Alma Mater Studiorum – Università di Bologna
Facoltà di Scienze Matematiche, Fisiche e Naturali

Dottorato di Ricerca in:

GEOFISICA

Ciclo: XXII

Settore scientifico-disciplinare di afferenza: **GEO-10**

Titolo Tesi

A new statistical model for eruption forecasting

Presentata da

Passarelli Luigi

Coordinatore

Prof. Michele Dragoni

Relatore

Dr. Warner Marzocchi

Esame finale anno 2010

Contents

Introduction **1**

1 Bayesian Hierarchical Time Predictable Model for eruption occurrence: an application to Kilauea Volcano **5**

1.1 Introduction 5

1.2 Bayesian Hierarchical Model 7

1.2.1 Data model 8

1.2.2 Process model 10

1.2.3 Parameter model 12

1.2.4 Posterior distribution for variables and parameters 13

1.3 Parameters estimation and forecasting 16

1.3.1 Parameters estimation 17

1.3.2 Model checking 20

1.3.3 Forecasts 21

1.4 Conclusions 24

References 27

Tables 30

Figures 32

2 A new Bayesian Time-Predictable Model for Open Conduit Volcanoes: The Case of Mt Etna and Kilauea **43**

2.1 Introduction 44

2.2 A Bayesian Hierarchical Model for Time-Predictability 46

2.2.1 Data Model 47

2.2.2 Process model 48

2.2.3 Parameters model 49

2.2.4 Posterior and full conditional distributions 50

2.2.5 Model Checking and Forecasting procedure 51

Application to Kilauea volcano, Hawaii, and Mount Etna volcano, Sicily 54
2.3 Kilauea volcano 54
2.3.1 Results for variables and parameters 55
2.3.2 Model checking and Forecasts 57
2.4 Mount Etna volcano 60
2.4.1 Results for variables and parameters 61
2.4.2 Model checking and Forecasts 63
2.5 Conclusions 67
Appendix A 69
References 71
Tables 75
Figures 79

3 The Correlation Between Run-Up and Repose Times of Volcanic Eruptions 97
3.1 Introduction 98
3.2 Definitions 99
3.3 Observations 102
3.3.1 Unusual Individual Eruptions 103
3.4 Interpretation in terms of viscosity 104
3.4.1 Viscosity based on Silica content 104
3.4.2 Model for Run-up Times 105
3.4.3 Model for Repose Times 107
3.5 Conclusions and Implications for Eruption Forecasts 108
References 111
Tables 115
Reference list for database in Table 3.1 121
Figures 132

Conclusions 137

Acknowledgements 139

References 141

List of Figures

1.1 *Plot of the cumulative number of eruptive events listed in Kilauea catalog. On the right side of the dashed line there are the events that have been used in BH_ TPM. This plot shows that the catalog is complete from 1918, but we have taken only eruptions from 1923 because 1919 and 1922 eruptions have missing volume data.* 33

1.2 *Posterior distributions of relevant parameters of BH_ TPM using a synthetic catalog with b=0.5. The first plot on the left represents the synthetic data sets (i.e. volumes and interevent times); the other sub-plots show the parameters inferred by BH_ TPM. For more information see the text.* 34

1.3 *Constructed Markov Chains for each variable and parameter of the BH_ TPM. For R and V we show just one of the 41 chains relative to each variable. In panel* **a**, *each chain (i.e. each subplot) reaches the convergence after few iterations, forgetting the initial guess very quickly. In this case the starting values is chosen to be 10 for all quantities. Iterations in panel* **a** *represent only the first 100 iteration of the burn-in phase, for more details please refer to the text. The remaining iterations (i.e. from 1001 to 10000), shown in* **b** *panel, represent the conditional posterior distributions for BH_ TPM variables and parameters.* . . . 35

1.4 *Posterior distribution for relevant parameters simulated using all data in catalog. In panel* **a** *it is shown the posterior distribution of parameter b; in panel* **b** *the posterior distribution for parameter K and in panel* **c** *the posterior distribution for parameter σ_R^2.* 36

1.5 *Blue stars show the posterior distributions of pairs of simulated variables (interevent times R_i and volumes V_i). These variables are simulated via MCMC-Gibbs sampling using all data in the catalog. Panel* **a** *is relative to R_i and V_i from 1 to 20 and panel* **b** *from 21 to 41. Red plus is the observed data.* 37

1.6 *Posterior distributions of: b parameter in panel* **a**, *K parameter in panel* **b** *and* σ_r^2 *in panel* **c**, *all calculated using the forward procedure discussed in the text. Black dashed line represents the learning phase. Red triangles are the mean of the distributions for b and K and the median for* σ_r^2 38

1.7 *Distributions of synthetic interevent times (blue bars) compared with observed values (red line) using descriptive statistic. This goodness-of-fit test (for more detail see the text) shows that our BH_ TPM predicts unreasonably long and short interevent times for Kilauea volcano.* 39

1.8 *"Punctual probability gain" of the BH_ TPM for each event after the learning phase against: in panel* **a** *Poisson Model (Klein, 1982), in panel* **b** *Log-Normal Model (Bebbington & Lai, 1996b) and in panel* **c** *Generalized Time Predictable Model (Sandri et al., 2005). Values greater than zero indicate when BH_ TPM model performs better forecast than the reference models. The inset in each panel is the total Probability gain, i.e. the sum of the punctual probability gains.* 40

1.9 *Regression analysis for BH_ TPM "punctual probability gain" against Poisson Model versus observed interevent times. The significant inverse linear relationship, whose best fit regression coefficients and* R^2 *are given, indicates a systematic negative probability gain for long interevent times. As discussed in the text, this means an additional complexity for long interevent times compared to the time predictable eruptive behavior. This causes a worse ability of our BH_ TPM, compared to Poisson model, to forecast long interevent times.* 41

2.1 *Autocorrelation function for MCMC realizations for parameters: b top left panel, c top right panel and* λ *bottom left panel. The autocorrelation function is zero at lag 20, so we run each MCMC chain for 201000 iterations thinning it every 20 MCMC-steps. We obtain 10000 independent realizations for each chain.* . . . 80

2.2 *Blue stars show the posterior distributions of pairs of simulated variables (interevent times* r_i *and volumes* v_i*). These variables are simulated via MCMC Gibbs sampling (*r_i*'s) and Metropolis Hastings (*v_i*'s) using all data in the catalog. The top panel is relative to* r_i*'s and* v_i*'s from 1 to 20 and the bottom panel from 21 to 41. Red plus is the observed data.* 81

2.3 *Posterior distributions for BH_ TPMII parameters obtained using all data in the catalog: top left panel refers to b, top right to c and bottom left to* λ. 82

2.4 *Posterior distributions of: b parameter in top left panel, c parameter in top right panel and λ in the bottom left panel, all calculated using the sequential procedure discussed in the text. Black dashed line represents the learning phase. Red triangles are the mean of each distribution.* 83

2.5 *Distributions of synthetic interevent times (blue bars) compared with observed values (red line) using descriptive statistic. This goodness-of-fit test (for more detail see the text) shows that BH_ TPMII predicts synthetic interevent times in good agreement with the observed data, except for the maximum and standard deviation where the observed quantities are reproduced in the tail behavior.* . . . 84

2.6 *Results for the SIR procedure applied to posterior distribution of λ's. In this plot we indicate with blue stars the posterior MCMC-realizations for λ^j while red stars refer to the resampled ones with SIR algorithm. Using the SIR procedure, described in Appendix A, we update each posterior distribution of λ with the information given by the observed volume under the sequential procedure discussed in the text. The SIR procedure is applied on λ's obtained after the learning phase as required in the sequential approach used (i.e. events from 14 to 41 in Table 2.1).* 85

2.7 *"Punctual probability gain" of the BH_ TPMII for each event after the learning phase against: in panel **a** Poisson Model (Klein, 1982), in panel **b** BH_ TPM (Passarelli et al, 2010), in panel **c** Log-Normal Model (Bebbington & Lai, 1996b) and in panel **c** Generalized Time Predictable Model (Sandri et al., 2005). Values greater than zero indicate when BH_ TPM model performs better forecast than the reference models. The inset in each panel is the total Probability gain, i.e. the sum of the punctual probability gains.* 86

2.8 *Regression analysis for BH_ TPMII "punctual probability gain" against Poisson Model versus observed interevent times. The significant inverse linear relationship, whose best fit regression coefficients and R^2 are given, indicates a systematic negative probability gain for long interevent times. As discussed in the text, this means an additional complexity for long interevent times compared to the time predictable eruptive behavior. This causes a worse ability of our model, compared to Poisson model, to forecast long interevent times.* 87

2.9 *Autocorrelation function for MCMC realizations for parameters: b top left panel, c top right panel and λ bottom left panel. The autocorrelation function is zero at lag 20. So, to obtain 10000 independent realizations for each chain, we run each MCMC chain for 201000 iterations thinning every 20 steps.* 88

2.10 *Blue stars show the posterior distributions of pairs of simulated variables (interevent times r_i and volumes v_i). These variables are simulated via MCMC Gibbs sampling (r_i's) and Metropolis Hastings (v_i's) using all data in the catalog. From top to bottom the first panel is relative to r_i and v_i from 1 to 20, the second panel from 21 to 40 and the third panel from 40 to 62. Red plus is the observed data.* 89

2.11 *Posterior distributions for BH_ TPMII parameters obtained using all data in the catalog: top left panel refers to b, top right to c and bottom left to λ.* 90

2.12 *Posterior distributions of: b parameter in top panel, c parameter in middle panel and λ in the bottom panel, all calculated using the sequential procedure discussed in the text. Black dashed line represents the learning phase. Red triangles are the mean* 91

2.13 *Distributions of synthetic interevent times (blue bars) compared with observed values (red line) using descriptive statistic. This goodness-of-fit test (for more detail see the text) shows that BH_ TPMII predicts synthetic interevent times in good agreement with the observed data, except for the maximum and standard deviation where the observed quantities are reproduced in the tail behavior.* . . . 92

2.14 *Results for the SIR procedure applied to posterior distribution of λ's. In this plot we indicate with blue stars the posterior MCMC-realizations for λ^j while red stars refer to the resampled ones with SIR algorithm. Using the SIR procedure, described in Appendix A, we update each posterior distribution of λ with the information given by the observed volume under the sequential procedure discussed in the text. The SIR procedure is applied on λ's obtained after the learning phase as required in the sequential approach used (i.e. events from 20 to 62 in Table 1.1).* 93

2.15 *Plot to detect the trend of intensity of a homogeneous Poisson process under the sequential procedure. Blue stars are the intensity λ_{MLE} calculated sequentially via MLE adding one data at a time plotted versus the time of each event. The λ_{MLE}'s are calculated after the learning phase. To figure out whether or not the intensity is increasing with time, we estimate its trend with linear regression, please refer to the text for more details. Red lines represent non significant regressions (at 1% level), green lines represents significant regressions. The black dashed line is the change point found by Smethurst et al 2009. Estimating sequentially the trend, one is able to detect the increasing trend only four events after the change point found by Smethurst et al., 2009, say, only after the 1975 AD eruption.* 94

2.16 *"Punctual probability gain" of the BH_ TPMII for each event after the learning phase against: in panel **a** Poisson Model (Klein, 1982), in panel **b** BH_ TPM (Passarelli et al, 2010), in panel **c** GTPM (Sandri et al, 2005), in panel **d** Salvi et al, 2006 model, in panel **e** Smethurst et al, 2009 model and in panel **f** modified piecewise linear model of Smethurst et al, 2009 under the sequential procedure (please see the text for more details). Values greater than zero indicate when BH_ TPM model performs better forecast than the reference models. The inset in each panel is the total Probability gain, i.e. the sum of the punctual probability gains.* 95

2.17 *Regression analysis for BH_ TPMII "punctual probability gain" against Poisson Model versus observed interevent times. The significant inverse linear relationship, whose best fit regression coefficients and R^2 are given, indicates a systematic negative probability gain for long interevent times. As discussed in the text, this means an additional complexity for long interevent times compared to the time predictable eruptive behavior. This causes a worse ability of our model, compared to Poisson model, to forecast long interevent times.* 96

3.1 *Repose time versus run-up time data. The error associate with the slope of the regression is equal to 0.3 and with the intercept is 0.1. Labels of individual points correspond to each eruption documented in Table 1. Magma composition is based on the Le Bas et al (1986) classification.* 133

3.2 *Regression analysis to infer an empirical relationship between silica content and viscosity. Viscosity is calculated using Conflow with reported compositional information (Mastin & Ghiorso, 2000). Please refer to Table 2 for more details.* 134

3.3 *Repose time versus run-up time with viscosity calculated using the regression line in Figure 2 for each eruption.* 135

3.4 *Schematic illustration of the physical model used in the text. Q_i is the magma supply rate. For more details, please refer to the text.* 136

3.5 *Average extrusion rate Q_e, red ones, are calculated using repose times and volumes in Table 1 and compared with those from White et al (2006), blue ones. The Q_e's are calculate for different class of magma composition. For more detail please refer to the text.* 136

List of Tables

1.1 Kilauea eruptive catalog 31
1.2 Overview of distribution used in BH_TPM 32

2.1 Catalog of eruptive events at Kilauea volcano 76
2.2 Mt Etna flank eruptions catalog 77

3.1 Dataset of al 54 eruptions used 119
3.2 Data used to infer the viscosity 120

Introduction

In this dissertation we present the three projects we have been involved during the three years of the PhD program in Geophysics at University of Bologna. The first two projects (in Chapters 1 and 2) are closely related, one being the enhancement of the other. They focus on the development and carrying out of two Bayesian Hierarchical Models for forecasting volcanic eruption of open conduit volcanoes, with application to Kilauea volcano, Hawaii, and Mount Etna volcano, Sicily. We have capitalized on the Bayesian methodology to test if these volcanoes are compatible with a time predictable eruptive model, and to implement a procedure for probabilistic forecast assessment. The third and last project (in Chapter 3) concerns the two main observables time-scales of the dynamics of eruptive processes, i.e. the interevent time or repose time and the magma run-up time. We have investigated the inter-relationship of these two quantities considering 26 different volcanoes around the world relative to 54 different eruptions with magma composition ranging from basaltic to dacitic. The final goal is to investigate the inter-relationship between the interevent time and repose time trying to constrain the role of magma viscosity in controlling these two physical observables.

In order to make the reading easier, we organize this introduction section keeping separated the two main topics reported above. So we will introduce first the main argumentation on the physical and statistical reasonings behind the two statistical models for eruption forecast. In the last part we will discuss widely of the last project.

One of the main challenges in modern volcanology is to forecast volcanic eruptions with the aim of mitigating the risk associated with. The extreme complexity, non linearity, limited knowledge and the large number of degrees of freedom of a volcanic system make deterministic prediction of the evolution of volcanic processes rather impossible (e.g. Marzocchi 1996; Sparks 2003). Volcanic systems are intrinsically stochastic. In general, eruption forecasting involves two different time scales: i) a *short-term* forecasting, mostly based on monitoring measures observed during an episode of unrest (e.g., Newhall & Hoblitt 2002, Marzocchi *et al* 2008 among others), and mostly related to a statistical description of the past eruptive catalogs (e.g. Klein, 1982, Bebbington, 1996a among others). Here, we focus our attention only on the long term forecast.

An incisive and useful forecast should be made before the onset of a volcanic eruption, using the data available at that time. Models implemented with forecast purposes have to take into account the possibility to provide "forward" forecasts and should avoid the idea of a merely "retrospective" fitting of the data available. Although several statistical models have been proposed in the past years aiming at the identification of possible recurrence or correlation in the volcanic time and/or volume data, none of those models has been carried out with a robust procedure acting to test the forecast performance of the model (see for example Klein 1982, Mulargia *et al* 1985, Bebbington & Lai 1996a and 1996b, Salvi *et al*, 2006, among others). The idea behind these works was to make efforts in best-fitting the data disregarding to check the forecast capability of the model. Here we want to tackle this problem constructing a model where the probabilistic forecast has to be one of the main goals in a perspective of probabilistic volcanic hazard assessment .

In addition, a statistical model should include a physical eruptive process and related information, if there is any, to give a better understanding of the overall phenomenon. These convictions lead us to use Bayesian methods in which the posterior distribution for the parameter vector is a compromise between the likelihood and the prior distribution (see for example Gelman et al., 2000). While the likelihood quantifies the probability of observation varying the parameters, the prior distribution, expresses in terms of probability density function some a priori belief about parameters. So, there is the possibility of assigning probability on the hypotheses using prior distributions together with the inferential use of the data as in a mere likelihood analysis. Therefore, probability distributions can be used to model and constrain extra-sample information in the prior distribution settings. We believe this possibility could be a suitable and helpful tool to get enhancement in forecasting geophysical system when the information provided by data are poor (for small or heterogeneous dataset for instance).

Here, following the aforementioned ideas, we will apply the Generalized Time Predictable model as presented by Sandri *et al* (2005) and Marzocchi & Zaccarelli (2006) for the eruptive process. The classical Time Predictable Model (De La Cruz-Reyna, 1991, Burt *et al* 1994) assumes eruptions occur when the volume in the storage system reaches a threshold value being recharged at constant rate from deeper crust. The size of eruptions is a random variable following some kind of statistical distribution. Mathematically, this implies that the interevent time, the time between two consecutive onset of eruption events (i.e. $r_i = t_{i+1} - t_i$), is linearly dependent on the volume erupted during the ith eruption. Here we will use the generalization of the classical time predictable model, proposed by Sandri *et al* (2005), where the input rate in the magma shallow reservoir could be variable in time, implying a power law relationship between interevent time and volume erupted.

In Sandri *et al* (2005), the authors have found that Mount Etna eruptions (both summit

and lateral events since 1970 AD) follow a time predictable behavior. Marzocchi & Zaccarelli (2006) have also showed that the Kilauea volcano eruptions are time predictable. Both models, however, do not take into account the measurement errors for interevent times and volumes, since volume data are affected by a large uncertainty.

As we will show in Chapter 1, using the Generalized Time Predictable model, we have built up the model for forecasting volcanic eruption with application to Kilauea volcano. We have used a Bayesian Hierarchical framework where variables and parameters of the process are described used log-normal and inverse-gamma distributions with the aim of using the information relative to the measurement error. The choices of this particular type of distribution, corroborated by goodness-of-fit tests, have come out for technical reasons making easier numerical simulations within the model. This model has showed problems in fitting data, while we have found the time-predictability of Kilauea volcano and have made probabilistic forecast as we will show later in Chapter 1. Attributing this discrepancy in data fitting with log-normal distributions, we have chosen to develop a further version of hierarchical model with more appropriate and general probability density function for interevent times and volumes. This choice was made in order to improve forecasts. We have chosen exponential-wise distributions for interevent times and volumes according with Klein (1982), Mulargia (1985), Marzocchi (1996) and Bebbington & Lai (1996a) and (1996b). We will present this second model in Chapter 2 with application to Kilauea eruption and Mount Etna flank eruptions. This project has been performed in collaboration with prof Bruno Sansò at Dept. of Applied Mathematics and Statistics at University of California, Santa Cruz under the Marco Polo exchange program of the University of Bologna.

Finally we will present in Chapter 3, the project developed with prof. Emily Brodsky at the Dept. of Earth and Planetary Sciences at University of California, Santa Cruz. The idea behind this exploratory work is that volcanoes usually show signs of unrest before an eruption. The intensity of these signals during the pre-eruptive phase varies greatly. So, establishing physical controls on the duration of precursory activity, i.e. run-up time, could improve understanding of the dynamics of magma ascent from a shallow magma reservoir to the surface. We also focused on another observable indicative of eruption dynamics: the interevent time or repose time, i.e., the time between magmatic eruptions. For sake of clarity, in Chapter 3 we will use repose time with the same meaning of interevent time. The repose time could be associated with the mechanism that recharges the magmatic system. Both of these dynamic quantities are strongly dependent on magma composition and hence magma viscosity. In this preliminary work, we have investigated the inter-relationship between run-up time, repose time and viscosity by collecting together a database of 54 eruptions from 26 different volcanoes around the world. The data ranges from basaltic to dacitic systems, so we

could investigate the gross influence of viscosity by using the silica content as a proxy.

This dissertation is organized as follows: in Chapter 1 we will present "Bayesian Hierarchical Time Predictable Model for eruption occurrence: an application to Kilauea Volcano" , in Chapter 2 we will present "A new Bayesian Time-Predictable Model for Open Conduit Volcanoes: The Case of Mt Etna and Kilauea", in Chapter 3 we will introduce "The Correlation Between Run-Up and Repose Times of Volcanic Eruptions ". We will give references, tables and figures at the end of each chapter, while the bibliography of this introduction section will be at the end of the dissertation.

Chapter 1

Bayesian Hierarchical Time Predictable Model for eruption occurrence: an application to Kilauea Volcano

Abstract

The physical processes responsible for volcanic eruptions are characterized by a large number of degrees of freedom, often non-linearly coupled. This extreme complexity leads to an intrinsic deterministic unpredictability of such events that can be satisfactorily described by a stochastic process. Here, we address the long-term eruption forecasting of open conduit volcanoes through a Bayesian Hierarchical Modeling information in the catalog of past eruptions, such as the time of occurrence and the erupted volumes. The aim of the model is twofold: 1) to get new insight about the physics of the process, using the model to test some basic physical hypotheses of the eruptive process; 2) to build a stochastic model for long-term eruption forecasting; this is the basic component of Probabilistic Volcanic Hazard Assessment that is used for rational land use planning and to design emergency plans. We apply the model to Kilauea eruption occurrences and check its feasibility to be included in Probabilistic Volcanic Hazard Assessment.

1.1 Introduction

The extreme complexity, non linearity, limited knowledge, and the large number of degrees of freedom of a volcanic system make deterministic prediction of the evolution of volcanic pro-

cesses impossible. Volcanic systems are intrinsically stochastic (e.g. Marzocchi 1996; Sparks 2003), and hazardous volcanic phenomena involve so many uncertainties that a probabilistic approach is practically always needed (e.g. Newhall & Hoblitt 2002; Sparks 2003; Marzocchi *et al.* 2004).

In general, eruption forecasting can be tackled in two different ways, related to two different time scales: i) a *short-term* forecasting, mostly based on monitoring measures observed during an episode of unrest (e.g., Marzocchi *et al.* 2008); ii) a *long-term* forecasting, usually made during a quiet period of the volcano, and mostly related to a statistical description of the past eruptive catalogs. Here, we focus our attention only on this second issue.

In a recent paper, Marzocchi & Zaccarelli (2006) found different behavior for volcanoes with "open" conduit regime (i.e., volcanoes with high frequency of eruption and repose periods less than few tens of years) compared to those with "closed" conduit regime (i.e., volcanoes with periods of quiescence longer than 30-40 years). According to that paper, open conduit volcanoes tested there (i.e. Mt Etna, Kilauea volcano) seem to follow a so-called *Time Predictable Model*, i.e. a model where the time to the next eruption depends on the size of the last eruption (De La Cruz-Reyna, 1991, Burt *et al.* 1994). Closed conduit volcanoes, tested by Marzocchi & Zaccarelli (2006) , conversely seem to follow mostly a Poisson distribution. These results have been used to build general probabilistic models for volcanic hazard assessment of open and closed conduit systems.

Different methods have been presented in the past years aiming at the identification of possible recurrence or correlation in the volcanic time and/or volume data. Klein (1982) and Bebbington & Lai (1996b) study the changes in volcanic regimes looking at the mean rate of occurrence of the volcanic events. Sandri *et al.* (2005) apply a generalized form of time predictable model to Mount Etna eruptions. De La Cruz-Reyna (1991) proposed a load-and-discharge model for eruptions in which the time predictable model could be seen as a particular case. Bebbington (2008) presented a stochastic version of the general load-and-discharge model also including a way to take into account of the history of the volcano discharging behavior. In this paper the author studied the time predictability as a particular case of his model with application to Mount Etna and Mauna Loa and Kilauea data series. Finally a different hierarchical approach has been presented by Bebbington (2007) using Hidden Markov Model to study eruption occurrences with application to Mount Etna flank eruptions. This model is able to find any possible underlying volcano activity resulting in volcanic regime changes.

Here, our goal is to improve significantly the modeling of open conduit systems through the implementation of a Bayesian Hierarchical Time Predictable Model (hereafter BH_TPM) for eruption occurrence. The model is a formal generalization of the Time Predictable Model in a full Bayesian framework. The Bayesian perspective allows accounting for stochastic

fluctuations in each parameter of the model and in each recorded measurement (Wikle 2003). In this way, each parameter of the model is described through a probability density function whose posterior distribution is conditioned by the available data. The numerical solution is obtained via MCMC-Gibbs sampling (Gelman *et al.*, 2000). The BH_TPM is then applied to the eruption record of Kilauea Volcano since 1923 published by the Hawaiian Volcano Observatory (see Table 1.1). The outcomes for model variables and parameters show good convergence properties for all model parameters and errors.

After describing the model in detail, we focus our attention on some specific issues: 1) to discuss the volcanological implications of the model parameters obtained; 2) to verify if the model describes the data satisfactorily; 3) to compare the forecasting capability of BH_TPM with other models in the literature; i.e. Poisson model (Klein, 1982) and Log-Normal model (Bebbington & Lai, 1996b) and Generalized Time Predictable Model (Sandri *et al.*, 2005). We would like to remark point 3) under a probabilistic forecast perspective. As we will show later in the text, we will use BH_TPM for forecasting purposes mimicking probabilistic eruption forecasts using Kilauea volcano dataset. In order to do this, we will use the first third part of the catalog as a learning phase for the model, and we will make probabilistic eruption forecast on the remaining part using a *forward* procedure discussed later in the text. This allows to test and use this model as a component of Probabilistic Volcanic Hazard Assessment (PVHA).

1.2 Bayesian Hierarchical Model

The formal ideas of hierarchical modelling arise from simple probability rules. Hierarchical modelling is based on the simple fact that the joint distribution of a collection of random variables can be decomposed into a series of conditional models (Wikle, 2002). That is, if X, Y, and Z are random variables, we can write the joint distribution in terms of a factorization such as $[X, Y, Z] = [Z|Y, X][Y|X][X]$. We make use of the bracket notation for probability distribution in which $[Y]$ refers to the distribution of Y and $[Y|X]$ refers to the conditional distribution of Y given X. This simple formula is the basic idea of hierarchical thinking. In general it is easier to specify the distribution of the relevant conditional models than to work with marginal distributions of variables involved in such models. In this case, the product of a series of relatively simple conditional models leads to a joint distribution that can be quite complicated.

In order to build the model, we follow the framework outlined by Wikle (2002; see also references therein). The idea is to approach the problem by breaking it into three primary stages:

- Data model : $[data|process, parameters]$

- Process model : $[process|parameters]$
- Parameter model : $[parameters]$

The first stage regards the observational process or data model, which specifies the distribution of the observed data given the process generating them and the parameters describing it. The second stage describes the process, conditional on its parameters. Finally, the third stage accounts for the uncertainty in the parameters. Ultimately, we are interested in the distribution of the process and parameters updated by the data. We obtain the joint posterior distribution for the process and parameters using Bayes' rule:

$$[process, parameters|data] \propto [data|process, parameters][process|parameters][parameters] \quad (1.1)$$

In order to make inference about the process and parameters governing the occurrence of volcanic eruptions for the case of "open" conduit volcano, we apply this simple approach. In the next subsections we will illustrate each stage that we have performed for our hierarchical model.

1.2.1 Data model

The dataset reported in Table 1.1 is taken from the Hawaiian Volcano Observatory web site (http://hvo.wr.usgs.gov/kilauea/history/historytable.html). The full catalog starts from 1823 but only the 42 volcanic events having occurred after 1922 are considered in our analysis, because only this latter part of the catalog can be considered complete in terms of occurrence time and erupted volume data. Figure 1.1 reports the cumulative number of events versus time, where the eruptive rate since 1923 is approximately constant except for a major quiescence period around the 40's. The catalog reports the onset of each eruption, the total volume of material ejected (lava and tephra) and the interevent time. The volume of the 1924/05/10 event is taken from http://www.volcano.si.edu/ and is only the tephra volume. For more details regarding the definition of interevent times see Klein (1982). Since the interevent time following the last eruption cannot be available, we have 41 pairs of data of interevent time (i.e. the time between the onset of ith and the onset of $(i+1)$th eruptions) and volume erupted (in the ith eruption), that from now on we indicate with d_{r_i} and d_{v_i} respectively.

In testing the independence of data via correlation function, the only significant correlation (P-value=0.06) appears between the volume and the subsequent interevent time. Therefore we assume that each pair of data (d_{r_i},d_{v_i}) is independent from the other pairs. In a Bayesian framework, the act of measurement does not lead simply to an observed value, but to a state of information described by a distribution where the single measurement is a random realization of this distribution.

In this paper, we assume that the logarithm of the data, made dimensionless by two gauge constant (i.e. $\hat{R} = 1\,\text{day}$ and $\hat{V} = 1 \times 10^6\ \text{m}^3$), i.e. $D_{r_i} = \ln(d_{r_i}/\hat{R})$ and $D_{v_i} = \ln(d_{v_i}/\hat{V})$,

are respectively random draws from normal distributions, with the means $R_i = \ln(r_i/\hat{R})$ for the interevent times and $V_i = \ln(v_i/\hat{V})$ for the volumes, where r_i's are the interevent time variables and v_i's are the volume variables. We test whether or not D_{r_i} and D_{v_i} are normally distributed using Anderson-Darling test (Anderson and Darling, 1952). The null hypothesis is that logarithm of the data comes from a normal distribution. We can not reject the null hypothesis of normality for D_{r_i} and D_{v_i} with P-value=0.625 and P-value=0.715 respectively (Trujillo-Ortiz *et al.*, 2007). We can conclude that normal distributions fit reasonably the logarithm of the data.

The variables r_i and v_i, and their natural logarithm, represent the variables of our model. The variances of such normal distributions are the data measurement errors for the interevent times $\sigma^2_{Dr_i}$ and for the volumes $\sigma^2_{Dv_i}$. In this view, each single pair is:

$$D_{r_i} \sim N(R_i, \sigma^2_{Dr_i}) \quad \text{and} \quad D_{v_i} \sim N(V_i, \sigma^2_{Dv_i}) \quad i = 1, \ldots, 41$$

where from now on $N(a, b^2)$ indicate a normal distribution with mean a and variance b^2 and the symbol $\sim$ means "is distributed as".

In order to give appropriate variances for R_i and V_i to each distribution, we use the error propagation. We assume two different values for measurement errors on volume data before and after 1960. Such division arises by considering that, after 1960, the measurements were taken by the Hawaiian Volcano Observatory, and we assume that these measurements are more accurate. Systematic and direct measurement of lava flow or modern measurement using satellite techniques should give a more precise estimation of the volume erupted. Indirect measurement on historical lava flow, inferred with geological field methodology probably underestimates the real erupted volume (e.g. Behncke *et al.*, 2005). This is the reason why we assume the relative error $(\Delta v_i/v_i)$ equal to 25% for the volumes before 1960 and equal to 15% for more recent data. For the interevent times we choose an error measurement equal to $\Delta r_i = 1$day. Therefore, applying the error propagation rule, we get:

$$\sigma_{Dr_i} = \frac{\partial R_i}{\partial r_i}\Delta r_i = \frac{\Delta r_i}{r_i} \quad i = 1, \ldots, 41$$

$$\sigma_{Dv_i} = \frac{\partial V_i}{\partial v_i}\Delta v_i = \frac{\Delta v_i}{v_i} = 0.25 \quad i = 1, \ldots, 13$$

$$\sigma_{Dv_j} = \frac{\partial V_j}{\partial v_j}\Delta v_j = \frac{\Delta v_j}{v_j} = 0.15 \quad j = 14, \ldots, 41$$

The error σ_{Dr_i} is coincident with the relative error on the interevent time, while σ_{Dv_i} is independent from the data value and error.

At this point we are able to write the joint distributions for the data model, assuming

independence among the pairs of data, as:

$$[D_r|R,\sigma^2_{Dr}] = \prod_{i=1}^{41} N(R_i,\sigma^2_{Dr_i}) \tag{1.2}$$

$$[D_v|V,\sigma^2_{Dv}] = \prod_{i=1}^{41} N(V_i,\sigma^2_{Dv_i}) \tag{1.3}$$

1.2.2 Process model

Before displaying our statistical considerations for the process model, we have to introduce the underlying physical eruptive process. We use a very simple stochastic process to explain the eruptive dynamic process. It is the Generalized Time-Predictable Model (GTPM, see Sandri *et al.* 2005) for volcanic eruptions, assuming that eruptions occur when the volume in the storage system reaches a threshold value, given that magma enters in the magma storage system with a variable rate and that the size of eruptions is a random variable, following some kind of statistical distribution. Under these assumptions, we have a generalized time-predictable system with longer/shorter interevent time following large/small volume output eruptions. In fact, for such a model, the time to the next eruption is determined by the time required for the magma entering the storage system to reach the eruptive level. In this view the more general form for a time-predictable model is a power law between the erupted volume and the interevent time:

$$r_i = cv_i^b \tag{1.4}$$

that we want to linearize by logarithmic transformation. For this reason we need dimensionless variables and so we introduce two gauge constants (i.e. $\hat{R}$ and $\hat{V}$ that are the same of previous section) in order to make r_i and v_i dimensionless. Therefore we choose $\hat{R} = 1\,\text{day}$ and $\hat{V} = 1 \times 10^6\,\text{m}^3$ and we define:

$$r_i^* = \frac{r_i}{\hat{R}} \qquad \text{and} \qquad v_i^* = \frac{v_i}{\hat{V}}$$

that we introduce in the previous equation and we obtain:

$$r_i^* = \alpha v_i^{*b}$$

where $\alpha = (c\hat{V}^b)/\hat{R}$ is a new constant. Now we can take the logarithm of this equation and we have:

$$R_i = K + bV_i \tag{1.5}$$

where $K = \ln\alpha$ is a constant and $R_i = \ln r_i^*$ and $V_i = \ln v_i^*$. This dimensionless transformation does not influence the following numerical solutions, but it is only an algebraic solution to make dimensionless the argument of the logarithms.

In the last equation, if the parameter b is equal to unity we are in a classical time predictable system (see De La Cruz Reyna 1991, Burt *et al.* 1994). If b is equal to 0 the system is not time predictable. If $b > 1$ we have a non-linear relationship implying a longer interevent time after a large volume eruption compared to a classical time predictable system. If $0 < b < 1$ we still have a non-linear relationship but for a big volume eruption it implies a shorter interevent time compared to a classical time predictable system. Assuming this process as a dynamic eruptive behavior for the volcano, we proceed to show our statistical consideration about this part of the hierarchical model implementation.

In building up the process model, we have to connect the model variables (R_i and V_i) with the physical model, i.e., with equation (1.5). Here, we assume that the R_i's are independent and each of them is normally distributed, with mean given by the generalized time-predictable model and unknown variance representing the model error. Hence:

$$R_i \sim N(bV_i + K, \sigma_R^2) \quad i = 1, \ldots, 41$$

and for the all variables R_i the resulting joint distribution given the model parameters is:

$$[R|V, b, K, \sigma_R^2] = \prod_{i=1}^{41} N(bV_i + K, \sigma_R^2) \tag{1.6}$$

In order to assign the distribution for the volume variables (V_i) we have to exert a little effort. We do not have information about the real size distribution of Kilauea eruptions. However, according to the Anderson and Darling test performed in the previous sub-section, the set of volume data, i.e. D_{v_i} $(i = 1, \ldots, 41)$, is satisfactorily fitted by a log-normal distribution. Because of this goodness-of-fit test, we assume that also the volume variables (i.e., v_i) in the BH_TPM have a log-normal distribution. The logarithm of variables, i.e. V_i, are therefore normally distributed with unknown mean μ_v and variance σ_v^2, and for each of them we can write:

$$V_i \sim N(\mu_v, \sigma_v^2) \quad i = 1, \ldots, 41$$

and the joint distribution is:

$$[V|\mu_v, \sigma_v^2] = \prod_{i=1}^{41} N(\mu_v, \sigma_v^2) \tag{1.7}$$

In addition, we assume that the parameter μ_v has uniform non informative vague prior distribution. A non informative prior expresses vague or general information about a variable. Non informative priors can express objective information (e.g., "the variable is positive") assigning equal probabilities to all possibilities within the defined domain (e.g., for all $x > 0$). The simplest case of non informative vague prior distribution is the uniform distribution with

unlimited domain (e.g., $-\infty < x < +\infty$). In this text when we refer to non informative vague prior distribution, we always use uniform distribution with unlimited domain, see Table 1.2.

The distribution of variance parameters, i.e. σ_R^2 and σ_v^2, are constructed from inverse gamma family, which is the natural conjugate family for the normal distribution (see Gelman *et al.*, 2000). The property of conjugacy is very useful in Bayesian prior to posterior analysis. The conjugacy is formally defined in this way: for a given vector of data $y = y_1, \ldots, y_n$ and a parameter vector $\theta = \theta_1, \ldots, \theta_n$, if Φ is a class of likelihood $[y \mid \theta]$, and Ψ is a class of prior distribution for θ, then the class Ψ *is conjugate* for Φ if $[\theta \mid y] \in \Psi$ for all $[y \mid \theta] \in \Phi$ and $[\theta] \in \Psi$ where data and parameters are linked by Bayes' theorem, i.e. $[\theta \mid y] \propto [\theta][y \mid \theta]$. In our case, if we model the prior distribution for variance by an inverse gamma distribution, the likelihood is normal (i.e. equation (1.6) and (1.7)), thus the posterior distribution (for the variance) becomes an inverse gamma distribution.

Therefore, the prior distributions for variances are:

$$[\sigma_R^2] = \Gamma^{-1}(\alpha_{\sigma_R}, \beta_{\sigma_R})$$

$$[\sigma_v^2] = \Gamma^{-1}(\alpha_{\sigma_v}, \beta_{\sigma_v})$$

where Γ^{-1} indicates the inverse gamma distribution with mean $\mu = \beta_{(.)}/(\alpha_{(.)} - 1)$ for $\alpha_{(.)} > 1$ and variance $s = \beta_{(.)}^2/(\alpha_{(.)} - 1)^2(\alpha_{(.)} - 2)$ for $\alpha_{(.)} > 2$, and α_{σ_R} and α_{σ_v} are shape parameters and β_{σ_R} and β_{σ_v} are scale parameters.

1.2.3 Parameter model

In a Bayesian perspective, we have to assign a distribution for the parameters (b and K) from equation (1.5), describing the physical model. From a Bayesian point of view, and for reasons of conjugacy properties of the distributions used, we simply assign a normal distribution to the parameters that we want to make inference on. The means (μ_b and μ_k) and variances (σ_b and σ_k) of those distribution are called *hyperparameters*. Hence we have:

$$[b|\mu_b, \sigma_b^2] = N(\mu_b, \sigma_b^2) \tag{1.8}$$

$$[K|\mu_k, \sigma_k^2] = N(\mu_k, \sigma_k^2) \tag{1.9}$$

The prior distributions for the hyperparameters are assumed to be independent. We assume non informative vague uniform prior distributions for the means (see Table 1.2), and the inverse-gamma prior distributions for the variances; the latter are

$$[\sigma_b] = \Gamma^{-1}(\alpha_{\sigma_b}, \beta_{\sigma_b})$$

$$[\sigma_K] = \Gamma^{-1}(\alpha_{\sigma_K}, \beta_{\sigma_K})$$

where α_{σ_b} and α_{σ_K} are shape parameters and β_{σ_b} and β_{σ_K} are scale parameters (see previous section).

1.2.4 Posterior distribution for variables and parameters

In Table 1.2 there is a summary of the all distributions assigned. The last step, now, is to calculate the joint posterior distribution as a product of data model, process model and parameters model. The posterior distribution is the process and parameters distribution updated by the observed data. Remembering equation (1.1) and the Bayes' rule, we have:

$$\begin{aligned}[R, V, b, K, \mu_b.\mu_k, \mu_v, \sigma_R^2, \sigma_v^2, \sigma_k^2, \sigma_b^2 | D_r, D_v] \propto \\ [D_r|R, \sigma_{Dr}^2][D_v|V, \sigma_{Dv}^2][R|V, b, K, \sigma_R^2][V|\mu_v, \sigma_v^2] \\ [b|\mu_b, \sigma_b^2][K|\mu_k, \sigma_k^2][\mu_v][\mu_b][\mu_k][\sigma_v^2][\sigma_b^2][\sigma_k^2][\sigma_R^2]\end{aligned} \tag{1.10}$$

The relevant BH_TPM parameters that we want to simulate from equation (2.7) are the parameters of the physical model b and K, and the error σ_R^2. Also, we want to simulate the variables R_i and V_i, in order to compare them with the observations. Finally we simulate μ_v and σ_v^2 for model check purpose, that will be explained in the following section. In order to simulate these parameters and variables, we have to integrate the joint posterior distribution given by equation 2.7.

We use a Monte Carlo integration using Markov Chain (MCMC), where the Markov Chain are constructed using Gibbs sampler (Gilks *et al.* 1996 and references therein).The Gibbs sampling algorithm generates an instance from the distribution of each variable in turn, conditional on the current values of the other variables/parameters. Therefore Gibbs sampling works by iteratively drawing samples from the full conditional distribution of each quantity of interest (i.e., variable or parameter); thus we calculate the full conditional distribution for every variable R_i and V_i, and every parameter b, K, σ_R^2, μ_v and σ_v^2. The analytic expression for each full conditional distribution calculated and used for sampling procedure is:

$$\begin{aligned}[R \mid \text{rest}] &\propto \prod_{i=1}^{41} \left[\mathrm{N}(D_{r_i} \mid R_i, \sigma_{Dr_i}^2)\mathrm{N}(R_i \mid bV_i + K\,,\, \sigma_R^2)\right] \\ &\propto \mathrm{N}\left(\left(\sum_{i=1}^{41} \frac{D_{r_i}}{\sigma_{Dr_i}^2} + \sum_{i=1}^{41} \frac{bV_i + K}{\sigma_R^2}\right), \left(\sum_{i=1}^{41} \frac{1}{\sigma_{D_{r_i}}^2} + \frac{1}{\sigma_R^2}\right)^{-1}\right)\end{aligned}$$

$$[V \mid \text{rest}] \propto \prod_{i=1}^{41} \left[\mathrm{N}(D_{v_i} \mid V_i, \sigma^2_{D_{v_i}}) \mathrm{N}(R_i \mid bV_i + K, \sigma^2_R) \mathrm{N}\left(V_i \mid \mu_v, \sigma_v\right) \right]$$
$$\propto \mathrm{N}\left(\left(\sum_{i=1}^{41} \frac{D_{v_i}}{\sigma^2_{Dv_i}} + \sum_{i=1}^{41} \frac{b(R_i - K)}{\sigma^2_R} + \frac{\mu_v}{\sigma^2_v} \right), \left(\sum_{i=1}^{41} \frac{1}{\sigma^2_{Dv_i}} + \frac{1}{\sigma^2_v} + \frac{1}{\sigma^2_R} \right)^{-1} \right)$$

$$[b \mid \text{rest}] \propto \prod_{i=1}^{41} \left[\mathrm{N}\left(R_i \mid bV_i + K, \sigma^2_R\right) \right] \mathrm{N}\left(b \mid \mu_b, \sigma^2_b\right)$$
$$\propto \mathrm{N}\left(\left(\sum_{i=1}^{41} \frac{(R_i V_i - K V_i)}{\sigma^2_R} + \frac{\mu_b}{\sigma^2_b} \right), \left(\sum_{i=1}^{41} \frac{V_i^2}{\sigma^2_R} + \frac{1}{\sigma^2_b} \right)^{-1} \right)$$

$$[K \mid \text{rest}] \propto \prod_{i=1}^{41} \left[\mathrm{N}\left(R_i \mid bV_i + K, \sigma^2_R\right) \right] \mathrm{N}\left(K \mid \mu_k, \sigma^2_k\right)$$
$$\propto \mathrm{N}\left(\left(\sum_{i=1}^{41} \frac{(R_i - bV_i)}{\sigma^2_R} + \frac{\mu_k}{\sigma^2_k} \right), \left(\frac{41}{\sigma^2_R} + \frac{1}{\sigma^2_k} \right)^{-1} \right)$$

$$[\mu_v \mid \text{rest}] \propto \prod_{i=1}^{41} \left[\mathrm{N}(V_i \mid \mu_v, \sigma^2_v) \right] \mathrm{U}\left(\mu_v \mid -\infty, +\infty\right)$$
$$\propto \mathrm{N}\left(\left(\sum_{i=1}^{41} \frac{V_i}{\sigma^2_v} \right), \left(\frac{41}{\sigma^2_v} \right)^{-1} \right)$$

$$[\sigma^2_R \mid \text{rest}] \propto \prod_{i=1}^{41} \left[\mathrm{N}\left(R_i \mid bV_i + K, \sigma^2_R\right) \right] \Gamma^{-1}\left(\sigma^2_R \mid \alpha_{\sigma_R}, \beta_{\sigma_R}\right)$$
$$\propto \Gamma^{-1}\left(\left(\frac{41}{2} + \alpha_{\sigma_R} \right), \left(\frac{1}{\beta_{\sigma_R}} + \sum_{i=1}^{41} \frac{(R_i - (bV_i + K))^2}{2} \right) \right)$$

$$[\sigma^2_v \mid \text{rest}] \propto \prod_{i=1}^{41} \left[\mathrm{N}(V_i \mid \mu_v, \sigma^2_v) \right] \Gamma^{-1}\left(\sigma^2_v \mid \alpha_{\sigma_v}, \beta_{\sigma_v}\right)$$
$$\propto \Gamma^{-1}\left(\left(\frac{41}{2} + \alpha_{\sigma_v} \right), \left(\frac{1}{\beta_{\sigma_v}} + \sum_{i=1}^{41} \frac{(V_i - \mu_v)^2}{2} \right) \right)$$

where the symbol $\mathrm{U}(a, b)$ indicate a uniform distribution on the domain $[a, b]$.

To implement the Gibbs algorithm, we have to set the starting values for each quantity of interest. The numerical solutions, obtained after 11000 iterations, exhibit good convergence properties for all model variables and parameters. Figure 1.3 shows the constructed Markov Chain using Monte Carlo integration for all values of BH_TPM. We discard the first 1000 iterations as the burn-in phase. For readers are not familiar with MCMC simulations, the burn-in phase is the number of iterations or the time steps needed by chains to reach convergence. After that burn-in phase, the constructed chain can be considered stationary. In Figure 1.3 each chain converges after very few iterations. Anyway, for sake of precision, we run each chain longer than needed (i.e., 11000 time steps), discarding the first 1000 iterations as the burn-in phase (mainly because the longer is the chain, the better is the approximation of the target stationary distribution, and moreover the Gibbs sampler simulation code is very fast to run). Hence the last 10000 Gibbs sampled time steps set up the posterior distributions for BH_TPM parameters and variables.

In order to ensure the convergence of each chain, regardless of starting values and the number of time steps (i.e. iterations) used, we finally calculate the Gelman and Rubin statistics (for a more detailed description of this method see Gelman *et al.* 2000, 331-332). For this reason we perform a number of different parallel simulations with different starting values, to check that the stationary distributions obtained are not sensitive to the random choice of starting values. We perform 10 parallel simulation of 15000 runs with different starting values and we monitor the convergence only for parameters b, K, σ_r^2, μ_v and σ_v^2. We use a higher number of simulations to avoid slow convergence problems related to extreme starting values.

The Gelman and Rubin approach is substantially based on comparing different simulated sequences by computing the between-sequence (i.e. B) and within-sequence (i.e. W) variance (using the same notation present in Gelman *et al.* 2000). For a general scalar ϕ_{ij} with $i = 1, \ldots, n$ and $j = 1, \ldots, J$, where n is the number of the simulations (i.e. 15000 in our case) and J is the number of parallel sequences (i.e. 10 in our case), we compute:

$$B = \frac{n}{J-1} \sum_{j=1}^{J} \left(\overline{\phi}_{.j} - \overline{\phi}_{..} \right)^2$$

where $\overline{\phi}_{.j} = \frac{1}{n} \sum_{i=1}^{n} \phi_{ij}$ is the mean of the j-th sequence and $\overline{\phi}_{..} = \frac{1}{J} \sum_{j=1}^{J} \overline{\phi}_{.j}$ is the grand

mean and

$$W = \frac{1}{J}\sum_{j=1}^{J} s_j^2$$

where $s_j^2 = \frac{1}{n-1}\sum_{i=1}^{n}\left(\phi_{ij} - \overline{\phi}_{.j}\right)^2$ is the variance within sequence j.

Hence we can estimate var(ϕ | data), the marginal posterior variance of the estimand, by a weighted average of W and B, namely:

$$\text{var}(\phi \mid \text{data}) = \frac{n-1}{n}W + \frac{1}{n}B$$

For a finite number of simulations n, the variance W should be an underestimate of var(ϕ | data) because the individual sequences do not cover all the range of target distribution and, as a result, will have less variability; in the limit $n \to \infty$, the expectation of W approaches var(ϕ | data). Therefore the aim is to monitor convergence by means of the factor

$$\mathcal{R} = \sqrt{\frac{\text{var}(\phi \mid \text{data})}{W}}$$

that has to be close to the unity. For the all parameters in our model, this $\mathcal{R}$-factor estimand is in practice equal to the unity. Therefore we have checked that the constructed Markov chain for BH_TPM parameters are independent of the starting values, then we can use the last 10000 sampling values as posterior distribution for the parameters b, K, σ_r, μ_v and σ_v.

1.3 Parameters estimation and forecasting

In this section we examine the results obtained via MCMC-Gibbs Sampling for the model variables and parameters. We explain the physical meaning of the simulated quantities and their reliability to reproduce observational data. We test the forecast capability of this model compared with some appropriate models previously published in the literature.

Before discussing the results obtained for Kilauea Volcano, we test the BH_TPM and its reliability by analyzing synthetic data. To this purpose, we generate a sample of 50 synthetic values v_{synt}^i from a log-normal distribution with zero mean and unit variance. By definition of log-normal distribution, we have that $V_{synt} = \log(v_{synt}^i)$ are normally distributed. This set of 50 V_{synt} are random draws from a normal distribution and they mimic a synthetic catalog of volume erupted. These synthetic volume data are substituted into the Time Predictable equation (1.5), setting different values for the parameters b and K, in order to obtain a "purely"

time predictable catalog of synthetic interevent times R^i_{synt}. Then, we add a white noise at each synthetic interevent time R^i_{synt} using the following equation:

$$R^i_{synt} = K + bV^i_{synt} + \varepsilon$$

where $\varepsilon \sim N(0,1)$ is a stochastic noise term.

Thus we generate three different synthetic data sets of R^i_{synt} and V^i_{synt} each one with a different value of b, i.e. $b = 0.5$, $b = 1$ and $b = 1.5$, and the same value of $K = 5$, in order to reproduce three different eruptive regimes achievable with a Time Predictable equation (1.4), i.e. $0 < b < 1$, $b = 1$ and $b > 1$. With this procedure we build up three synthetic data sets consisting each of 50 pairs of intervent times and volumes. The idea is to use them to test our BH_TPM. Eventually, if the model is robust, we expect to find as outcomes the same b and K values used to obtain the synthetic interevent times R^i_{synt} for each data sets. The results of this synthetic test show a good reproducibility of the model respect to the parameters used generating the R_{synt}'s. In Figure 1.2 there are the BH_TPM simulations for the parameters b, K and σ^2_r when the synthetic interevent time R_{synt}'s are generated with $b = 0.5$ and $K = 5$. We obtain similar results in the other cases (i.e. $b = 1$ and $b = 1.5$); we do not show them to avoid redundancy. It is even interesting in Figure 1.2 that the numerical value of the variance of interevent times distribution of BH_TPM, i.e. σ^2_r, is comparable with the noise term ε. Yet, we acknowledge that the three data sets do not contain outliers, so there is a very small variability inside them. Finally, as the model seems to be robust, we apply it to a "real" dataset.

1.3.1 Parameters estimation

Using the great flexibility of the implemented Markov Chain, we obtain the numerical values for model variables and parameters in two ways:

1. using all the first 41 events in the catalog (Table 1.1), but discarding the $42nd$ because it is ongoing, to obtain the distributions of the variables R and V and the parameters b, K and σ^2_R, see Figure 1.4, 1.5;

2. sampling b, K and σ^2_R through a *forward* procedure. At first, we use only the first event in the catalog (see Table 1.1), and we add one pair of volume and interevent time data at a time. Then, we simulate the distribution of each sampled parameter. Therefore we

obtain 41 distributions for the model parameters, each one with an increasing number of data used (see Figure 1.6. In this case, the last distribution in Figure 1.6 is the same of the one in Figure 1.4.

Note that the second procedure provides interesting information; for example, it allows us to investigate which is the minimum amount of data necessary to have an accurate and informative distribution for model parameters. In other words we can control the amount of data necessary to correctly perform the learning phase for the model. Moreover, this procedure is particularly suitable to mimic a realistic eruption forecasting, since it uses only data available at a specific time to forecast what will happen in the next future.

As it is shown in Figure 1.4, the inferred slope parameter b of the GTPM equation (1.5) has a well defined distribution. First, we test the null hypothesis H_0:$b \leq 0$ and we reject it at 5% level of significance, stating that b has a distribution of values significantly greater than zero. Its numerical values are between 0 and 0.5, with mean $\overline{b} = 0.21$ and standard deviation $\overline{\sigma_b} = 0.10$. This means that GTPM works out for eruptive behavior at Kilauea Volcano. Moreover its numerical value less than one implies a non-linear relationship in equation (1.4) between interevent times and erupted volumes. Such non-linear relationship implies the possibility of having a non costant input rate in the magma storage system. Therefore, after a large erupted volume, we expect a shorter interevent time compared with a classic Time Predictable System where the magma input rate is assumed constant in time.

A possible explanation might be represented by an increment in the magma input rate from the depth to the shallow magma storage system after an eruption characterized by a large volume. This might be due to an additional pressure gradient inside the magma chamber ought to magma discharging process, because a large eruption drains the magma chamber and decreases the effective pressure inside it (see Aki & Ferrazzini, 2001). This reduction of pressure inside the magma storage system may trigger an increasing of magma buoyancy and, obviously, an increase of the magma input rate. In addition, Takada, 1999 shows, as a result of his deterministic model for dike migrations and stationing in the level of neutral buoyancy, the possibility to have a constant supply rate with oscillations or fluctuations beneath intraplate volcanoes (i.e. Mauna Loa and Kilauea volcanoes).

Another result is reported in Figure (1.4), where we show the distribution of intercept K in equation (1.5). In terms of its physical meaning, we can consider it as a gauge parameter

(see equation (1.4)) that links together two non-homogeneous quantities, i.e. interevent time and erupted volume. As it is shown in Figure 1.4, the mean and standard deviation of the parameter K are respectively $\overline{K} = 5.27$ and $\overline{\sigma_k} = 0.22$. The main result is that K has a proper finite distribution, that represents the appropriate dimensional constant for equation (1.4). The parameter K can also be seen as a function of the average recharge rate: in equation (1.5) $K = \ln \alpha$, where $\alpha = (c\hat{V}^b)/\hat{R}$, and $\alpha = r_i^*/v_i^{*b}$ from equation (1.4). So the dimensionless α parameter, or better the dimensional parameter c is function of the inverse average recharge rate. However, due to the fact that b is different from 1, the term v_i^b makes it difficult to compare physically $1/c$ with the average recharge rate at Kilauea volcano for the period 1923-1983.

The parameter σ_R^2 (see Figure 1.4) depends on the quantity $R_i - (bV_i + K)$ and it can be seen as a measure of the discrepancy between the simulated interevent times and the Time Predictable equation. This error is a measure of how close the BH_TPM model realizations for R and V fit the data (D_r and D_v) when the variables simulated are constrained by the data in the MCMC-Gibbs Sampling. In the process model distribution for interevent times (i.e. equation (1.6)) errors are additive on the logarithm. After an exponential transformation, this error becomes multiplicative respect to r_i. The median of the distribution in Figure 1.4 is 1.33, and so an error of about 4 times the relative interevent time comes out. Nevertheless we cannot consider σ_R^2 as a measure of goodness-of-fit for BH_TPM to the data; this aspect is discussed in the next subsection when we simulate and compare synthetic datasets with observational data. This feature of the model in reproducing data with relatively small errors is shown in Figure 1.5. The various panels in Figure 1.5 represent the simulated volumes and interevent times (blue stars), plotted together with the observed data (red plus) that are always within the simulated distributions.

As mentioned above, Figure 1.6 represents the distributions for model parameters b, K and σ_R^2 using the sampling *forward* procedure described above at the point 2. Those figures show the learning phase, before the dashed line, and the remaining part used to model checking and forecasting. We choose the first third part of the catalog, i.e first 14 events, as a learning phase; this means that we test the model on the remaining 27 events. We test again the null hypothesis H_0:$b \leq 0$ and we can reject it a 5% level of significance for all b distributions after the learning phase. The physical interpretation is the same as it was given before in describing

results obtained using all catalog.

In particular we want to point out that results in Figure 1.6 are important to understand the framework of the forward procedure to infer parameters distribution. This kind of sampling, i.e. adding one pair of data at a time, will be particularly useful when we make forecast for future interevent times (see below).

1.3.2 Model checking

The final goal is to check if the model is capable to reproduce satisfactorily the observed data. To this purpose, we follow the approach suggested by Gelman et al. (2000,161), and we compare the synthetic realizations given by BH_TPM with the real data via descriptive statistics. We choose this approach instead of the classical goodness-of-fit tests, because in this way we can control directly the possible model failures computing the discrepancy between the synthetic realizations (the so called posterior predictive distribution) and data. This is an easy task in Bayesian statistics, because it is always possible to simulate the quantities of interest from their posterior distribution.

In order to compare model realizations and data, we simulate a 10000 synthetic catalogs from BH_TPM. The first step is to draw a random volume V from the process equation (1.7) using its own mean μ_v and variance σ_v^2 already simulated via MCMC-Gibbs sampling using all data. The second step is to simulate an interevent time relative to the simulated volume V from equation (1.6), using the parameters b, K and σ_R^2 in Figure 1.4. We iterate this pattern to replicate the 41 pairs of interevent times and volumes, ending up with a new synthetic catalog. By replicating this scheme 10000 times, we obtain 10000 catalogs each one containing 41 events. The last step is to compare real catalog (41 observed interevent times) with the 10000 replicated by BH_TPM, using descriptive statistics. For both real and synthetic catalogs, we calculate the mean number of events (or mean rate of occurrence) λ, the maximum, the minimum, the median and the standard deviation of the interevent times.

The results are displayed in Figure (1.7), where we show the distributions for the above quantities both for the synthetic realizations (blue bars) and for the real data (red line in figure). The figures suggest that the model generates synthetic data that are reasonably in agreement with real data, even though with some important discrepancies. In particular, the model tends systematically to overestimate the maximum of R_i and, as a consequence, it tends

to underestimate the mean rate of occurrence. Owing to the overestimate of the maximum, the standard deviation is overestimated too. Besides, the minimum is underestimated. In spite of this lack-of-fit, however the median of the distribution shows a better agreement.

A possible explanation of these discrepancies may be linked to the use of log-normal distribution for inter-event times and volumes. This choice has been mostly adopted for technical reasons; in fact, the use of conjugate distributions (i.e. normal and inverse gamma distributions) for each level in data model, process model and parameters model, makes the calculations much easier. The log-normal distribution has a fat tail, so when we generate synthetic data by drawing independent samples from such distribution, we obtain large values (both for volumes and interevent times). In this way, in each catalog generated, there is at least a synthetic eruption with unreasonably large erupted volume. Consequently, there is systematically at least one very large interevent time, implying an overestimate of the maximum. An analogous problem arises for the minimum. We attribute the lack-of-fit for the minimum again to the tail behavior of the log-normal distribution close to zero. Likely, the log-normal is not the optimal choice to capture the behavior of the extreme values of the data in Table 1.1. Further developments of the model will drop the assumption of conjugacy in order to improve the model. For now, we argue that these discrepancies do not affect the conclusions about the existence of a time predictable model behind the eruption process. Most important, as we will see in the next section, they do not affect too much the forecasting performances of the model.

1.3.3 Forecasts

The last check on the reliability of the model consists of comparing the forecasting performances of BH_TPM against others model already present in literature. We endeavor to compare the forecast capability of BH_TPM with those of a Poisson model (Klein, 1982), Log-Normal model (Bebbington & Lai, 1996b) and Generalized Time Predictable Model (GTPM) (Sandri *et al.*, 2005). The test mainly consists of calculating the gain in probability of BH_TPM with respect to the cited models, under the framework of a probabilistic forecast made on the observed data.

The homogeneous Poisson model is a totally random and memoryless model and it is the simplest model to describe the eruptive process (e.g., Klein, 1982; Marzocchi, 1996).

If the events follow a Poisson distribution, then the interevent times follow an exponential distribution (see Klein 1982; Mulargia *et al.* 1985; Bebbington & Lai 1996a).

A Log-Normal model has been proposed by Bebbington & Lai (1996b) as a best fit distribution for Kilauea data. According to those authors, a log-normal distribution should take into account the possible eruption cyclicity at Kilauea volcano. The authors test interevent time distribution at Kilauea volcano on "all" data available (i.e. period 1823 to 1977 AD) trying different possible distributions. The best fit is given by a log-normal one. At the same time, the authors also state that the hypothesis of an exponential interevent time distribution (Poisson process) can not be rejected when focusing only on data from 1918 to 1977 AD. This latter results is in agreement with Klein (1982). This may mean that for our dataset (only eruption form 1923 to 1983, see Table 1.1) a Poisson model could be preferred. Nevertheless, we compare our model both with Poisson and Log-Normal models.

The GTPM proposed by Sandri *et al.* (2005) is substantially the non-hierarchical version of the present model (i.e. BH_TPM). Those authors have applied a regression analysis on the logarithm of the interevent time and volume data at Mount Etna volcano, finding a time predictability for this volcano. However, in that model there is no possibility to use the information given by the volume errors; volume data in GTPM are assumed to be affected only by the scatter around the regression line. Here, we also compare BH_TPM to GTPM. In this way we point out some justifications for our choice of introducing a hierarchy to better capture the time predictable behavior, which in turn is mainly due to the necessity of accounting for the volume errors.

To this purpose, following the scheme proposed in seismology by Kagan & Knopoff (1997), we calculate the probability gain of BH_TPM versus Poisson, and Log-Normal and GTPM models as the difference between the log-likelihood of the two models. Because of the complexity of BH_TPM, we do not have a classical analytical likelihood function, but equation (1.6) contains the sample information and the process information, therefore we consider this equation as the likelihood of our model. The probability gain is calculated over the data following the learning phase (see Figure 1.6). For each of these eruptions, we calculate the probability of having an event in a time window of one month around the observed interevent time. For the BH_TPM such probability is obtained by equation (1.6) with the observed volume datum and parameters estimated from the previous data. For example, in forecasting

the $20th$ interevent time,we use the volume erupted in event number 20 in the catalog and the parameters inferred from the first 19 events. For the other models, we use the likelihood function to calculate the probability in the same one month time window around observed data.

For sake of clarity, this procedure deserves further explanation. To calculate the probability for BH_TPM we first simulate 10000 interevent times from the posterior predictive distribution, then we calculate the empirical cumulative distribution function for the simulated interevent times and finally we calculate the probability from the empirical distributions. For Poisson, and Log-Normal models, we instead use the analytical cumulative distribution function. We fit the parameters of those distributions via Maximum Likelihood Estimation using the same *forward* procedure used for BH_TPM. For GTPM we first calculate the regression line following the *forward* procedure described above, then we forecast the interevent time using the regression parameters and the volume datum. The probability here is calculated from the cumulative normal distribution on the logarithm of the data with mean equal to the log-interevent time forecasted and variance equal to the residual mean sum of square. Probability is always calculated as the difference in the one month time window around the observed interevent time.

The results are displayed in Figure (1.8), where we show the probability gain for each event (the so called "punctual probability gain"), and its total value obtained summing up all punctual probability gains. If the probability gain is greater than zero, our model makes better forecast than others. Figure (1.8) shows that not all the punctual probability gains are positive, although the total probability gain is positive for all tests. In particular, BH_TPM does better forecast than all the other models we tested. Our choice of introducing this kind of hierarchy is corroborated by the highest probability gain value which is obtained against GTPM. In order to check if there are some systematic co-variation between the punctual probability gain and the interevent times, we check a possible correlation between these two quantities. We show only for the probability gain against the Poisson process, because this model represents a totally random and memoryless eruptive behavior for Kilauea. Comparison with a Poisson model allows us to speculate on the physical processes possibly involved in the eruption dynamics.

Figure 1.9 shows the relationship between interevent times and punctual probability gains.

The inverse linear relationship (the slope is significantly less than zero, P-value$\leq$ 0.01) means that, for very long interevent times, BH_TPM performs worse than Poisson model. Performing the same analysis for the punctual probability gain against the Log-Normal model, it shows a weaker but still significant, inverse relationship. The slope is less than zero with P-value=0.0125.

There are different possible explanations for the inverse linear relationship: 1) for long interevent times, Kilauea volcano becomes memoryless in its eruptive behavior (see Marzocchi & Zaccarelli, 2006); 2) our assumption on the time predictable model as a dynamic eruptive behavior is too simple to describe events with long repose time; 3) the assumption used to consider eruption as a point event in time without taking into account the eruption duration may become distorting for the model forecast purposes (see Bebbington, 2008); 4)with BH_TPM at Kilauea, we neglect magma intrusions not followed by an eruption (Takada, 1999, Dvorak & Dzurisin, 1993); 5) also we neglect possible changes in magma chamber geometry after an eruption (see Gudmundsson, 1986). Further explanations could be derived focusing on the volumes instead of the interevent times. The volume erupted may change the physical and chemical conditions of the magma chamber and the magma conduit. However performing the same regression analysis as in Figure 1.9, but for the volumes instead of interevent times, it does not provide any significative correlation.

1.4 Conclusions

In this work we have developed a time predictable model embedded in a hierarchical Bayesian structure (BH_TPM), to describe the behavior of eruptive catalog of open conduit volcanoes. The use of a Bayesian structure allows to explicitly and formally include in the analysis any kind of uncertainty (relative to data, models, and parameters). We have applied the model to Kilauea eruptive catalog from 1923 to 1983 AD. The results show that interevent times depend on the previous erupted volume, as in a generalized time predictable model (Sandri *et al.* 2005; Marzocchi & Zaccarelli 2006). The model shows a reasonable fit with the data observed at Kilauea volcano, although it is not able to capture all the features and variability of the real catalog. We find also that the Kilauea volcano has a weak time predictable eruptive behavior; likely this model could work better when applied to other "open" conduit volcanoes. However, these discrepancies do not seem to affect the forecasting capability of BH_TPM, that remains

superior to the forecasting capability of a stationary Poisson model, a Log-Normal model and Generalized Time Predicable Model. We suggest that the present model could be included in a long-term Probabilistic Volcanic Hazard Assessment as a basic component for modelling the occurrence of eruptions in time at Kilauea Volcano.

Bibliography

[1] Aki, K. & Ferrazzini, V., 2001. Comparison of Mount Etna, Kilauea, and Piton de la Fournaise by a quantitative modeling of their eruption histories, *J. Geophyis. Res.*, 106, B3, 4091–4102.

[2] Anderson, T. W. and Darling, D. A. 1952. Asymptotic theory of certain 'goodness-of-fit' criteria based on stochastic processes. *Annals of Mathematical Statistics*, 23:193-212.

[3] Bebbington M.S., Lai C. D. 1996a. Statistical analysis of New Zealand volcanic occurrence data, *J. Volcanol. Geotherm. Res.*, 74, 101–110.

[4] Bebbington M.S., Lai C. D. 1996b. On nonhomogeneous models for volcanic eruptions, *Math. Geology*, 28,5, 585–600.

[5] Bebbington M.S., 2007. Identifying volcanic regimes using Hidden Markov Models. *Geophys. J. Int.* 171, 921-941.

[6] Bebbington M, 2008. Incorporating the eruptive history in a stochastic model for volcanic eruptions. *J. Volcanol. Geotherm. Res.* 175, 325-333.

[7] Behncke, B., Neri, M., Nagay, A., 2005. Lava flow hazard at Mount Etna (Italy): new data from GIS-based study, in *Kinematics and dynamics of lava flow*, Manga, M., and Ventura, G., eds, Geological Society of America, Special Paper 396, 189-208,doi:10.1130/2005.2396(13).

[8] Burt M.L., Wadge G. & Scott W.A., 1994. Simple stochastic modelling of eruption history of basaltic volcano: Nyamuragira, Zaire, *Bull. Volcanol.*, 56, 87–97.

[9] De la Cruz-Reyna S., 1991. Poisson-distributed patterns of explosive eruptive activity, *Bull. Volcanol.*, 54, 57–67

[10] Dvorak, J.J., & Dzurisin, D., 1993. Variations in magma-supply rate at Kilauea volcano, Hawaii, *J. Geophys. Res.*, 98, 22255-22268.

[11] Gelman A., Carlin J.B., Stern H.S. & Rubin D.B.,2000. *Bayesian Data Analysis*,1st edn, Chapman & Hall/CRC,Boca Raton-Florida.

[12] Gilks W.R., Richardson S. & Spiegelhalter D.J., 1996. *Markov chain Monte Carlo in practice*, 2nd edn, Chapman & Hall, London.

[13] Gudmundsson A, 1986. Possible effect of aspect ratios of magma chambers on eruption frequency. *Geology* 14, 991-994.

[14] Kagan Y.Y. & Knopoff L., 1987. Statistical Short-Term Earthquake Prediction, *Science*, 236(4808), 1563–1567

[15] Klein F.W.,1982 Patterns of historical eruptions at Hawaiian Volcanoes, *J. Volcanol. Geotherm. Res.*, 12 , 1–35

[16] Marzocchi W.,1996. Chaos and stocasticity in volcanic eruptions the case of Mount Etna and Vesuvius, *J. Volcanol. Geotherm. Res.*,70, 205-212.

[17] Marzocchi, W., Sandri, L., Gasparini, P., Newhall, C. G., Boschi, E., 2004. Quantifying probabilities of volcanic events: the example of volcanic hazard at Mt. Vesuvius. *J. Geophys. Res.*, 109, B11201, doi:10.1029/2004JB003155.

[18] Marzocchi W., Sandri L. & Selva J.,2008. BET_EF: a probabilistic tool for long- and short-term eruption forecasting, *Bull. Volcanol.*, 70, 623–632

[19] Marzocchi W. & Zaccarelli L.,2006. A quantitative model for the time size distribution of eruptions, *J. Geophys. Res.*, 111, doi:10.1029/2005JB003709.

[20] Mulargia F.,Tinti S. & Boschi E.,1985. A statistical analysis of flank eruptions on Etna Volcano, *J Volcanol Geotherm Res*, 23, 263–272.

[21] Newhall C.G. & Hoblitt,R.P., 2002. Constructing event trees for volcanic crises, *Bull. Volcanol.*, 64, 3–20.

[22] Sandri L., Marzocchi W. & Gasperini P., 2005. Some inside on the occurrence of recent volcanic eruptions of Mount Etna volcano (Sicily,Italy), *J. Geophys. Res.*, 163, 1203–1218.

[23] Sparks, R.S.J., 2003. Forecasting volcanic eruptions,*Earth Planet. Sci. Lett.*, 210, 1–15.

[24] Takada, A., 1999. Variations in magma supply and magma partitioning: the role of the tectonic settings, *J. Volcanol. Geotherm. Res.*, 93, 93–110.

[25] Trujillo-Ortiz, A., Hernandez-Walls, R., Barba-Rojo, K. and Castro-Perez, A., 2007. AnDartest:Anderson-Darling test for assessing normality of a sample data. A MATLAB file. [WWW document]. http://www.mathworks.com/matlabcentral/fileexchange/loadFile.do?objectId=14807

[26] Wikle C. K.,2003. Hierarchical Models in Environmental Science, *Internat. Statist. Rev.*, 71-2, 181–199.

Eruption #	**Onset** yyyymmdd	**Interevent time** [days]	**Volume** lava e tephra $[10^6 m^3]$
1	1923 08 25	259	0.073
2	1924 05 10	70	0.79
3	1924 07 19	1083	0.234
4	1927 07 07	594	2.30
5	1929 02 20	155	1.40
6	1929 07 25	482	2.60
7	1930 11 19	399	6.20
8	1931 12 23	988	7.00
9	1934 09 06	6504	6.90
10	1952 06 27	703	46.70
11	1954 05 31	273	6.20
12	1955 02 28	1720	87.60
13	1959 11 14	60	37.20
14	1960 01 13	408	113.20
15	1961 02 24	7	0.022
16	1961 03 03	129	0.26
17	1961 07 10	74	12.60
18	1961 09 22	441	2.20
19	1962 12 07	257	0.31
20	1963 08 21	45	0.80
21	1963 10 05	517	6.60
22	1965 03 05	294	16.80
23	1965 12 24	681	0.85
24	1967 12 05	291	80.30
25	1968 08 22	46	0.13
26	1968 10 07	138	6.60
27	1969 02 22	91	16.10
28	1969 05 24	812	185.00

Eruption #	**Onset** yyyymmdd	**Interevent time** [days]	**Volume** lava e tephra $[10^6 m^3]$
29	1971 08 14	41	9.10
30	1971 09 24	132	7.70
31	1972 02 03	457	162.00
32	1973 05 05	189	1.20
33	1973 11 10	251	2.70
34	1974 07 19	62	6.60
35	1974 09 19	103	10.20
36	1974 12 31	333	14.30
37	1975 11 29	654	0.22
38	1977 09 13	794	32.90
39	1979 11 16	896	0.58
40	1982 04 30	148	0.50
41	1982 09 25	100	3.00
42	1983 01 03		ongoing

Table 1.1: Catalog of eruptive events at Kilauea volcano

Data Model	**Process Model**	**Parameter Model**
$D_{r_i} \sim N(R_i, \sigma^2_{Dr_i})$	$R_i \sim N(bV_i + K, \sigma^2_R)$	$b \sim N(\mu_b, \sigma^2_b)$
$D_{v_i} \sim N(V_i, \sigma^2_{Dv_i})$	$V_i \sim N(\mu_v, \sigma^2_v)$	$K \sim N(\mu_K, \sigma^2_K)$
$\sigma^2_{Dv_i}$ = known	$\mu_v \sim U(-\infty, +\infty)$ *	$\mu_b \sim U(-\infty, +\infty)$ *
$\sigma^2_{Dr_i}$ = known	$\sigma^2_R \sim \Gamma^{-1}(\alpha_{\sigma_R}, \beta_{\sigma_R})$*	$\mu_K \sim U(0, +\infty)$*
	$\sigma^2_V \sim \Gamma^{-1}(\alpha_{\sigma_V}, \beta_{\sigma_V})$*	$\sigma^2_b \sim \Gamma^{-1}(\alpha_{\sigma_b}, \beta_{\sigma_b})$*
		$\sigma^2_K \sim \Gamma^{-1}(\alpha_{\sigma_K}, \beta_{\sigma_K})$*

Table 1.2: Overview of distributions used in BH_TPM. The distributions highlighted with * are prior distributions for the BH_TPM. The prior distribution parameters for inverse gamma's (i.e. Γ^{-1}) are taken equal to 1. U means uniform distribution.

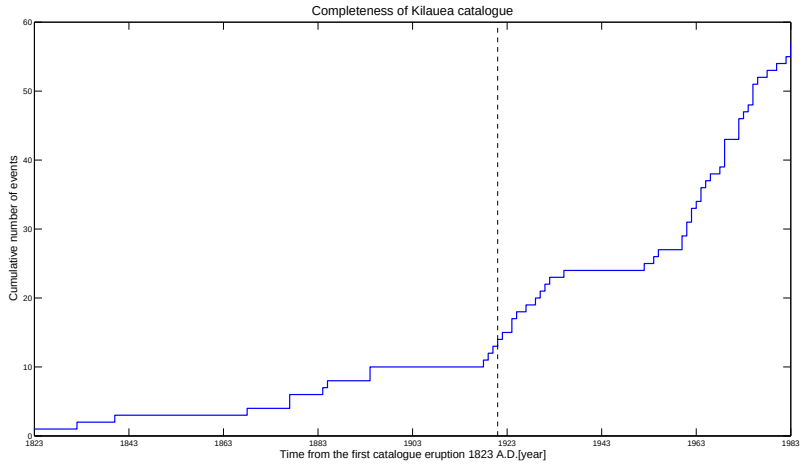

Figure 1.1: *Plot of the cumulative number of eruptive events listed in Kilauea catalog. On the right side of the dashed line there are the events that have been used in BH_TPM. This plot shows that the catalog is complete from 1918, but we have taken only eruptions from 1923 because 1919 and 1922 eruptions have missing volume data.*

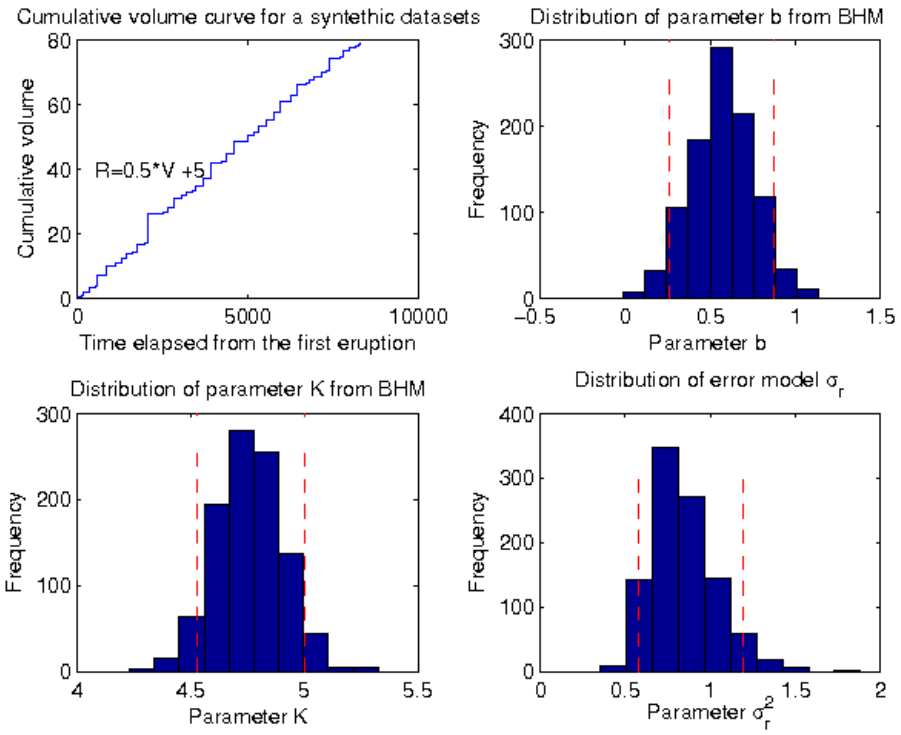

Figure 1.2: *Posterior distributions of relevant parameters of BH_ TPM using a synthetic catalog with b=0.5. The first plot on the left represents the synthetic data sets (i.e. volumes and interevent times); the other sub-plots show the parameters inferred by BH_ TPM. For more information see the text.*

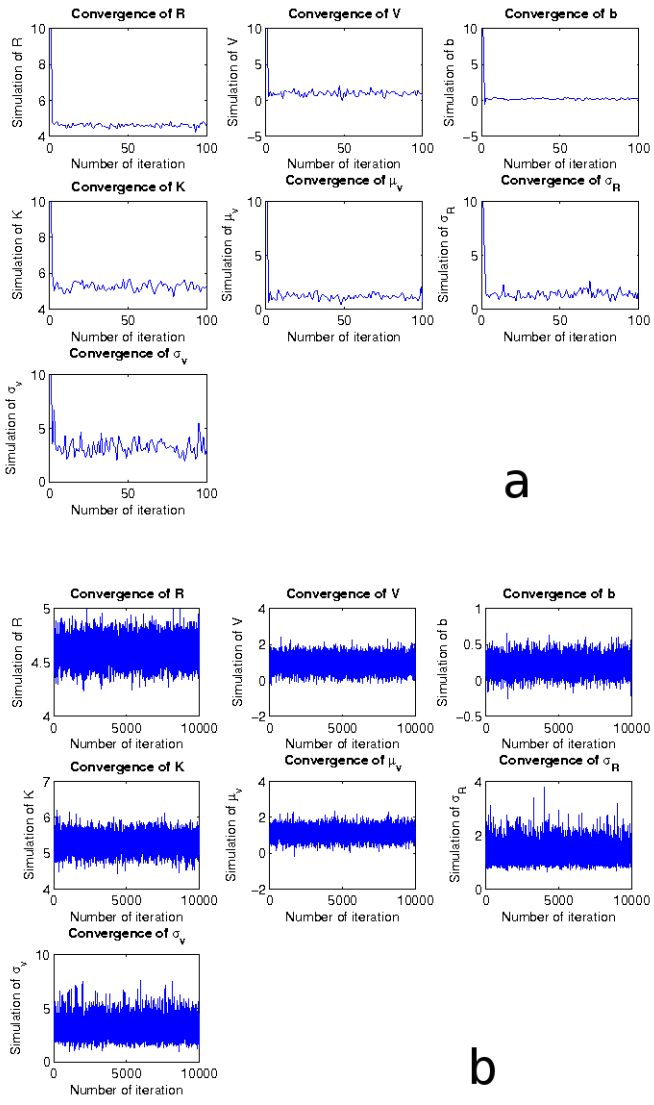

Figure 1.3: *Constructed Markov Chains for each variable and parameter of the BH_ TPM. For R and V we show just one of the 41 chains relative to each variable. In panel* ***a****, each chain (i.e. each subplot) reaches the convergence after few iterations, forgetting the initial guess very quickly. In this case the starting values is chosen to be 10 for all quantities. Iterations in panel* ***a*** *represent only the first 100 iteration of the burn-in phase, for more details please refer to the text. The remaining iterations (i.e. from 1001 to 10000), shown in* ***b*** *panel, represent the conditional posterior distributions for BH_ TPM variables and parameters.*

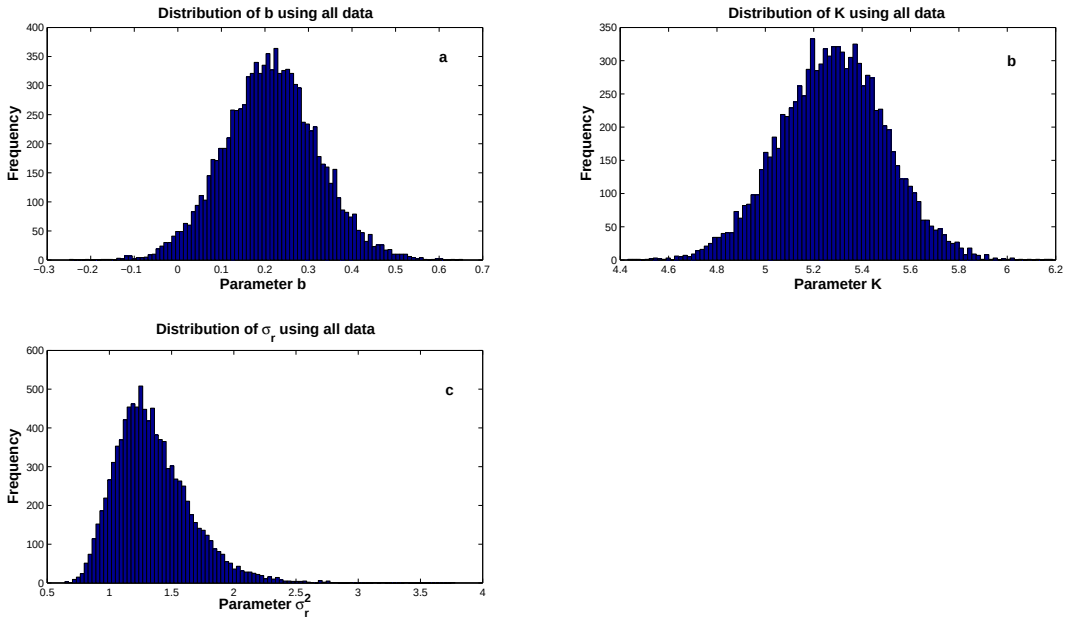

Figure 1.4: *Posterior distribution for relevant parameters simulated using all data in catalog. In panel* ***a*** *it is shown the posterior distribution of parameter b; in panel* ***b*** *the posterior distribution for parameter K and in panel* ***c*** *the posterior distribution for parameter σ_R^2.*

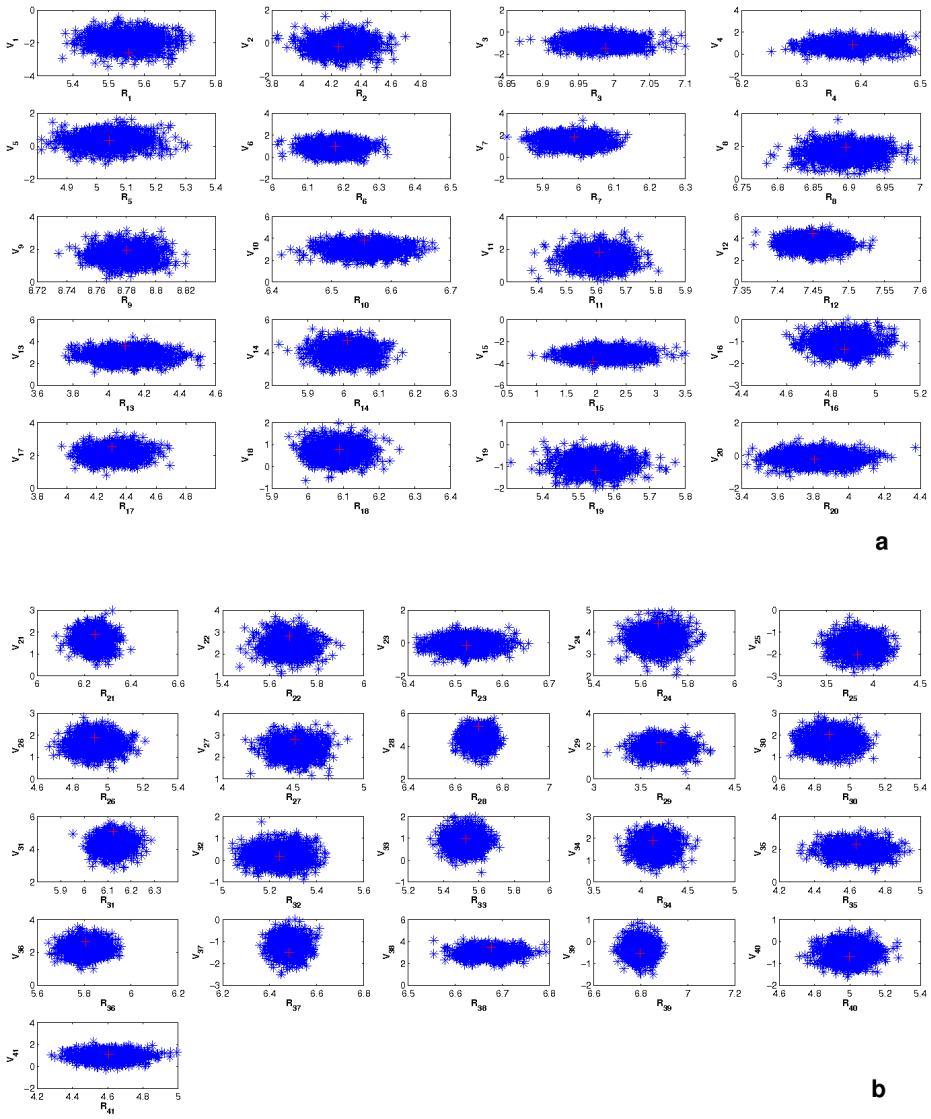

Figure 1.5: *Blue stars show the posterior distributions of pairs of simulated variables (interevent times R_i and volumes V_i). These variables are simulated via MCMC-Gibbs sampling using all data in the catalog. Panel* **a** *is relative to R_i and V_i from 1 to 20 and panel* **b** *from 21 to 41. Red plus is the observed data.*

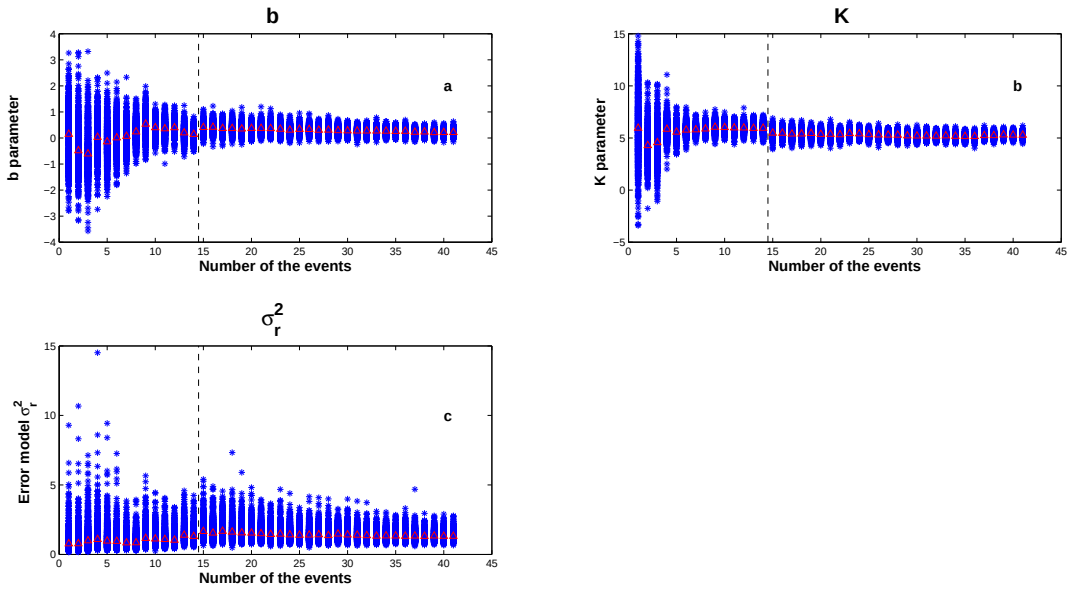

Figure 1.6: *Posterior distributions of: b parameter in panel* **a**, *K parameter in panel* **b** *and* σ_r^2 *in panel* **c**, *all calculated using the forward procedure discussed in the text. Black dashed line represents the learning phase. Red triangles are the mean of the distributions for b and K and the median for* σ_r^2

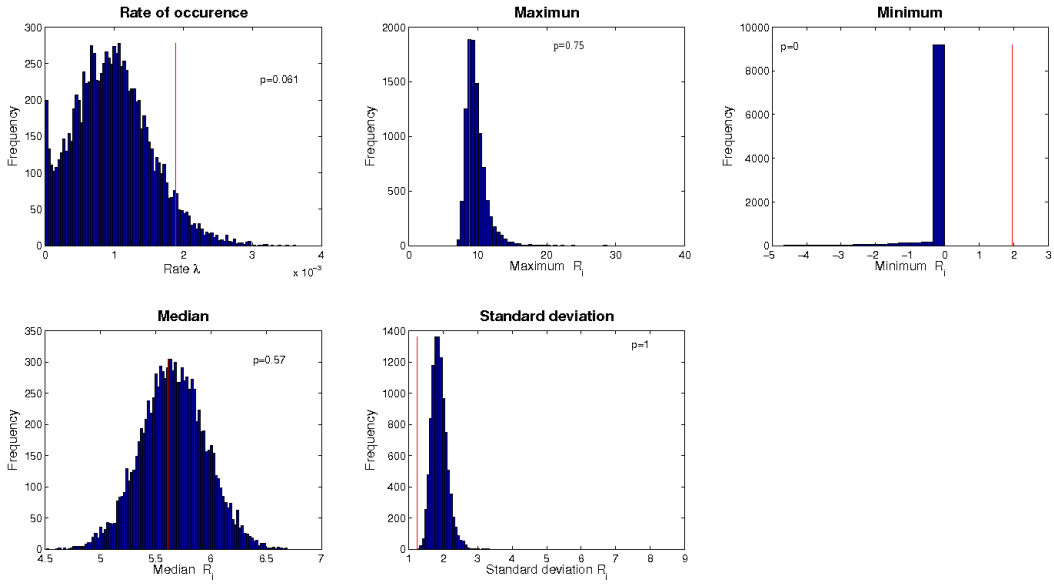

Figure 1.7: *Distributions of synthetic interevent times (blue bars) compared with observed values (red line) using descriptive statistic. This goodness-of-fit test (for more detail see the text) shows that our BH_ TPM predicts unreasonably long and short interevent times for Kilauea volcano.*

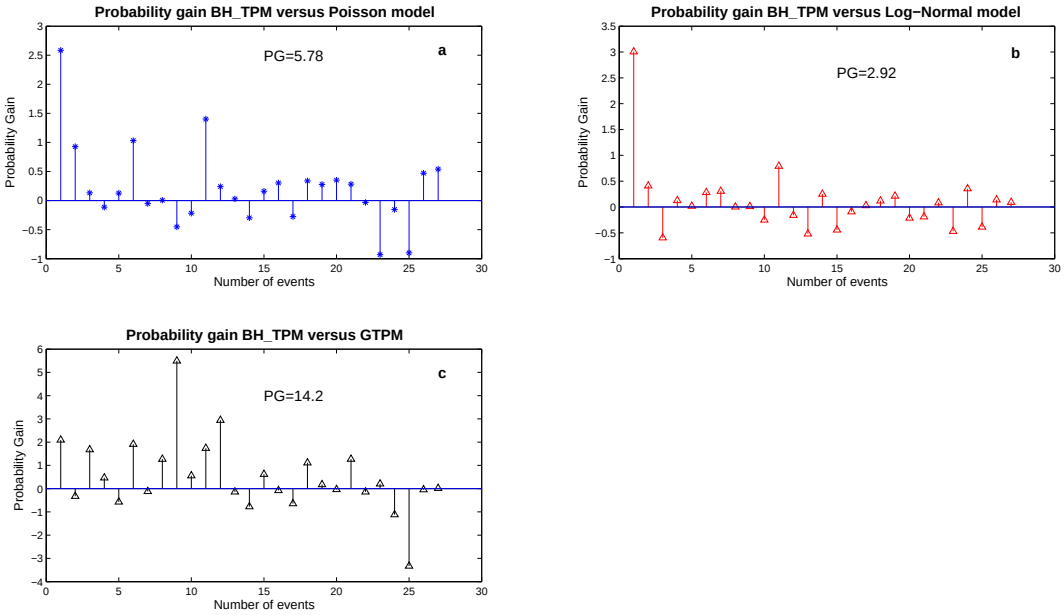

Figure 1.8: *"Punctual probability gain" of the BH_ TPM for each event after the learning phase against: in panel* ***a*** *Poisson Model (Klein, 1982), in panel* ***b*** *Log-Normal Model (Bebbington & Lai, 1996b) and in panel* ***c*** *Generalized Time Predictable Model (Sandri et al., 2005). Values greater than zero indicate when BH_ TPM model performs better forecast than the reference models. The inset in each panel is the total Probability gain, i.e. the sum of the punctual probability gains.*

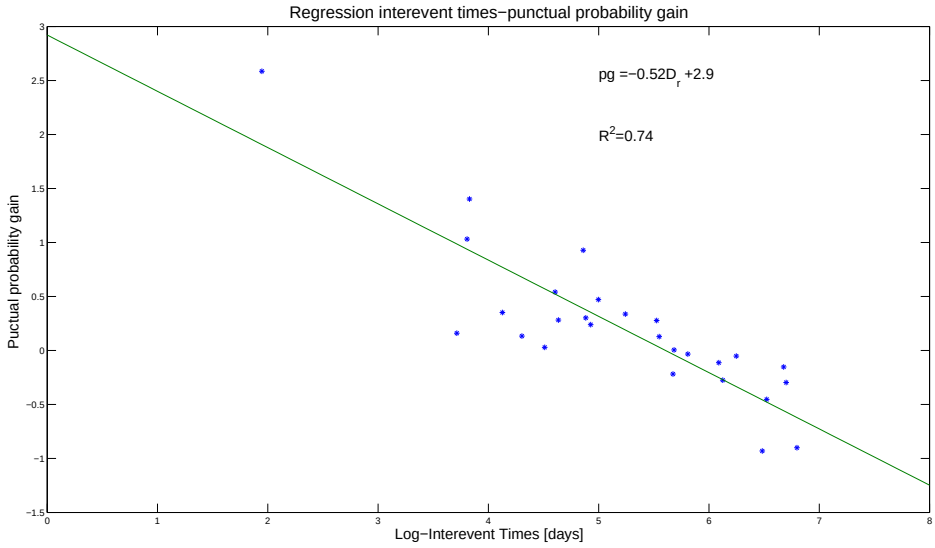

Figure 1.9: *Regression analysis for BH_ TPM "punctual probability gain" against Poisson Model versus observed interevent times. The significant inverse linear relationship, whose best fit regression coefficients and* R^2 *are given, indicates a systematic negative probability gain for long interevent times. As discussed in the text, this means an additional complexity for long interevent times compared to the time predictable eruptive behavior. This causes a worse ability of our BH_ TPM, compared to Poisson model, to forecast long interevent times.*

Chapter 2

A new Bayesian Time-Predictable Model for Open Conduit Volcanoes: The Case of Mt Etna and Kilauea

Abstract

One of the main goals in volcanology is to forecast volcanic eruptions. A trenchant forecast should be made before the onset of a volcanic eruption, using the data available at that time, with the aim of mitigating the volcanic risk associated to the volcanic event. In other words, models implemented with forecast purposes have to take into account the possibility to provide "forward" forecasts and should avoid the idea of a merely "retrospective" fitting of the data available. In this perspective, the main idea of the present model is to forecast the next volcanic eruption after the end of the last one, using only the data available at that time. We focus our attention on volcanoes with open conduit regime and high eruption frequency. We assume a generalization of the classical time predictable model to describe the eruptive behavior of open conduit volcanoes and we use a Bayesian hierarchical model to make probabilistic forecast. We apply the model to Kilauea volcano eruptive data and Mount Etna volcano flank eruption data.

The aims of this model are: 1) to test whether or not the Kilauea and Mount Etna volcanoes follow a time predictable behavior; 2) to discuss the volcanological implications of the time predictable model parameters inferred; 3) to compare the forecast capabilities of this

model with other models present in literature. The results obtained using the MCMC sampling algorithm show that both volcanoes follow a time predictable behavior. The numerical values inferred for the parameters of the time predictable model suggest that the amount of the erupted volume could change the dynamics of the magma chamber refilling process during the repose period. The probability gain of this model compared with other models already present in literature is appreciably greater than zero. This means that our model provides better forecast than previous models and it could be used in a probabilistic volcanic hazard assessment scheme.

Keywords. Effusive volcanism, Bayesian modeling, Mount Etna, Kilauea, Probabilistic forecasting, Volcanic hazards and risks.

2.1 Introduction

One of the main goals in modern volcanology is to provide reliable forecast of volcanic eruptions with the aim of mitigating the risk associated with. The extreme complexity and non linearity of a volcanic system make deterministic prediction of the evolution of volcanic processes rather impossible (e.g. Marzocchi 1996; Sparks 2003). Volcanic systems are intrinsically stochastic. In general, eruption forecasting involves two different time scales: i) a *short-term* forecasting, mostly based on monitoring measures observed during an episode of unrest (e.g., Newhall & Hoblitt 2002, Marzocchi *et al.* 2008 among others); ii) a *long-term* forecasting, usually made during a quiet period of the volcano, and mostly related to a statistical description of the past eruptive catalogs (e.g. Klein, 1982, Bebbington, 1996a among others). Here, we focus our attention only on this second issue. An incisive and useful forecast should be made before the onset of a volcanic eruption, using the data available at that time, with the aim of mitigating the volcanic risk associated. In other words, models implemented with forecast purposes have to take into account the possibility to provide "forward" forecasts and should avoid the idea of a merely "retrospective" fitting of the data available.

Different methods have been presented in the past years aiming at the identification of possible recurrence or correlation in the volcanic time and/or volume data for long-term eruption forecast. Klein (1982), Bebbington & Lai (1996a and 1996b) and Mulargia et al (1985) studied the time series of volcanic events looking at the mean rate of occurrence. Sandri *et al.* (2005) applied a generalized form of time predictable model to Mount Etna eruptions using regression

analysis. Marzocchi & Zaccarelli (2006) found different behavior for volcanoes with "open" conduit regime compared to those with "closed" conduit regime. Open conduit volcanoes (Mt Etna, Kilauea volcano there tested) seem to follow a so-called *Time Predictable Model*. While closed conduit volcanoes seem to follow a homogeneous Poisson process. De La Cruz-Reyna (1991) proposed a load-and-discharge model for eruptions in which the time predictable model could be seen as a particular case. Bebbington (2008) presented a stochastic version of the general load-and-discharge model also including a way to take into account of the history of the volcano discharging behavior. In this paper the author studied the time predictability as a particular case of his model with application to Mount Etna and Mauna Loa 3and Kilauea data series. A different hierarchical approach has been presented by Bebbington (2007) using Hidden Markov Model to study eruption occurrences with application to Mount Etna flank eruptions. This model is able to find any possible underlying volcano activity resulting in changes of the volcanic regime. Salvi *et al* (2006) carried out analysis for Mt Etna flank eruption using an Non Homogeneous Poisson process with a power law intensity, while Smethurst *et al* (2009) applied a Non Homogeneous Poisson process with a piecewise linear intensity to Mt Etna flank eruptions

In a recent paper Passarelli *et al* (2010) (in Chapter 1) proposed a Bayesian Hierarchical Model for interevent time-volumes distribution using the time predictable process with application to Kilauea volcano. The model presents a new Bayesian methodology for an open conduit volcano that allows to take into account uncertainties in observed data. Besides, the authors present and test the forecast ability of the model retrospectively on the data through a forward sequential procedure. While the model seems to perform better forecast compared with others model in literature, it produced fits to eruption volumes and interevent times that were too large and this reduces the forecast performances. This is due to the use of normal distributions for the log-transformed data. This is a restrictive distributional assumption that creates very long tails. Here we propose a more general modeling strategy that allows for more flexible distributions for the interevent times and volumes data.

Using the same framework of Passarelli et al (2010), we will model the interevent times and volumes data through distributions with exponential decay (Klein, 1982, Mulargia, 1985, Marzocchi, 1996, Bebbington, 1996a, 1996b and 2007, Salvi *et al*, 2006, Smethurst *et al*, 2009). This provide a general treatment of the volume and interevent time series, hopefully

improving the forecast capability of the model. As a eruptive behavior we use the Generalized Time Predictable Model (Sandri et al, 2005 and Marzocchi & Zaccarelli, 2006). This model assumes: 1) eruptions occur when the volume of magma in the storage system reaches a threshold value, 2) magma recharging rate of the shallow magma reservoir could be variable and 3) the size of eruptions is a random variable, following some kind of statistical distribution. Under these assumptions, the time to the next eruption is determined by the time required for the magma entering the storage system to reach the eruptive threshold. The more general form for a time-predictable model is a power law between the erupted volume and the interevent time:

$$r_i = cv_i^b \tag{2.1}$$

where, if the parameter b is equal to unity we are in a classical time predictable system (see De La Cruz Reyna 1991, Burt *et al.* 1994). If b is equal to 0 the system is not time predictable. If $b > 1$ or $0 < b < 1$ we have a non-linear relationship implying a longer or shorter interevent time after a large volume eruption compared to a classical time predictable system. The goal of the present work is to infer the parameters of Generalized Time Predictable equation (2.1).

In the remainder part of the paper, we focus our attention on some specific issues: 1) to discuss the physical meaning and implications of parameters inferred; 2) to verify if the model describes the data satisfactorily; 3) to compare the forecasting capability of the present model with other models previously published in literature using the sequential forward procedure discussed in Passarelli *et al* (2010) (see section 1.3 in Chapter 1). In the first part of this paper, we will introduce the generality of the model by considering three stages: 1) a model for the observed data; 2) a model for the process and 3) a model for the parameters (Wikle, 2003). Then we will discuss how: 1) to simulate the variables and parameters of the model, 2) to check the model fit, 3) to use the model to assess probabilistic forecast in comparison with other statistical published models. The last part of the paper contains the application of the model to Kilauea volcano and Mount Etna eruptive data.

2.2 A Bayesian Hierarchical Model for Time-Predictability

In the following sections we present a detailed description of our proposed model. We will denote it as Bayesian Hierarchical Time Predictable Model II (BH_TPM II), while the model

proposed in Passarelli *et al* (2010) will be denoted as BH_TPM. In Section 2.2.1 we discuss the modeling the measurement errors. In Section 2.2.2 we consider a model for the underlying process (equation (2.1)), which is based on the exponential distribution. In Section 2.2.3 we discuss the distributions that are placed on the parameters that control the previous two stages of the model. In Section 2.2.4 we introduce the simulation procedure and in Section 2.2.5 we consider model assessment and forecasting of volcanic eruptions.

2.2.1 Data Model

The dataset for this model has n observations with two components: erupted volumes and interevent times. We will denote the volumes as d_{v_i} and the interevent times as d_{r_i}. We assume independence between the measurement errors of interevent times and volumes. This is justified by the fact that these two quantities are measured using separate procedures. Dependence between interevent times and volumes will be handled at the process stage, following the power law in (2.1). In addition, we assume that, conditional on the process parameters, the interevent times or volumes are independent within their group. This is a natural assumption within a hierarchical model framework. It is equivalent to assuming that the volumes (times) are exchangeable between them. Exchangeability implies that all permutations of the array of volumes (times) will have the same joint distribution. Exchangeability is weaker than independence, and it is implied by it.

Our measurement error model assumes a multiplicative error for the observations. This follows from BH_TPM where it was assumed that

$$\log(d_{r_i}) = \log r_i + \log \epsilon_{r_i} \tag{2.2}$$

with $\log \epsilon_{r_i} \sim N(0, \sigma^2_{D_{r_i}})$ where $\sigma^2_{D_{r_i}} = (\frac{\Delta d_{r_i}}{d_{r_i}})^2$ (Passarelli *et al* 2010, data model in Chapter 1). The analogous assumption $\log(d_{v_i}) = \log v_i + \log \epsilon_{v_i}$ and $\log \epsilon_{v_i} \sim N(0, \sigma^2_{D_{v_i}})$ where $\sigma^2_{D_{v_i}} = (\frac{\Delta d_{v_i}}{d_{v_i}})^2$, was considered for the volumes. Exponentiating on both sides of Equation (2.2) we have

$$d_{r_i} = \epsilon_{r_i} r_i \tag{2.3}$$

which is the data stage model we propose in BH_TPM II.

The error in Equation (2.3) follows a probability distribution with positive support. We choose an inverse gamma distribution. This is a flexible distribution defined by two parameters

which will provide computational advantages. We fix the two defining parameters by assuming $\mathrm{E}(\epsilon_{r_i}) = 1$ and calculating $\mathrm{var}(\epsilon_{r_i})$ using a delta method approximation. Specifically, from the assumption that $\log \epsilon_{r_i} \sim N(0, \sigma^2_{D_{r_i}}))$, we have that $\mathrm{E}(\log \epsilon_{r_i}) = 0$ and $\mathrm{var}\,(\log \epsilon_{r_i}) = \sigma^2_{D_{r_i}} = (\frac{\Delta d_{r_i}}{d_{r_i}})^2$. Thus

$$\mathrm{var}\,(\epsilon_{r_i}) = \sigma^2_{D_{r_i}} \left[g' \left(\mathrm{E} \left(\frac{\Delta d_{r_i}}{d_{r_i}} \right) \right) \right]^2 = \left(\frac{\Delta d_{r_i}}{d_{r_i}} \right)^2$$

where $g(x) = \exp(x)$ and g' is the first derivative. At this point, remembering that a random variable X that follows an inverse gamma distribution with parameters α_{r_i} and β_{r_i} has expected value is $E(X) = \frac{\beta_{r_i}}{\alpha_{r_i}-1}$ and variance $\mathrm{var}(X) = \frac{\beta^2_{r_i}}{(\alpha_{r_i}-1)^2(\alpha_{r_i}-2)}$, we then have that

$$\begin{cases} \frac{\beta_{r_i}}{\alpha_{r_i}-1} = 1 \\ \frac{\beta^2_{r_i}}{(\alpha_{r_i}-1)^2(\alpha_{r_i}-2)} = \left(\frac{\Delta d_{r_i}}{d_{r_i}} \right)^2 \end{cases}.$$

Solving for α_{r_i} and β_{r_i} gives $\alpha_{r_i} = (\frac{d_{r_i}}{\Delta d_{r_i}})^2 + 2$ and $\beta_{r_i} = (\frac{d_{r_i}}{\Delta d_{r_i}})^2 + 1$ where $\frac{\Delta d_{r_i}}{d_{r_i}}$ is the relative error. Analogous calculations can be done for the volumes. The joint distributions for the measurement errors $\epsilon_r = (\epsilon_{r1}, \ldots, \epsilon_{r_n})$ and $\epsilon_v = (\epsilon_{v1}, \ldots, \epsilon_{v_n})$ result in

$$[\epsilon_r | \alpha_{r_i}, \beta_{r_i}] = \prod_{i=1}^{n} \Gamma^{-1}(\alpha_{r_i}, \beta_{r_i}) \quad \text{and} \quad [\epsilon_v | \alpha_{v_i}, \beta_{v_i}] = \prod_{i=1}^{n} \Gamma^{-1}(\alpha_{v_i}, \beta_{v_i}) \tag{2.4}$$

where $\alpha_{v_i} = \left(\frac{d_{v_i}}{\Delta d_{v_i}} \right)^2 + 2$ and $\beta_{v_i} = \left(\frac{d_{v_i}}{\Delta d_{v_i}} \right)^2 + 1$. We use $[X]$ to denote a distribution of random variable X and Γ^{-1} to denote an inverse gamma.

The distribution for the observed variables d_{r_i} and d_{v_i} can be obtained from the error distributions specified by the expression in (2.4). Noting that $\left| \frac{d\epsilon_{r_i}}{d(d_{r_i})} \right| = \frac{1}{r_i}$ we have from the change of variables formula for probability density functions that

$$[d_r | \alpha_{r_i}, \beta_{r_i}, r_i] = \prod_{i=1}^{n} \Gamma^{-1}(\alpha_{r_i}, \beta_{r_i} r_i) \quad \text{and} \quad [d_v | \alpha_{v_i}, \beta_{v_i}, v_i] = \prod_{i=1}^{n} \Gamma^{-1}(\alpha_{v_i}, \beta_{v_i} v_i). \tag{2.5}$$

The expression in (2.5) will be used to obtain the likelihood function for our data. For sake of clarity, assuming X is a random variable with continuous probability density function f. Suppose that $Y = r(X)$, where r is a differentiable function, then the change variables formula gives $g(y) = f(r^{-1}(y)) \mid d\, r^{-1}(y)/dy \mid$, where g is the probability density function of Y.

2.2.2 Process model

The starting point for the model pertaining the unobserved quantities r_i is the assumption that volcanic eruptions correspond to a homogeneous Poisson process. A homogeneous Poisson

process in times has the property that the number of events that occur during a given time interval follow a Poisson distribution with mean proportional to the length of the interval. Additionally the time between consecutive events is distributed as an exponential random variable (Klein, 1982, Mulargia, 1985, Marzocchi, 1996, Bebbington & Lai, 1996a, 1996b). Thus we assume that $r_i \sim \text{Exp}(\lambda)$ implying that the joint distribution of $r = (r_1, \ldots, r_n)$ is given by $[r|\lambda] = \prod_{i=1}^{n} \text{Exp}(\lambda)$. Given the distributional assumption for the interevent times we can obtain the distribution of the volumes v_i using Equation (2.1). Recalling that $r_i = cv_i^b$ and $\left|\frac{dr_i}{dv_i}\right| = cbv_i^{b-1}$. the change of variable formula for probability density functions yields $[v_i] = cb\lambda v_i^{b-1} \mathrm{e}^{-\lambda c v_i^b}$ Written in distributional form we have: $v_i \sim \text{Wb}\left(b, \left(\frac{1}{\lambda c}\right)^{\frac{1}{b}}\right)$ where $Wb(\cdot, \cdot)$ denotes a Weibull distribution. The joint distribution for the volumes $v = (v_1, \ldots, v_n)$ is given as

$$[v|\lambda, b, c] = \prod_{i=1}^{n} \text{Wb}\left(b, \left(\frac{1}{\lambda c}\right)^{\frac{1}{b}}\right). \tag{2.6}$$

This completes the specification of the second stage of our model.

2.2.3 Parameters model

To complete our model we need to specify distributions for the parameters b, c and λ. Our choices are based on prior information obtained from previous modeling efforts. In a Bayesian setting, like the one proposed in this work, we have the ability to include structural information, like the one used to build the second stage model, as well as prior information. The final product consists of the posterior distribution of all model parameters. This contains a blend of the information provided by all the stages of the model: data, process and prior knowledge.

We choose for λ a gamma distributions with known parameters, from now on hyperparameters. This is denoted as have: $\lambda \sim \text{Ga}(\alpha_\lambda, \beta_\lambda)$ where α_λ and β_λ are calculated by fitting the interevent times data with a gamma distribution, via maximum likelihood estimation. For the time predictable equation parameters, i.e. b and c, we use normal distributions with moments calculated using the posterior distributions taken from BH_TPM (Passarelli et al., 2010). Thus $[b] = \text{N}(\mu_b, \sigma_b^2)$ and $[c] = \text{N}(\mu_c, \sigma_c^2)$.

By choosing the values of the hyperparameters we are introducing a certain degree of subjectivity in our modeling. We believe that this is a desirable feature of the Bayesian approach, as it allows to incorporate knowledge from similarly behaved open conduit volcanoes. We remark the subjective approach allowed in Bayesian Statistics could be a suitable tool in

modeling geophysical phenomena where available data are scarce. This provides the possibility of incorporating knowledge obtained from other sources in a probabilistic way, through the prior distributions. This allows for the introduction of physical and/or statistical constraints, when available, on the parameters governing the examined phenomenon. In principle this methodology could be helpful to improve the understanding of a particular system. We want to point out, though, that subjective statistical modeling choices need careful justification, possibly relying on physical or phenomenological constraints.

2.2.4 Posterior and full conditional distributions

The three stage model specification developed in the previous sections produces a posterior distribution for the model parameters r, v, b, c and λ that, using Bayes theorem, can be written as

$$[r, v, b, c, \lambda | d_r, d_v \Delta d_r \Delta d_v] \propto \tag{2.7}$$
$$[d_r | \alpha_{d_r}, \beta_{d_r}, r][d_v | \alpha_{d_v}, \beta_{d_v}, v][v | c, \lambda, b][r|\lambda][\lambda][b][c] \quad .$$

To make inference about the posterior distribution specified by Equation (2.7) we draw samples from it using Monte Carlo Markov Chain (MCMC) methods (Gelman *et al*, 2000, Gilks *et al*, 1996). This requires the full conditional distributions for each parameter in the model. In the equations below we specify each of them using the notation $[X|\ldots]$ to indicate the distribution of variable X conditional on all other variables.

$$[r_i|\ldots] \propto r_i^{\alpha_{r_i}} \exp\left\{-r_i\left(\lambda + \frac{\beta_{r_i}}{d_{r_i}}\right)\right\} = \mathrm{Ga}\left(\alpha_r + 1\,,\, \lambda + \frac{\beta_r}{d_{r_i}}\right)$$

$$[v_i|\ldots] \propto v_i^{\alpha_{v_i}+b-1} \exp\left\{\left(\lambda c v_i^b + \frac{\beta_{v_i} v_i}{d_{v_i}}\right)\right\}$$

$$[\lambda|\ldots] \propto \lambda^{2n+\alpha_\lambda - 1} \exp\left\{-\lambda\left(\beta_\lambda + c\sum_{i=1}^{n} v_i^b + \sum_{i=1}^{n} r_i\right)\right\} =$$
$$\mathrm{Ga}\left(\alpha_\lambda + 2n\,,\, \beta_\lambda + c\sum_{i=1}^{n} v_i^b + \sum_{i=1}^{n} r_i\right)$$

$$[c|\ldots] \propto c^n \exp\left\{-c\lambda\sum_{i=1}^{n} v_i^b + \frac{\mu_c c}{2\sigma_c^2} - \frac{c^2}{2\sigma_c^2}\right\}$$

$$[b|\ldots] \propto \prod_{i=1}^{n}\left(bv^{b-1}\right)\exp\left\{-\lambda c\sum_{i=1}^{n} v_i^b + \frac{\mu_b b}{2\sigma_b^2} - \frac{b^2}{\sigma_b^2}\right\}$$

The full conditional distributions of $r_i, i = 1,\ldots,n$ and λ can be sampled from directly, as they correspond to gamma distributions. So those parameters can be sampled using Gibbs steps. The full conditionals of the other parameter do not have standard forms. So we use Metropolis steps to obtain samples from them. Once samples from the MCMC are obtained we discard the first part of the chain as a burn-in phase (see for example Gilks *et al*, 1996); then we do a "thinning" of the chain by subsampling the simulated values at a fixed lag k. This strategy ensures that, setting k to some value high enough, successive draws of the parameters are approximately independent (Gelman, 1996). To define the lag we use the auto-correlation function as we will show afterwards in the text.

2.2.5 Model Checking and Forecasting procedure

We have presented, so far, the hierarchical structure of the model and the fitting procedure for the model parameter, based on MCMC sampling. We now address the issues of (1) testing the goodness of the proposed model and (2) forecasting future interevent times.

Bayesian model checking is based on the idea that predictions obtained from the model should be compatible with actual data. So our strategy consists of simulating data from the predictive posterior distribution and compare them to actual observations. The predictive posterior distribution quantifies the uncertainty in future observations given the observed data. By denoting $\tilde{r}$ future values of interevent times we have that the posterior predictive is

$$[\tilde{r} \mid Data] = \int_{R^+} [\tilde{r} \mid \lambda][\lambda \mid Data]d\lambda \tag{2.8}$$

To obtain samples from the expression in Equation (2.8) we start from the MCMC sample of λ. Suppose we have N of them and denote them as λ^j. Conditional on λ^j, for $j = 1,\ldots,N$ we simulate $\tilde{r}^j$ from $[\tilde{r} \mid \lambda^j]$, which are products of exponential. In this way we obtain N synthetic catalogs each one with n pairs of interevent time and volume data. These are compared to

the observed data using descriptive statistics. As descriptive statistics we choose the mean number of events, maximum, minimum, median and standard deviation for both real and synthetic data.

To test the ability of the model to forecast future volumes and interevent times we use a sequential approach. We proceed by fitting the model to the first data pair, then we add the data of the second event to the model fitting. We continue adding data sequentially until the last event. This provides an assessment of the number of data needed for the model to effectively "learn" the model parameters. Using this sequential approach, we are able to decide the minimum amount of data needed to define the learning phase for the model. For the remaining part of data (i.e. voting phase), we use the sequentially sampled parameters to generate the distribution for the next event (interevent time). In this way we can compare the forecasted interevent times with the observed data and with other other possible models already present in literature (see *forward* procedure discussed in Passarelli et al., 2010, see Section 1.3 this volume).

A close look at Equation (2.8) reveals a practical forecasting problem. We observe that the posterior predictive distribution of the interevent times depends on the distribution of the interevent times given the parameter λ. While this is statistically correct, it is not a realistic forecasting procedure. In fact, in a generalized time predictable system the time to the next eruption is strongly dependent on the volume of the previous eruption. More explicitly, in our current framework, after the end of the n-th eruption we have samples of λ that are simulated using only the information up to $(d_{r_{(n-1)}}, d_{v_{(n-1)}})$. We would like to incorporate the information on d_{v_n}. We do this by resampling the posterior realizations of λ using the Sampling Importance Resampling algorithm (hereafter SIR), (Rubin,1988, Smith and Gelfand, 1992) together with the Bayes theorem.

Let $\theta_{n-1} = b, c, \lambda$ the samples obtained from our model using the first $n-1$ data. For the n-the interevent time we have

$$[\tilde{r_n} \mid d_{v_n}] = \int_{R^+} [\tilde{r_n} \mid d_{v_n}, v_{n-1}, \theta_{n-1}][\theta_{n-1} \mid d_{v_n}, v_{n-1}] d\theta_{n-1} \tag{2.9}$$

Obtaining samples from the predictive distribution in Equation (2.9) requires samples of $[\theta_{n-1} \mid d_{v_n}, v_{n-1}]$, which are not available. Our MCMC algorithm produces samples of

$[\theta_{n-1} \mid d_{v_{n-1}}, v_{n-1}]$ instead. Using Bayes theorem we have that

$$[\theta_{n-1} \mid d_{v_n}, v_{n-1}] \propto [d_{v_n} \mid v_{n-1}, \theta_{n-1}][\theta_{n-1} \mid v_{n-1}] \ . \tag{2.10}$$

In Equation (2.10) we recognize $[d_{v_n} \mid v_{n-1}, \theta_{n-1}]$ as the inverse gamma distribution used for volume data in Equation (2.5). $[\theta_{n-1} \mid v_{n-1}]$ is the posterior distribution for parameters λ, b and c up to the first $n-1$ events. The SIR algorithm consists of resampling the output from the MCMC, say θ^j_{n-1}, with replacement, using the normalized weights defined as

$$w^*(\theta^i_{n-1}) = \frac{w(\theta^i_{n-1})}{\sum_{j=1}^m w(\theta^j_{n-1})}$$

where $w(\theta^i_{n-1}) = [d_{v_n} \mid v^i_{n-1}, \theta^i_{n-1}]$. The weights w correspond to the inverse gamma distribution in Equation (2.5) for the observed volume of the n-th event conditional on the sampled volumes of the previous event and the remaining parameter, as simulated by the MCMC. The output from the SIR algorithm can be used within Equation (2.9) to obtain the desired samples of the n interevent time. A brief description of the SIR algorithm is in Appendix A.

Finally we make explicit comparison for the probability of eruption calculating the probability gain or information content as proposed by Kagan & Knopoff (1987). We calculate the information gain for the present model with respect to other statistical models previously published, sharing the sequential approach above discussed and only on the voting phase. Let A and B two statistical models, the probability gain is simply defined as the difference between the log-likelihood distributions, i.e.:

$$PG = \sum_{i=m}^{n} l_A(\delta d_{r_i}) - \sum_{i=m}^{n} l_B(\delta d_{r_i}) \tag{2.11}$$

where l_A is the natural logarithm of the likelihood of the model A and l_B of the model B calculated in a temporal window δd_{r_i} of one month around the observed interevent time in the voting phase (i.e. on the $n-m$ events).

If PG is greater than zero, model A performs better forecast than model B, if PG is zero the two models provide the same information to the forecast. Together with the total probability gain given by equation (2.11), we can calculate the "punctual" probability gain, i.e. the probability for each event $l_A(\delta d_{r_i}) - l_B(\delta d_{r_i})$ with $i = m, \ldots, n$ (Passarelli *et al*, 2010).

Application to Kilauea volcano, Hawaii, and Mount Etna volcano, Sicily

We apply the BH_TPM II to Kilauea volcano and Mt Etna volcano eruption data. Marzocchi and Zaccarelli (2006) found that Kilauea volcano and Mt. Etna volcano follow a time predictable eruptive behavior. They also stated that these volcanoes are in open conduit regime because their high eruptive frequency and consequently short duration of interevent times. Bebbington (2007) showed evidence of the time-predictable character of Mt. Etna flank eruptions using a catalog since 1610 AD. The same results on time-predictability are attained by Sandri *et al* (2005) only focusing on the Mt Etna flank eruptions in the period 1971-2002. Passarelli *et al* (2010) (in Chapter 1) found time-predictability of Kilauea volcano for eruptive catalog since 1923 AD.

These findings led us to use Kilauea and Mt Etna as the best candidate for the model. In applying the model to these two volcanoes we will able to test: 1) whether or not they follow a time predictable behavior; 2) the reliability of the assumptions used in the model; 3) improvements in using the information given by the volume measurement errors; 4) the ability in fitting the observed data and 5) the forecast capability of the model compared with models previously published in literature for Kilauea and Mt Etna.

2.3 Kilauea volcano

Kilauea volcano is the youngest volcano on the Big Island of Hawaii. The subaerial part of Kilauea is a domelike ridge rising to a summit elevation of about 1200 m, it is about 80 km long and 20 km wide, and covers an area of about 1500 km^2. Kilauea had a nearly continuous summit eruptive activity during the $19th$ century and the early part of the $20th$ century. During the following years, Kilauea's eruptive activity had shown little change. After 1924, summit activity had become episodic and after a major quiescence period during 1934-1952, the rift activity raised increasing the volcanic hazard (Holcomb, 1987). It is widely accepted that Kilauea has its own magma plumbing system extending from the surface to about 60 km deep in the Earth, with a summit shallow magma reservoir at about 3 km depth. The shallow magma reservoir is an aseismic zone beneath the South zone of the Kilauea caldera and it is surrounded on two sides by active rift conduits (Klein *et al* 1987).

The eruption history of Kilauea volcano directly documented dates back to 18*th* century, however before the 1923 the recorded eruptions are spotty and in most of the events the volume erupted is unknown. Therefore, in our analysis we consider all 42 events after 1923 AD (please refer to Passarelli et al., 2010 for more details on the Kilauea catalog completeness, Chapter 1). The data are listed in Table 2.1 where we report the onset date of each eruption together with the erupted volume (lava + tephra) and the relative interevent time. The volume of the 1924/05/10 event is taken from http://www.volcano.si.edu/ and is only the tephra volume. Since the eruption that began in 1983 is still ongoing with a volume erupted greater than 3 km^3, we have 41 pairs of data of interevent time (i.e. the time between the onset of i-*th* and the onset of (i+1)-*th* eruptions) and erupted volume (in the i-*th* eruption).

In the next two subsections we will present the results of the model for the Kilauea dataset. We will show first the results obtained for the model parameters both using all data and the sequential procedure discussed in section 2.2.5, together with the ability of the model in fitting the data (model checking). Then we will show the forecasts obtained using this model; we will compare it with forecasts provided by other models previously published.

2.3.1 Results for variables and parameters

Before to embark on the discussion of the results achieved, we need first to specify the values for the measurement errors $(\Delta d_{r_i}, \Delta d_{v_i})$ and the hyperparameters $(\mu_b, \sigma_b^2, \mu_c \,\text{and}\, \sigma_c^2)$ of the prior distributions of b and c. For interevent times we choose an error (Δd_{r_i}) of 1 day for all data in the catalog; for volumes errors we assign a relative errors $(\Delta d_{v_i}/d_{v_i})$ of 0.25 for data before the 1960 AD (i.e. $i = 1, \ldots, 13$) and of 0.15 for data after the 1960 AD (i.e. $i = 14, \ldots, 41$) (see discussion in Passarelli *et al*, 2010, Section 1.2.1 in this volume). The values for the hyperparameters are taken running the BH_TPM and calculating the mean and standard deviation of the posterior distribution for b and c, i.e. $\mu_b = 0.2$, $\sigma_b = 0.1$, $\mu_c = 200$ and $\sigma_c = 50$ (see Passarelli *et al*, 2010, see Figure 1.4 in Chapter 1).

We simulate the variables and parameters from the posterior distribution (2.7) using MCMC algorithm. As stated in the section 2.2.4, we use both Metropolis-Hastings and Gibbs sampling algorithms. Those simulation techniques do not provide independent samples; successive values for each chain (i.e. each full conditional distribution) are potentially highly correlated. The optimal number of iterations needed to obtain independent draws from the

posterior distribution is determined by using the autocorrelation function. We calculate the autocorrelation function to determine at which lag the values for variables and parameters are independent. In Figure 2.1 is plotted the autocorrelation function for lag 1 to 20 for the parameters b, c and λ, we do not show the same plot for the 41 variables r_i's and 41 v_i's because they give zero correlation almost at the first lags. It is easy to see that the autocorrelation function is close to zero when lag is equal to 20. Hence we run each chain in the MCMC algorithm for 201000 iteration and we thin it with every 20 iteration discarding the first 1000 iteration as a burn-in phase. At the end we have that each variable and parameter is composed by 10000 simulations.

Simulations obtained are presented in Figures 2.2 and 2.3. In Figure 2.2 we show the MCMC realizations for the model variables r_i and v_i (blue stars) compared with the observed data (red pluses). Those variables are calculated using all data in the catalog and are representative of how the model can reproduce the data. The data reproduction is optimal when the variables are constrained into their full conditionals by the data. It is worth to underline, looking at the scale for x-axis and y-axis, how the model is able to reproduce errors measurements, simulating interevent times with little errors and volumes with bigger ones.

In Figure 2.3 we present the results for the model parameters b, c and λ using all data. A close look at their value gives that Kilauea volcano has a time predictable behavior, since b (top left panel) is less than 1 and greater than zero with mean $\overline{b} = 0.45$ and standard deviation $\overline{\sigma_b} = 0.05$. This results are similar to those achieved by Passarelli *et al* (2010), however there the mean value for b distribution is lower. The discrepancy could be imputed at two factor: a different parametrization used in the models and the fact that here we do not use the logarithm of the interevent times and volumes. For the distribution for c (top right panel), which is function of the average magma recharge process, we find a mean value $\overline{c} = 164$ days/10^6 m^3 with error (1 standard deviation) $\overline{\sigma_c} = 24$ days/10^6 m^3. In the bottom left panel we have the posterior distribution for λ, the rate of occurrence or the number of events over the length of the catalog. Their mean value is $\overline{\lambda} = 2.0 \times 10^{-3}$ days^{-1} and standard deviation $\overline{\sigma_\lambda} = 0.3 \times 10^{-3}$ days^{-1} which are totally compatible to the occurrence time calculated directly by the data with Maximum Likelihood Estimation (MLE) technique, i.e. $\lambda_{MLE} = 1.9 \times 10^{-3}$ days^{-1} with 95 % confidence interval $[1.4, 2.5] \times 10^{-3}$ days^{-1}.

In the Figure 2.4 we present the parameters b, c and λ using the sequential approach dis-

cussed in section 2.2.5.The black dashed lines determine the division between the learning and voting phases. In particular the events on the left of the dashed line are the learning phase (first third of the catalog, i.e. 14 events), while we use the remaining part to test the eruption forecasts (i.e. 27 events). We will use these realizations into the forecast procedure and we will discuss it in the next section.

The results obtained imply a power law relationship between interevent times and volumes. As discussed in Passarelli *et al* (2010) this non linear relationship underlines the role played by magma discharging process onto the eruption frequency. Such relationship implies the possibility of having a non costant input rate in the magma storage system. Therefore, large erupted volume may trigger the increasing of the magma upwelling process inside a shallow reservoir. We expect a shorter quiescence period after an eruption characterized by a large volume compared with a process where the magma recharging rate is constant (i.e. Classical Time Predictable model). A simple explanation could be thought as an additional gradient of pressure ought to the drainage process of the shallow magma system by a large erupted volume. This pressure gradient may increase the magma upwelling process from the deep crust. Non constant magma input rate for the shallow magma reservoir for Kilauea volcano has been found by Aki & Ferrazzini (2001) and Takada, (1999). This possible non-stationarity should be taken into account in modeling the magma chamber dynamics at Kilauea volcano.

2.3.2 Model checking and Forecasts

The model check is a way to assess the fit of the model to the data. This sensitivity analysis quantify the uncertainties of the model in regard to future observations; on the other hand, it is a way to understand the limits of the model in reproducing data. In checking the model, we simulate 10000 synthetic catalogs using the procedure described in Section 2.2.5. Then we calculate for both synthetic catalogs and observed data, the rate of occurrence, the maximum, the minimum, the median and the standard deviation. In Figure 2.5 we plot the synthetic data as histograms (blue bars) and the relative quantities calculated over the real dataset (red line). For each plotted quantity the p-value (i.e. fraction of synthetic simulations with value greater than the observed quantity) is indicated. It is easy to see a good agreement for the rate of occurrence, the minimum and the median. The are some discrepancies for the maximum and consequently for the standard deviation. In these cases the observed value falls in the

tails of the predictive distributions. This is due to the fact that the maximum corresponds to the 18 years of quiescence of the Kilauea volcano (i.e. 1934-1952 AD). This is a extraordinary long period of rest for the Kilauea and it could be considered as an extreme value. The second longest interevent time is about 5 years of quiescence (i.e. 1955-1959 AD). Such value falls right at the center of the distribution with p-value=0.7. In summary, the model is capable of reproducing the data, with the exception of future extreme events that correspond to the tails of the predictive distribution.

The last check on the reliability of the model is to evaluate its forecast performances and compare them with already published models for the Kilauea volcano interevent times. We make probabilistic forecast comparison of this model with homogeneous Poisson process (Klein *et al*, 1982), Log-Normal model (Bebbington & Lai, 1996b), Generalized Time Predictable Model (GTPM) (Sandri *et al.*, 2005) and BH_TPM (Passarelli *et al*, 2010, Chapter 1 in this volume) using the sequential procedure described in Section 2.2.5.

The homogeneous Poisson process was proposed by Klein (1982) to describe the Kilauea interevent time data. This model implies a totally random and memoryless eruptive behavior; while the number of events in time is distributed according with a Poisson distribution, the time intervals between two consecutive events has exponential distribution. The Log-Normal model was proposed by Bebbington & Lai (1996b); in this model interevent times are described using a log-normal distribution. The mode of a log-normal distribution could reveal a certain degree of cyclicity in the eruptive behavior for Kilauea volcano. The GTPM was proposed by Sandri et al., 2005. It is a linear regression among pairs of logarithm of interevent times and of volumes. The BH_TPM is a hierarchical model where the interevent times and volumes are described via log-normal distributions and uses the logarithm of the generalized time predictable model equation as eruptive behavior.

We calculate the probability for BH_TPMII drawing simulations from equation (2.9), where the λ^j are resampled with the SIR algorithm using the information given by volume data. The results of the SIR procedure are plotted in Figure 2.6 where the blues stars refer to the MCMC's output and the red ones are the resampled. It is worth to underline that the information provided by the volume data into the SIR procedure shrinks and shifts the λ distributions. Besides the mode of the resampled λ's has a higher value than the mode of the non resampled ones. Now, using the resampled λ's, we can calculate the probability gain.

The results are plotted in Figure 2.7 where we show the " punctual" probability gain and we report the total probability gain as calculated using equation (2.11). The model shows an improvement in forecasting capability respect to the other models because the total probability gain is always greater than zero in all tests. The best results is for the test against the Poisson model (panel a) where the model performs better forecasts for 20 out of 27 eruptions. Good results are those against the Log-Normal model (panel c) and the highest probability gain is obtained testing against the GTPM (panel d). This latter result implies that the information on the error measurements are helpful in the model budget. The test against the counterpart of this model, i.e. BH_TPM (panel b), shows a weaker results, however the total probability gain is greater than zero. BH_TPMII gives better forecasts over 19 out of 27 events. PG, here, is influenced by two events (i.e. the $1st$ and $11th$ in Figure 2.7) where the "punctual" probability gain is particularly negative. It seems that, despite of some local discrepancies, the BH_TPMII shows a better behavior in forecasting the eruptive events. Evidence toward this statement is the fact that in all tests BH_TPMII gives better forecast for more than 50% of events manifesting a higher reliability in case of its potential use in probabilistic volcanic hazard assessment.

Finally we investigate some possible correlation between the "punctual" probability gains and the interevent times or volumes using linear regression analysis. We do not find any correlation between volumes and probability gain. The only significant linear dependence (p-value≤ 0.01) we find is between "punctual " probability gain calculated against homogeneous Poisson process and observed interevent times, as in Figure 2.8. The inverse relationship imply that systematically we perform worse forecast for long interevent times. We can justify this results stating that for long quiescence period the Kilauea volcano becomes memoryless (see Marzocchi & Zaccarelli, 2006). In addition, considering the events as points in time could be distorting when eruptions last months to years (see Bebbington, 2008), together with the fact that we do not consider intrusions not followed by eruptions (Takada, 1999, Dvorak & Dzurisin, 1993). Finally another possible explanation could be related to possible modification of the shallow magma reservoir geometry after an eruption (Gudmundsson, 1986).

2.4 Mount Etna volcano

Mount Etna volcano is a basaltic stratovolcano located in the North-Eastern part of the Sicily Island. It is one of the best known and monitored volcano in the world and records of its activity date back to several centuries B.C. The sub-aerial part of Mount Etna is 3300 m high covering an area of approximately 1200 km^2. Two styles of activity occur at Mt Etna: a quasi-continuous paroxysmal summit activity, often accompanied with explosions, lava fountains and minor lava emission; a less frequent flank eruptive activity, typically with higher effusion rate originate from fissures that open downward from the summit craters. The flank activity is sometimes accompanied by explosions and lava spattering; recently, two flank eruptions have been highly explosive and destructive, the 2001 and 2002-2003 events (Behncke & Neri, 2003, Andronico *et al*, 2005, Allard *et al*, 2006).

At present there are petrological, geochemical and geophysical evidences for a 20-30 km deep reservoir controlling the volcanic activity (Tanguy *et al*, 1997), but it is still debated whether or not Mt Etna has one o more shallower plumbing systems. Results from seismic tomography do not reveal any low velocity zone in the uppermost part of the volcanic edifice, while a high-velocity body at depth of $<$ 10 km b.s.l. is interpreted as a main solidified intrusive body (Chiarabba *et al*, 2000, Patanè *et al*, 2003). However, a near-vertical shallower plumbing system has been recently inferred at about 4.5 km b.s.l. using deformation data (Bonforte *et al*, 2008 for a review). It is widely accepted that a central magma conduit feeds the near-continuous summit activity, while lateral eruption are triggered by lateral draining of magma from its central conduit. Only few events appear to be independent from the central conduit being fed by peripheral dikes (see Acocella & Neri, 2003 among others).

The recorded eruptive activity for Mt Etna dates back to 1500 B.C. (Tanguy *et al*, 2007). Unfortunately, the eruptive catalog can be considered complete only since 1600 AD for flank eruptions (Mulargia *et al*, 1985). Instead summit activity, was recorded carefully only after the World War II (Andronico & Lodato, 2005) and only after 1970 all summit eruptions were systematically registered (Wadge, 1975, Mulargia *et al*, 1987). Thus the Mt Etna catalog is considered complete since 1970 AD for summit eruptions. There are several catalogs for Mt Etna eruptions available in literature, the most recent ones being those compiled by Behncke *et al* (2005), Branca & Del Carlo (2005) and Tanguy *et al* (2007); the Andronico & Lodato (2005) catalog is detailed only for events in the $20th$ century. In this study we use only the

flank eruptions since 1600 AD using the Behncke *et al* (2005) catalog as it appears the most complete, at least for volume data. We also integrate and double-check the volume data for the $20th$ century events with the Andronico & Lodato (2005) catalog. The Behncke *et al* (2005) catalog lists events up to 2004/09/07 eruption, so we update it for 2006 AD and 2008 AD eruptions using information available in Burton *et al* (2005) and Behncke *et al* (2008). A raw estimation for the volume of the 2008/05/13 eruption was kindly provided by Marco Neri (Marco Neri personal communication, 2010).

The choice of using only lateral eruptions needs qualification. Although it could be arguable and could explain only one aspect of the eruption activity at Mt Etna volcano, we are pushed in this direction by the quality of data available. Besides, from a statistical point of view, it is better not to use an incomplete dataset with the awareness of the risk of losing one piece of information, than using incomplete data and find false correlations (Bebbington, 2007). Flank eruptions, however, constitute one of the most important threat for a volcanic hazard assessment at Mt Etna (see Behncke *et al*, 2005 and Salvi *et al*, 2006 among others). Thus, in our opinion, the choice of using only flank eruptions seems the best available in a volcanic hazard assessment perspective. In Table 2.2 the data of flank eruptions at Mt Etna are reported; we indicate the onset date, interevent times (d_{r_i}) and volumes (d_{v_i}). The are 63 eruptive events and consequently 62 pairs of interevent time and volume data.

The next two subsections are organized as follows: we first show the results obtained for the model parameters both using all data and the sequential procedure discussed in Section 2.2.5, then the ability of the model in fitting the data (model checking) and the forecast obtained. Finally, we will compare them with forecast provided by other models previously published (when the comparison is possible).

2.4.1 Results for variables and parameters

In order to apply the model to the Mt Etna flank eruptions, first we need to specify the measurements errors ($\Delta d_{r_i}, \Delta d_{v_i}$) and the hyperparameters (μ_b, σ_b^2, μ_c and σ_c^2) for the priors distribution for b and c. In the Behncke *et al* (2005) catalog there is no mention about the interevent time errors whereas relative errors are given for volume data. Therefore, we assign an error of 1 day for Δd_{r_i} for interevent times. According to Behncke *et al* (2005) we assign relative errors as follows: $\Delta d_{v_i}/d_{v_i} = 0.25$ for $i = 1, \ldots, 43$ (eruptions from 1607 to 1970AD),

$\Delta d_{v_i}/d_{v_i} = 0.05$ for $i = 44, \ldots, 60$ (eruptions form 1970 to 2004 AD) and $\Delta d_{v_i}/d_{v_i} = 0.25$ for $i = 61, 62$. The latter errors are relative to the 2006 and 2008 AD events not in Behncke *et al* (2005) catalog; whose volumes are first raw estimate not reparametrized yet (Marco Neri personal communication, 2010).

The MCMC simulations here are performed following the thinning procedure already discussed. In Figure 2.9 there are the autocorrelation function results from lag 1 to 20 for the parameters b, c and λ, we do not show the same figures for the 62 variables r_i's and 62 v_i's because they provide zero correlation at almost the first lags. The autocorrelation function is practically zero at lag 20 for all parameters. Therefore we run 201000 simulations discarding the first 1000, as a burn-in, and than thinning the chains every 20 iterations. In this way we obtain posterior distributions for variables and parameters of 10000 simulation each. For the hyperparameters we choose the same parameters as the Kilauea case, i.e.$\mu_b = 0.2$, $\sigma_b = 0.1$, $\mu_c = 200$ and $\sigma_c = 50$.

Simulations obtained are presented in Figures 2.10 and 2.11. The data reproduction here is optimal when the variables are constrained in their full conditionals by data, see Figure 2.10 where simulation are blue stars and data red pluses. Also here, as in the Kilauea case, the model reproduces reliably the measurement errors assigned. In Figure 2.3 we present the results for the model parameters b, c and λ using all data. The value obtained for b (top left panel in Figure 2.11) suggests that Mt Etna flank eruptions follow a time predictable eruptive behavior. The numerical value for $0 < b < 1$ implies a power law time predictable behavior, the mean and standard deviation are $\overline{b} = 0.35$ and $\overline{\sigma_b} = 0.04$ respectively. For the distribution for c (top right panel), which is function of the average magma recharge process, we find a mean value $\overline{c} = 330$ days/10^6 m^3 with error (1 standard deviation) $\overline{\sigma_c} = 40$ days/10^6 m^3. In the bottom left panel we have the posterior distribution for the rate of occurrence λ. The mean value and standard deviation are $\overline{\lambda} = 5.4 \times 10^{-4}$ days^{-1} and $\overline{\sigma_\lambda} = 0.6 \times 10^{-4}$ days^{-1} respectively, and are totally compatible with the rate of occurrence calculated directly by the data with MLE technique, i.e. $\lambda_{MLE} = 4.2 \times 10^{-4}$ with 95 % confidence interval $[3.2, 5.4] \times 10^{-4}$.

In the Figure 2.12, we present the parameters $b, c \text{and} \lambda$ using the sequential approach discussed in section 2.2.5. The black dashed lines determine the division between the learning and voting phase; the events on the left of the dashed line constitute the learning phases (first

third of the catalog, i.e. 20 events), while we use the remaining part to test the eruption forecasts (i.e. 42 events). We will use these realizations into the forecast procedure and we will discuss it in the next section.

By looking at the outcomes of the MCMC simulations for the parameters b and c, it is clear that flank eruptions at Mt Etna follow a time predictable eruptive behavior. The value of b less than one implies a non-linear relationship between interevent times and volumes. The time predictable equation (2.1) is a power law similar to the one we infer for Kilauea volcano. These findings lead to speculate about the role played by the magma chamber feeding system in the eruption frequency as we have speculated in Section 2.3.1. Under this perspective the Mt Etna volcano seems to act as a non-stationary volcano (Mulargia *et al*, 1987), and the non-stationarity could also imply some sort of cyclicity in the eruption frequency (Behncke & Neri, 2003, Allard *et al*, 2006). This possible non-stationarity should be taken into account in modeling the magma chamber dynamics at Kilauea volcano.

2.4.2 Model checking and Forecasts

The results of the model check are presented in Figure 2.13. It is immediate to realize the agreement of the synthetic simulations (blue bars) with values calculated from the data (red bar) for the rate of occurrence, maximum, minimum and median. For the rate of occurrence where the p-value=0.87, we can speculate that the model predicts interevent times slightly longer that the observed one. Although the model works well for minimum, median and rate, it is less satisfactorily for the maximum and as a consequence for the standard deviation. Again here as for Kilauea, the model can reproduce the maximum only within the tail behavior of the synthetic realizations. A close look at Mt Etna catalog reveals that the maximum interevent time is relative to a long quiescence period from 1702 to 1755 AD. This value could be considered an extreme value (53 years) because the second longest interevent time is only 20 years, being the quiescence period from 1614 AD to 1634 AD. This second longest interevent time is compatible with the synthetics maximum simulation with p-value=0.7. As we verified in checking the model for Kilauea data, BH_TPMII model is able to capture the main data features except for the extreme value, or better, is able to reproduce the extreme value only within the tail of the distribution for the synthetic catalogs.

The final task, now, is to test the forecast performance of the model and compare it with

other models for Mt Etna interevent times already present in literature using the sequential approach discussed in Section 2.2.5. Before to embark in this comparison, we present the results of the SIR procedure used to resample the λ^j's in the right side of equation (2.9). In Figure 2.14 the λ^j are plotted as they are from the MCMC simulation (blue stars) with superimposed the outcome of the resampling procedure (red stars). The information provided by the volume data in the SIR procedure shrinks and shifts the λ^j distributions and as a results the mode of the distributions for the resampled quantities is higher than the non resampled ones. Now, as soon as we get the resampled λ^j's, we can use them to simulate the integral in equation (2.9).

There are several statistical model in literature describing statistically the eruptive data series for Mt Etna. The model are: BH_TPM proposed by Passarelli *et al* (2010) (Chapter 1), a Non Homogeneous Poisson process with a power law intensity proposed by Salvi *et al* (2006), a Non homogeneous Poisson process with piecewise linear intensity by Smethurst *et al* (2009); the GTPM by Sandri *et al* (2005) and the Hidden Markov Models of Bebbington (2007). The latter model is a model that allows to identify change in volcanic activity using Hidden Markov Models. In this work the activity level of Mt Etna volcano is tested through the onset count data, the interevent time data and the quiescence time data (interonset in the Bebbington 2007 terminology) together with time and size-predictable model. To be honest, we are not able to apply the sequential procedure to the Bebbington (2007) model due to its intrinsic computational complexity, so we do not perform the probability gain test against it.

We have already discussed the BH_TPM and GTPM in the previous sections (see Section 2.3.2), thus we present the main peculiarity of the Salvi *et al* (2006) model and the Smethurst *et al* (2009) model. Salvi et al (2006) model is an Non Homogeneous Poisson model. The intensity of the process has a power law time dependence whose parameters can be estimated using MLE. This model implies that the intensity can increase or decrease with time, depending on the value of the exponent. In this way the model can take into account and fit any trend in eruptive activity. In Smethurst *et al* (2009), authors study different Non Homogeneous Poisson processes, finding the best model is one with a piecewise linear intensity. In other words, fitting the model via numerical MLE, the intensity of the process is constant (Homogeneous Poisson process) for eruption before 1970 AD, and then it starts to increase linearly with time. This is a process with a change point and is not easy to handle under our sequential procedure.

The change point found by Smethurst et al. (2009) works only if the numerical MLE is done using all data (with the benefit of hindsight). On the other hand, applying the sequential procedure, i.e. adding one data at a time after the learning phase, does not guarantee to find the same change point and not even to find exactly one change point (see Gasperini *et al*, 1990). In addition, the parameters of the process in the Smethurst *et al* (2009) model are not in closed form, so the stability of the numerical maximization could produces further problems in applying the sequential approach.

To tackle this complicated change point problem and compute "forward" probabilities of eruptions, we choose to employ two different approaches. The first one is to keep the change point (i.e. 1964 AD) found by Smethurst *et al* (2009) using all data and simulate sequentially the other two parameters of the model. In this way we calculate the probability gain in equation (2.11) assuming a constant intensity up to the change point, and then assuming a linearly increasing intensity. Anyway, in the forward sequential approach perspective we want to use, this is not a fair game to get eruption probabilities, as we are using the value of the change point calculated using all data.

The second approach is instead based on the empirical estimation of the trend for the intensity of the process calculated under the sequential procedure. As we show in Figure 2.15, after the learning phase, we examine and evaluate the trend for the intensity λ_{MLE} (blue stars in the graph), calculated by adding one data at a time, assuming a homogeneous Poisson process. We find that the intensity shows a slow increase with important fluctuations up to the change point found by Smethurst et al. (2009) (black dashed line). Then, after the change point, the intensity rises more markedly. To figure out whether or not the intensity after each event is increasing with time, we estimate its trend with linear regression. In particular, we perform linear regression on the intensity since the datum before the last change of sign in its trend assessing the goodness of the regression (F-test on the slopes at 1% significance level). In Figure 2.15, we show positive slopes with significant regression with green lines, and negative slopes or positive ones with not significant regression with red lines. It is clear from the graph that intensity does not show any significant trend up to four events after the change point found by Smethurst *et al* (2009). This is something widely known, that is to say, in order to recognize a significant trend in a forward study, one needs several data points (see for example Cornelius & Voight, 1995).Hence, in calculating the parameters under the forward

sequential procedure, we keep a homogeneous Poisson process on the events where the above regressions are not significant (i.e. four events after the Smethurst *et al*, 2009 change point), then we use the Non Homogeneous Poisson process with linearly increasing intensity.

Finally we present the results for the probability gain in Figure 2.16. As it is shown in the inset of each panel, PG's are always greater than zero, showing the present model performs better forecast compared to the others. In particular, the forecasting test against the homogeneous Poisson process (panel a) shows only 14 eruptions out of 42 with a negative "punctual" probability gain, corroborating the fact that Mt Etna flank eruptions are non stationary in time (Mulargia *et al* 1987, Bebbington, 2007, Salvi *et al* 2006 and Smethurst *et al*, 2009). While in testing against BH_TPM (panel b), only 17 eruptions have a negative probability gain indicating that modeling Mt Etna interevent times with log-normal distributions does not seem to be the best choice. The result in panel c against the GTPM is the best one and remarks the limitation of a regression technique in modeling linear relationship between the logarithm of interevent times and of volumes, without using measurement errors. Salvi *et al* (2006) model, in panel d, performs worse forecasts compared with BH_TPMII, confirming that a power law intensity is not appropriate for Mt Etna eruption occurrences (Smethurst *et al* 2009). In panel e, the test against the Smethurst *et al* (2009) model, with fixed change point as they found, is the worse one, although the PG is still slightly positive. On one hand, this test shows that modeling the intensity with a linear increasing function for events in the last 40 years seems more appropriate. At the same time, it shows some limitations: a close look to the subplot e shows that event 38 have a very high gain in favor of the BH_TPMII. This event is the 2001 AD eruption, started after 10 years of quiescence. Therefore, the Smethurst *et al* (2009) model, with the ad hoc fitted piecewise linear intensity, could be misleading for real forecasting purposes as the observed eruption frequency decreases in the future. Finally we present, in panel f, the probability gain against the modified Smethurst *et al* (2009) model following the specification discussed in the previous section for the "forward" application. Respect to panel e, here the probability gain is considerably higher although the linear intensity fits better the last part of the catalog.

It seems that, despite some local discrepancies, the BH_TPMII shows a better overall behavior in forecasting the eruptive events providing better forecast for more than 50% of events and manifesting a higher reliability if used in probabilistic volcanic hazard assessment.

To get geophysical insights, we investigate some possible correlation between the "punctual" probability gains and the interevent times or volumes using linear regression analysis. We do not find any correlation between volumes and probability gain. The only significant linear relationship (p-value≤ 0.01) we find, as in the Kilauea case, is between "punctual " probability gain calculated against the homogeneous Poisson process and interevent times, as in Figure 2.17. The inverse relationship implies that we systematically perform worse forecast for long interevent times. We can justify this results stating that for long quiescence periods the volcano becomes memoryless with transition from open and closed conduit regime (see Marzocchi & Zaccarelli, 2006 and Bebbington, 2007). An other explanation could be related to the complexity of the volcano eruption system not considered in this model. The time predictable model seems to be more appropriate when the eruption are close in time, conversely, when the quiescence period are extremely long, other compelling physical processes may control the volcanic activity. Finally, neglecting the summit activity, we lose one piece of information related to the amount of erupted volume from summit crater during the quiescence period. This may introduce a bias that could explain this inverse relationship.

2.5 Conclusions

In this work we have carried out a Bayesian Hierarchical model to test time predictable model for open conduit volcanoes (BH_TPMII). The use of Bayesian Hierarchical modeling provides a suitable tool to take into account the physical uncertainties related to the eruption process and relative to the data, parameters and variables. We have applied the model to Kilauea eruptive catalog from 1923 to 1983 AD and to Mount Etna flank eruptions from 1607 to 2008 AD. The results show that both volcanoes have a generalized time predictable eruptive behavior where interevent times depend on the previous volume erupted. The numerical values of the time predictable model parameters inferred suggest that the amount of the erupted volume could change the dynamics of the magma chamber refilling process during the subsequent repose period.

The model shows a good fit with the observed data for both volcanoes and is also able to capture extreme values as a tail behavior of the distributions. The forecasts obtained by BH_TPM II are superior to those provided by other statistical models for both volcanoes. In particular we have improved the forecast performance compared with those of BH_TPM,

corroborating the hypotheses of building up the present model. We want to point out that an Non Homogeneous Poisson process, as the one developed in Smethurst *et al* (2009), could provide better forecast if the flank eruptive activity on Mt Etna keeps increasing in time as it did in the last 40 years. We suggest that the present model could be included in a long-term Probabilistic Volcanic Hazard Assessment as a basic component for modeling the occurrence of eruptions in time at Kilauea Volcano and Mount Etna volcano.

A Sampling Importance Resampling algorithm

The Sampling Importance Resampling (SIR) is a non iterative procedure proposed by Rubin (1988). The SIR algorithm generates an approximately independent and identically distributed (i.i.d.) sample of size m from the target probability density function $f(x)$. It starts by generating M $(m \leq M)$ random numbers from a probability density function $h(x)$ as inputs to the algorithm. The output is a weighted sample of size m drawn from the M inputs, with weights being the importance weights $w(x)$. As expected, the output of the SIR algorithm is good if the inputs are good ($h(x)$ is close to $f(x)$) or M is large compared to m.

The SIR consists of two steps: a sampling step and an importance resampling step as given below:

1. (Sampling step) generate $X_1, \ldots, X_M$ i.i.d. from the density $h(x)$ with support including that of $f(x)$;

2. (Importance Resampling Step) draw m values $Y_1, \ldots, Y_m$ from $X_1, \ldots, X_M$ with probability given by the importance weights:

$$w^*(X_1, \ldots, X_M) = \frac{w(X_i)}{\sum_{j=1}^{M} w(X_j)} \quad \text{for} \quad i = 1, \ldots, M.$$

   where $w(X_j) = f(X_j)/h(X_j)$ for all j.

The resampling procedure can be done with or without replacement.

Bibliography

[1] Acocella, V. & Neri, M., What makes flank eruptions? The 2001 Etna eruption and its possible triggering mechanisms. *Bull Volcanol*, 65:517–529,doi: 10.1007/s00445-003-0280-3.

[2] Aki, K. & Ferrazzini, V., 2001. Comparison of Mount Etna, Kilauea, and Piton de la Fournaise by a quantitative modeling of their eruption histories, *J. Geophys. Res.*, 106, B3, 4091–4102.

[3] Allard, P., Behncke, B., D'Amico, S., Neri, M. & Gambino, S., 2006. Mount Etna 1993-2005: anatomy of an evolving eruptive cycle. *Earth Science Reviews* 78 85–114 doi:10.1016/j.earscirev.2006.04.002.

[4] Andronico, D. & Lodato, L., 2005. Effusive activity at Mount Etna volcano (Italy) during the 20th century: a contribution to volcanic hazard assessment.*Nat. Hazards*, 36, 407–443.

[5] Andronico, D., Branca, S.,Calvari, S., Burton, M., Caltabiano, T., Corsaro, A.R., Del Carlo, P., Garfì, G., Lodato, L., Miraglia,L., Murè, F., Neri, M., Pecora, E., Pompilio, M., Salerno, G. & Spampinato, L., A multi-disciplinary study of the 2002-03 Etna eruption: insights into a complex plumbing system. 2005. *Bull Volcanol* 67,314–330 doi:10.1007/s00445-004-0372-8.

[6] Bebbington M.S., Lai C. D. 1996a. Statistical analysis of New Zealand volcanic occurrence data, *J. Volcanol. Geotherm. Res.*, 74, 101–110.

[7] Bebbington M.S., Lai C. D. 1996b. On nonhomogeneous models for volcanic eruptions, *Math. Geology*, 28,5, 585–600.

[8] Bebbington M.S., 2007. Identifying volcanic regimes using Hidden Markov Models. *Geophys. J. Int.* 171, 921-941.

[9] Bebbington M, 2008. Incorporating the eruptive history in a stochastic model for volcanic eruptions. *J. Volcanol. Geotherm. Res.* 175, 325-333.

[10] Behncke, B., Calvari, S., Giammanco, S., Neri, M. & Pinkerton, H., 2008. Pyroclastic density currents resulting from the interaction of basaltic magma with hydrothermally altered rock: an example from the 2006 summit eruptions of Mount Etna. *Bull Volcanol*, 70:1249–1268.

[11] Behncke B & Neri M 2003. Cycles and trends in the recent eruptive behaviour of Mount Etna (Italy). *Can J Earth Sci* 40:1405–1411 doi:10.1139/E03-052.

[12] Behncke, B., Neri, M.& Nagay, A., 2005. Lava flow hazard at Mount Etna (Italy): new data from GIS-based study, in *Kinematics and dynamics of lava flow*, Manga, M., and Ventura, G., eds, Geological Society of America, Special Paper 396, 189-208,doi:10.1130/2005.2396(13).

[13] Bonforte, A., Bonaccorso, A., Guglielmino, F., Palano, M. & Puglisi, G.,2008. Feeding system and magma storage beneath Mt. Etna as revealed by recent inflation/deflation cycles, *J Geophys Res*, 113 B05406, doi:10.1029/2007JB005334.

[14] Branca, S. & Del Carlo, P., 2005. Types of eruptions of Etna volcano AD 1670-2003: implication for short term eruptive behavior. *Bull Volcanol* 67: 732 – 742, doi:10.1007/s00445-005-0412-z.

[15] Burt M.L., Wadge G. & Scott W.A., 1994. Simple stochastic modelling of eruption history of basaltic volcano: Nyamuragira, Zaire, *Bull. Volcanol.*, 56:87–97.

[16] Burton, M., Neri, M., Andronico, D., Branca, S., Caltabiano, T., Calvari, S., Corsaro, R. A., Del Carlo, P., Lanzafame, G., Lodato, L., Miraglia, L., Salerno, G. & Spampinato, L., 2005. Etna 2004-2005: an archetype for geodynamically-controlled effusive eruptions. *Geophys Res Lett*, 32, L09303, doi:10.1029/2005GL022527.

[17] Chiarabba, C., Amato, A., Boschi, E., Barberi, F., 2000. Recent seismicity and tomographic modeling of the Mount Etna plumbing system. *J Geophys Res*, 105, B5, 10923–10938.

[18] Cornelius, R R, & Voight, B, 1995. Graphical and PC-software analysis of volcano eruption precursors according to the Material Failure Forecast Method (FFM), *J Volcanol Geotherm Res*, 64, 295–320.

[19] De la Cruz-Reyna S., 1991. Poisson-distributed patterns of explosive eruptive activity, *Bull. Volcanol.*, 54, 57–67

[20] Dvorak, J.J., & Dzurisin, D., 1993. Variations in magma-supply rate at Kilauea volcano, Hawaii, *J. Geophys. Res.*, 98, 22255-22268.

[21] Gasperini, P, Gresta, S, & Mulargia, F, 1990. Statistical analysis of seismic and eruptive activities at Mount Etna during 1978-1987, *J Volcanol Geotherm Res*, 40, 317 – 325.

[22] Gelman,A., 1996 Inference and monitoring convergence, in *Markov chain Monte Carlo in practice*, pp 131–143, eds Gilks W.R., Richardson S. & Spiegelhalter D.J., Chapman & Hall, London, 2nd edn.

[23] Gelman A., Carlin J.B., Stern H.S. & Rubin D.B.,2000. *Bayesian Data Analysis*,1st edn, Chapman & Hall/CRC,Boca Raton-Florida.

[24] Gilks W.R., Richardson S. & Spiegelhalter D.J., 1996. Introducing Markov chain Monte Carlo, in *Markov chain Monte Carlo in practice*, pp 1–19, eds Gilks W.R., Richardson S. & Spiegelhalter D.J., Chapman & Hall, London, 2nd edn.

[25] Gudmundsson A, 1986. Possible effect of aspect ratios of magma chambers on eruption frequency. *Geology* 14, 991-994.

[26] Holcomb, R.T.,Eruptive history and long term behavior of Kilauea volcano, in *Volcanism in Hawaii*, pp. 261–350 U.S. Geol. Surv. Prof. Pap. 1350.

[27] Kagan Y.Y. & Knopoff L., 1987. Statistical Short-Term Earthquake Prediction, *Science*, 236(4808), 1563–1567

[28] Klein F.W.,1982 Patterns of historical eruptions at Hawaiian Volcanoes, *J. Volcanol. Geotherm. Res.*, 12 , 1–35

[29] Klein F.W., Koyanagi,R.Y., Nakata, J.S. & Tanigawa, W.R., The seismicity of Kilauea's magma system, in *Volcanism in Hawaii*, pp. 1019–1185 U.S. Geol. Surv. Prof. Pap. 1350.

[30] Marzocchi W.,1996. Chaos and stocasticity in volcanic eruptions the case of Mount Etna and Vesuvius, *J. Volcanol. Geotherm. Res.*,70, 205-212.

[31] Marzocchi, W., Sandri, L., Gasparini, P., Newhall, C. G., Boschi, E., 2004. Quantifying probabilities of volcanic events: the example of volcanic hazard at Mt. Vesuvius. *J. Geophys. Res.*, 109, B11201, doi:10.1029/2004JB003155.

[32] Marzocchi W., Sandri L. & Selva J.,2008. BET_EF: a probabilistic tool for long- and short-term eruption forecasting, *Bull. Volcanol.*, 70, 623–632

[33] Marzocchi W. & Zaccarelli L.,2006. A quantitative model for the time size distribution of eruptions, *J Geophys Res*, 111, doi:10.1029/2005JB003709.

[34] Mulargia F.,Tinti S. & Boschi E.,1985. A statistical analysis of flank eruptions on Etna Volcano, *J Volcanol Geotherm Res* , 23, 263–272.

[35] Mulargia F., Gasperini, P., & Tinti S. ,1987. Identifying different regimes in eruptive activity: an application to Etna volcano, *J Volcanol Geotherm Res*, 34, 89–106.

[36] Newhall C.G. & Hoblitt,R.P., 2002. Constructing event trees for volcanic crises, *Bull. Volcanol.*, 64, 3–20.

[37] Patanè, D., De Gori, P., Chiarabba, C., Bonaccorso, A., 2003. Magma ascent and the pressurization of Mount Etna's volcanic system, *Science*, 299, 29 March 2003.

[38] Passarelli, L., Sandri, L., Bonazzi, A. & Marzocchi, W., 2010. Bayesian Hierarchical Time Predictable Model for eruption occurrence: an application to Kilauea Volcano, accepted to *Geophysical Journal International*

[39] Rubin, D. B. 1988. Using the SIR algorithm to simulate posterior distributions, in *Bayesian Statistics-3*, pp. 395-402, eds Bernardo, J.W., DeGroot, M. H., Lindley, D. V. & Smith, A.F.M. Oxford: Oxford University Press.

[40] Salvi, F., Scandone, R. & Palma, C., 2006. Statistical analysis of the historical activity of Mount Etna, aimed at the evaluation of volcanic hazard, *J Volcanol Geotherm Res*, 154, 159–168, doi:10.1016/j.jvolgeores.2006.01.002.

[41] Sandri L., Marzocchi W. & Gasperini P., 2005. Some inside on the occurrence of recent volcanic eruptions of Mount Etna volcano (Sicily,Italy), *J. Geophys. Res.*, 163, 1203–1218.

[42] Smethurst, L., James, M. R., Pinkerton, H., Tawn, J.A., 2009. A statistical analysis of eruptive activity on Mount Etna, Sicily, *Geophys J Int*, 179 655–666.

[43] Smith, A.F.M. & Gelfand, A.E., 1992. Bayesian statistics without fear: a sampling resampling perspective, *Am Statist*, 46, 84–88.

[44] Sparks, R.S.J., 2003. Forecasting volcanic eruptions,*Earth Planet. Sci. Lett.*, 210, 1–15.

[45] Takada, A., 1999. Variations in magma supply and magma partitioning: the role of the tectonic settings, *J. Volcanol. Geotherm. Res.*, 93, 93–110.

[46] Tanguy, J.C., Condomines, M. & Kieffer, G., 1997. Evolution of the Mount Etna magma: constraints on the present feeding system and eruptive mechanism, J Volcano Geotherm Res, 221–250.

[47] Tanguy, J.C., Condomines, M.,Le Goff,M., Chillemi, V., La Delfa, S. & Patanè, G., 2007. Mount Etna eruptions of the last 2,750 years: revised chronology and location through archeomagnetic and ^{226}Ra-^{230}Th dating. *Bull Volcanol* 70:55–83, doi:10.1007/s00445-007-0121-x.

[48] Wadge, G., Walker, W.P.L. & Guest, J.E., 1975. The output of Etna volcano, *Nature*, 255, 385–387.

[49] Wikle C. K.,2003. Hierarchical Models in Environmental Science, *Internat. Statist. Rev.*, 71-2, 181–199.

Table 2.1: Catalog of eruptive events at Kilauea volcano

Eruption#	**Onset** (yyyy mm dd)	**Interevent time** [days]	**Volume** lava e tephra $[10^6 m^3]$
1	1923 08 25	259	0.073
2	1924 05 10	70	0.79
3	1924 07 19	1083	0.234
4	1927 07 07	594	2.30
5	1929 02 20	155	1.40
6	1929 07 25	482	2.60
7	1930 11 19	399	6.20
8	1931 12 23	988	7.00
9	1934 09 06	6504	6.90
10	1952 06 27	703	46.70
11	1954 05 31	273	6.20
12	1955 02 28	1720	87.60
13	1959 11 14	60	37.20
14	1960 01 13	408	113.20
15	1961 02 24	7	0.022
16	1961 03 03	129	0.26
17	1961 07 10	74	12.60
18	1961 09 22	441	2.20
19	1962 12 07	257	0.31
20	1963 08 21	45	0.80
21	1963 10 05	517	6.60
22	1965 03 05	294	16.80
23	1965 12 24	681	0.85
24	1967 12 05	291	80.30
25	1968 08 22	46	0.13
26	1968 10 07	138	6.60
27	1969 02 22	91	16.10
28	1969 05 24	812	185.00
29	1971 08 14	41	9.10
30	1971 09 24	132	7.70
31	1972 02 03	457	162.00
32	1973 05 05	189	1.20
33	1973 11 10	251	2.70
34	1974 07 19	62	6.60
35	1974 09 19	103	10.20
36	1974 12 31	333	14.30
37	1975 11 29	654	0.22
38	1977 09 13	794	32.90
39	1979 11 16	896	0.58
40	1982 04 30	148	0.50
41	1982 09 25	100	3.00
42	1983 01 03		ongoing

Table 2.2: Catalog of eruptive events at Mount Etna volcano

Eruption #	**Onset** yyyymmdd	**Interevent time** [days]	**Volume** lava e tephra $[10^6 m^3]$
1	1607 06 28	954	158.00
2	1610 02 06	86	30.00
3	1610 05 03	1520	91.71
4	1614 07 01	7476	1071.00
5	1634 12 19	2985	203.03
6	1643 02 20	1369	4.12
7	1646 11 20	1519	162.45
8	1651 01 17	6628	497.53
9	1669 03 11	7308	1247.50
10	1689 03 14	4741	20.00
11	1702 03 08	19359	16.94
12	1755 03 09	2891	4.73
13	1763 02 06	132	21.08
14	1763 06 18	197	149.96
15	1764 01 01	847	117.20
16	1766 04 27	5135	137.25
17	1780 05 18	4391	29.35
18	1792 05 26	3824	90.13
19	1802 11 15	2324	10.43
20	1809 03 27	944	38.19
21	1811 10 27	2769	54.33
22	1819 05 27	4906	47.92
23	1832 10 31	4034	60.74
24	1843 11 17	3199	55.70
25	1852 08 20	4519	134.00
26	1865 01 03	3525	94.33
27	1874 08 29	1731	1.47

Eruption #	**Onset** yyyymmdd	**Interevent time** [days]	**Volume** lava e tephra [$10^6 m^3$]
28	1879 05 26	1396	41.93
29	1883 03 22	1154	0.25
30	1886 05 19	2243	42.52
31	1892 07 09	5772	130.58
32	1908 04 29	693	2.20
33	1910 03 23	536	65.20
34	1911 09 10	2638	56.60
35	1918 11 30	1660	1.20
36	1923 06 17	1965	78.50
37	1928 11 02	4988	42.50
38	1942 06 30	1700	1.80
39	1947 02 24	1012	11.90
40	1949 12 02	358	10.20
41	1950 11 25	1923	152.00
42	1956 03 01	4329	0.50
43	1968 01 07	1184	1.00
44	1971 04 05	1031	78.00
45	1974 01 30	40	4.40
46	1974 03 11	350	3.20
47	1975 02 24	278	11.80
48	1975 11 29	882	29.40
49	1978 04 29	118	27.50
50	1978 08 25	90	4.00
51	1978 11 23	253	11.00
52	1979 08 03	592	7.50
53	1981 03 17	741	33.30
54	1983 03 28	713	100.00
55	1985 03 10	599	30.03
56	1986 10 30	1106	60.00

Eruption #	**Onset** yyyymmdd	**Interevent time** [days]	**Volume** lava e tephra [$10^6 m^3$]
57	1989 11 09	765	38.40
58	1991 12 14	3503	250.00
59	2001 07 17	467	40.90
60	2002 10 27	681	131.50
61	2004 09 07	675	40.00
62	2006 07 14	669	25.00
63	2008 05 13		35.00

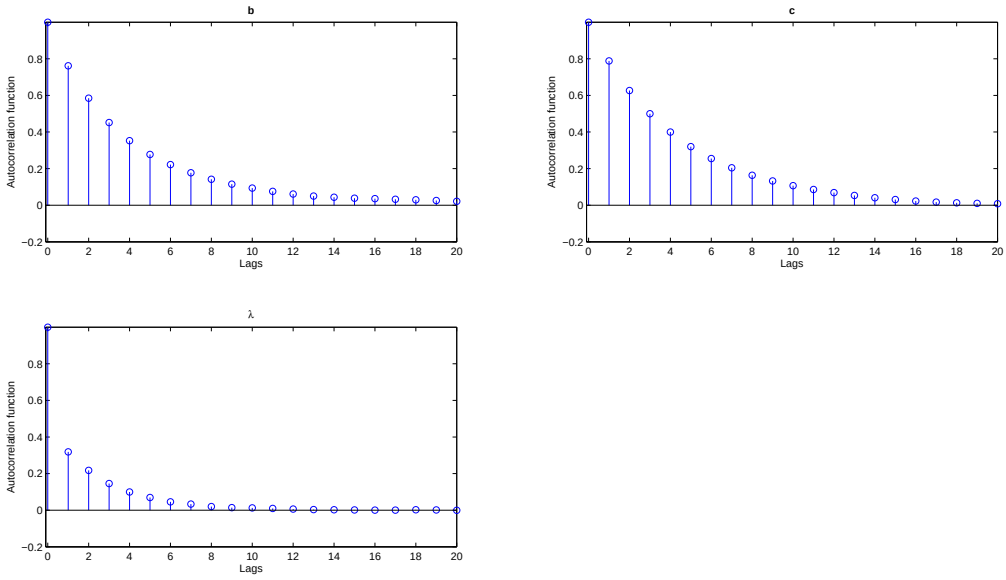

Figure 2.1: *Autocorrelation function for MCMC realizations for parameters: b top left panel, c top right panel and λ bottom left panel. The autocorrelation function is zero at lag 20, so we run each MCMC chain for 201000 iterations thinning it every 20 MCMC-steps. We obtain 10000 independent realizations for each chain.*

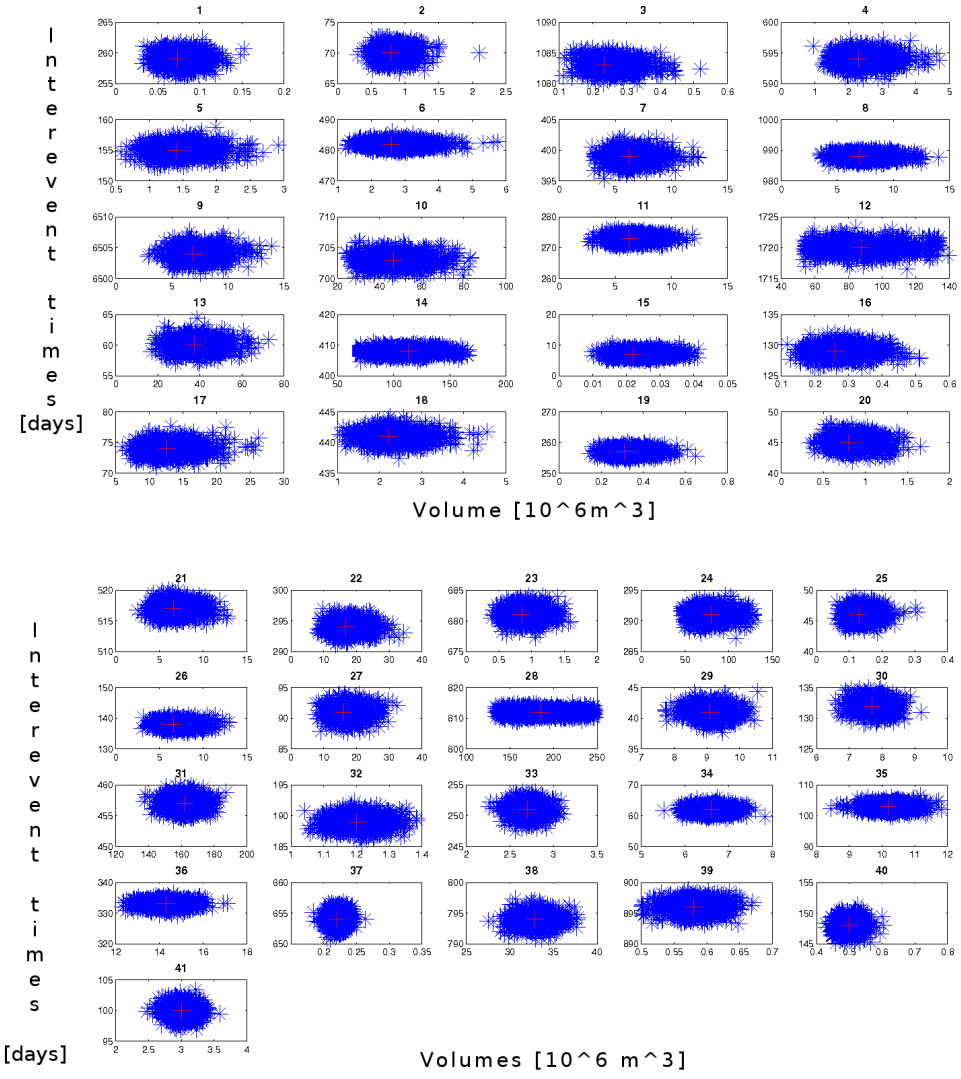

Figure 2.2: *Blue stars show the posterior distributions of pairs of simulated variables (interevent times r_i and volumes v_i). These variables are simulated via MCMC Gibbs sampling (r_i's) and Metropolis Hastings (v_i's) using all data in the catalog. The top panel is relative to r_i's and v_i's from 1 to 20 and the bottom panel from 21 to 41. Red plus is the observed data.*

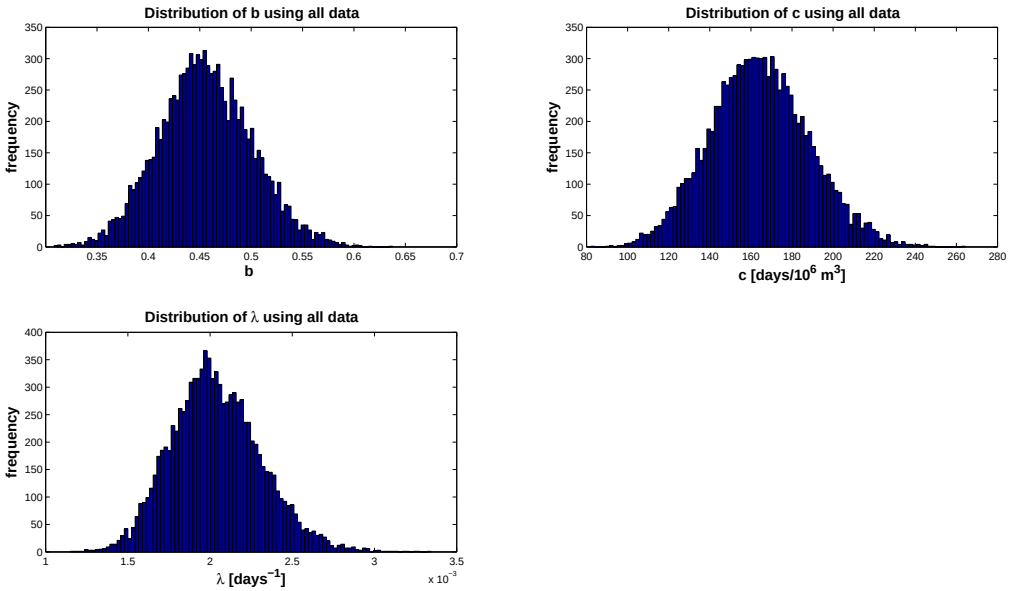

Figure 2.3: *Posterior distributions for BH_TPMII parameters obtained using all data in the catalog: top left panel refers to b, top right to c and bottom left to* λ.

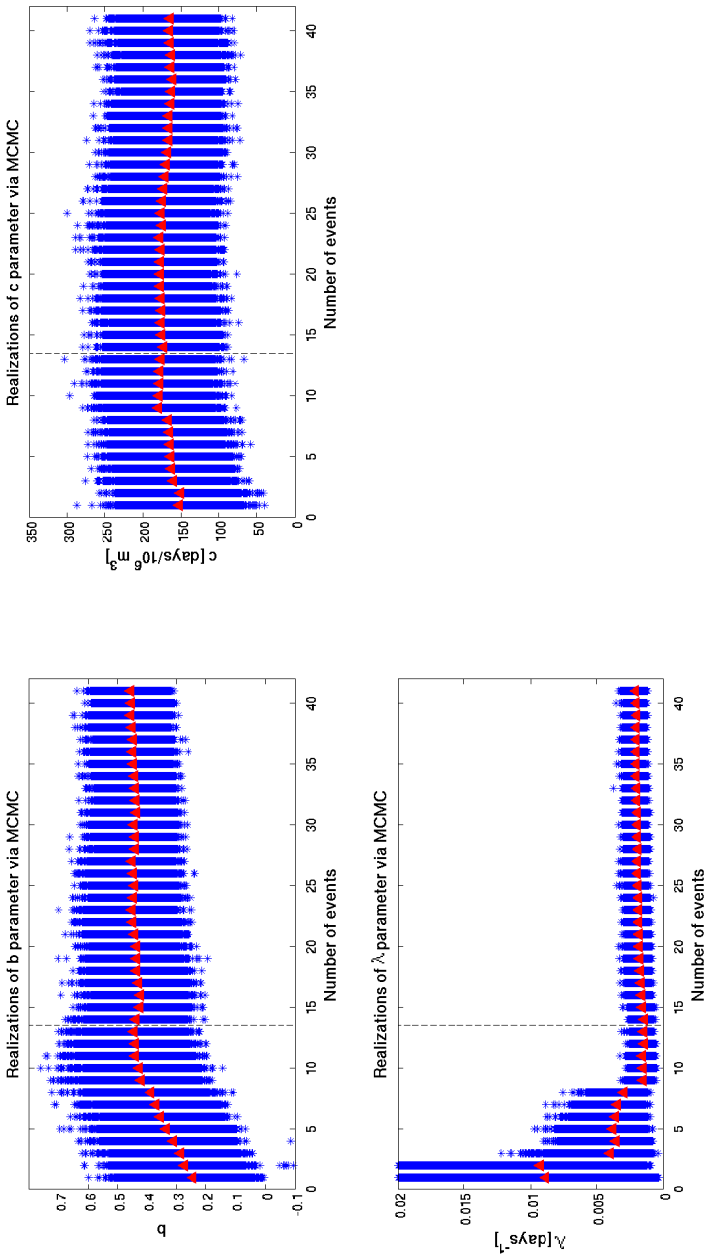

Figure 2.4: *Posterior distributions of: b parameter in top left panel, c parameter in top right panel and λ in the bottom left panel, all calculated using the sequential procedure discussed in the text. Black dashed line represents the learning phase. Red triangles are the mean of each distribution.*

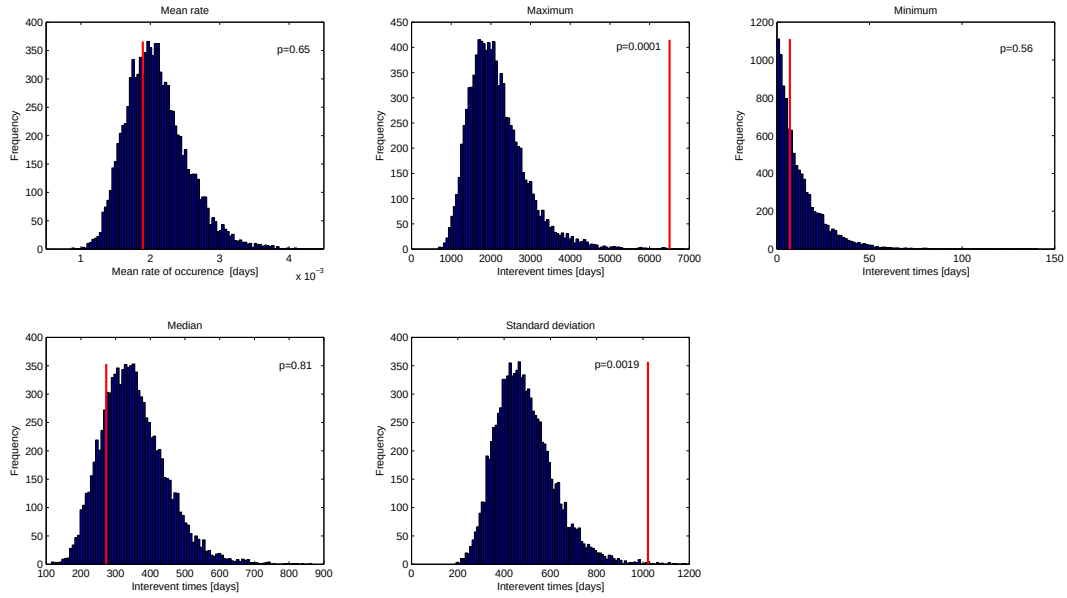

Figure 2.5: *Distributions of synthetic interevent times (blue bars) compared with observed values (red line) using descriptive statistic. This goodness-of-fit test (for more detail see the text) shows that BH_TPMII predicts synthetic interevent times in good agreement with the observed data, except for the maximum and standard deviation where the observed quantities are reproduced in the tail behavior.*

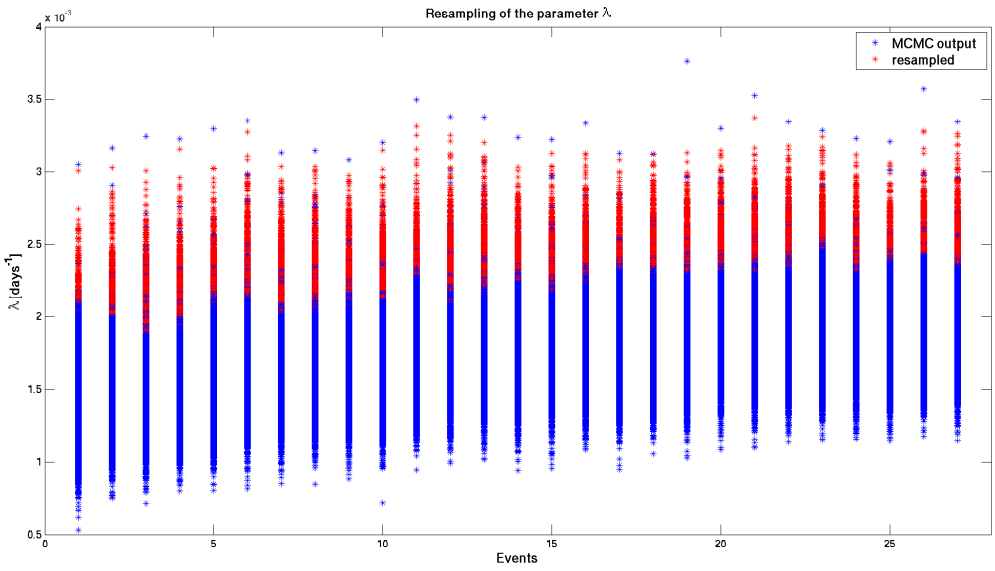

Figure 2.6: *Results for the SIR procedure applied to posterior distribution of λ's. In this plot we indicate with blue stars the posterior MCMC-realizations for λ^j while red stars refer to the resampled ones with SIR algorithm. Using the SIR procedure, described in Appendix A, we update each posterior distribution of λ with the information given by the observed volume under the sequential procedure discussed in the text. The SIR procedure is applied on λ's obtained after the learning phase as required in the sequential approach used (i.e. events from 14 to 41 in Table 2.1).*

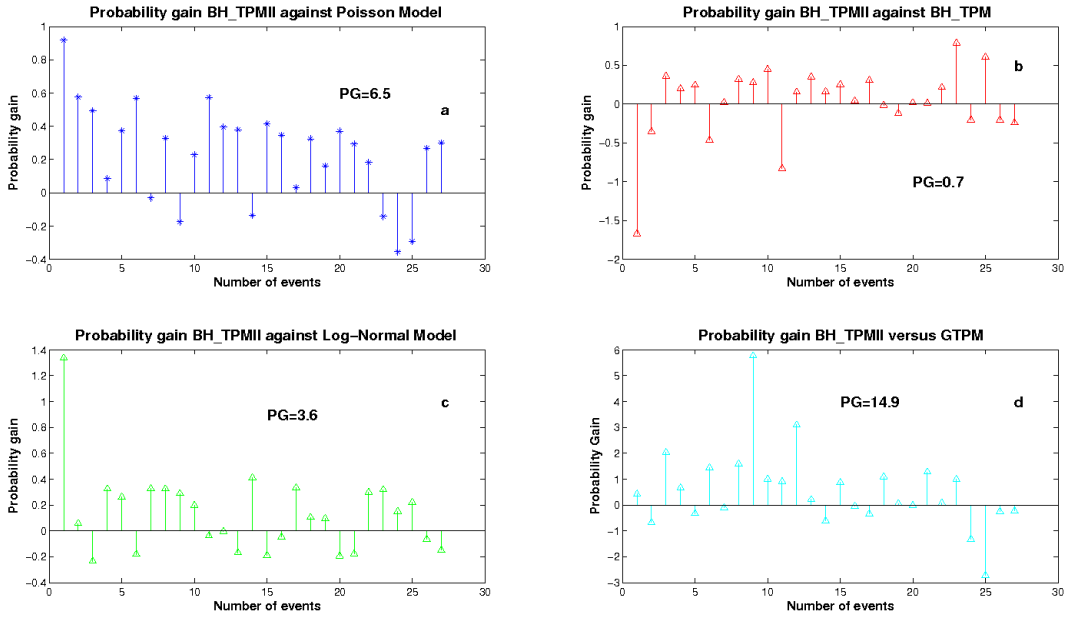

Figure 2.7: *"Punctual probability gain" of the BH_ TPMII for each event after the learning phase against: in panel* **a** *Poisson Model (Klein, 1982), in panel* **b** *BH_ TPM (Passarelli et al, 2010), in panel* **c** *Log-Normal Model (Bebbington & Lai, 1996b) and in panel* **c** *Generalized Time Predictable Model (Sandri et al., 2005). Values greater than zero indicate when BH_ TPM model performs better forecast than the reference models. The inset in each panel is the total Probability gain, i.e. the sum of the punctual probability gains.*

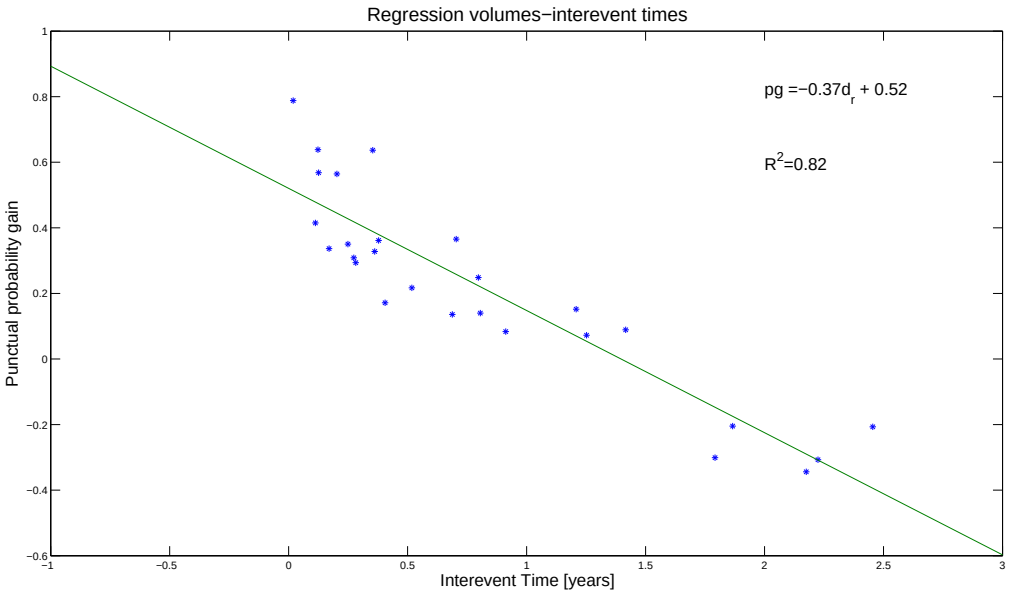

Figure 2.8: *Regression analysis for BH_ TPMII "punctual probability gain" against Poisson Model versus observed interevent times. The significant inverse linear relationship, whose best fit regression coefficients and* R^2 *are given, indicates a systematic negative probability gain for long interevent times. As discussed in the text, this means an additional complexity for long interevent times compared to the time predictable eruptive behavior. This causes a worse ability of our model, compared to Poisson model, to forecast long interevent times.*

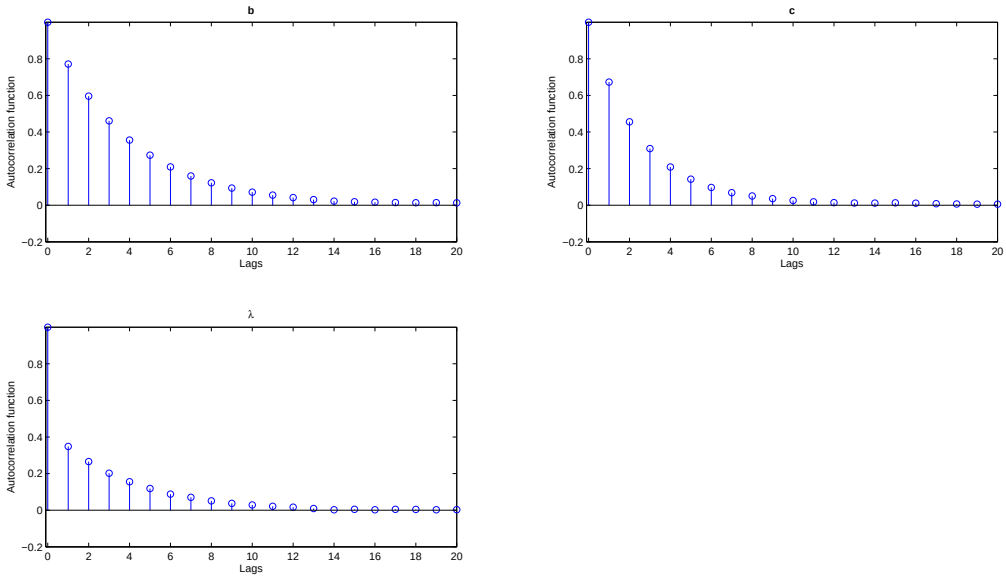

Figure 2.9: *Autocorrelation function for MCMC realizations for parameters: b top left panel, c top right panel and λ bottom left panel. The autocorrelation function is zero at lag 20. So, to obtain 10000 independent realizations for each chain, we run each MCMC chain for 201000 iterations thinning every 20 steps.*

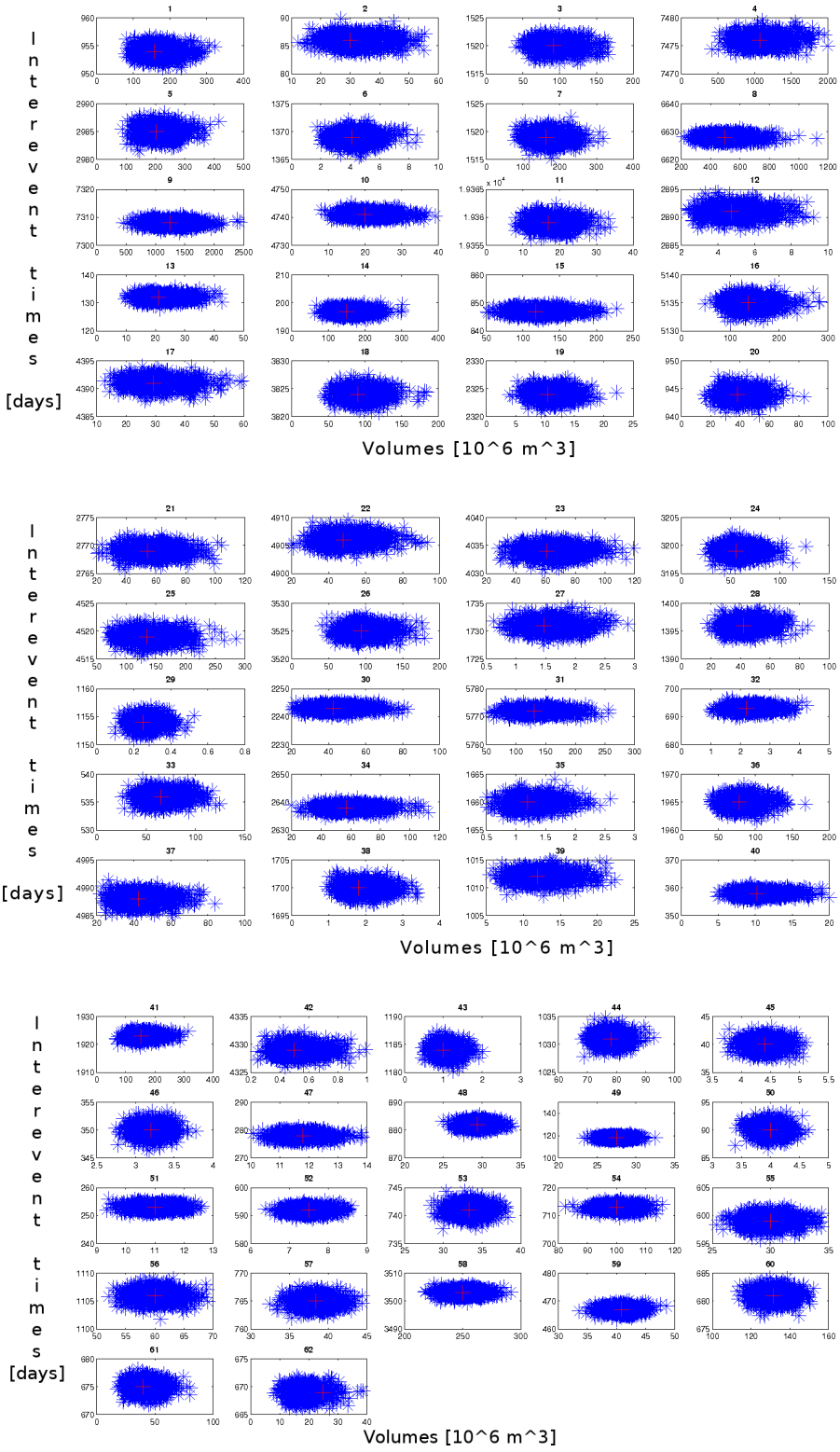

Figure 2.10: *Blue stars show the posterior distributions of pairs of simulated variables (interevent times r_i and volumes v_i). These variables are simulated via MCMC Gibbs sampling (r_i's) and Metropolis Hastings (v_i's) using all data in the catalog. From top to bottom the first panel is relative to r_i and v_i from 1 to 20, the second panel from 21 to 40 and the third panel from 40 to 62. Red plus is the observed data.*

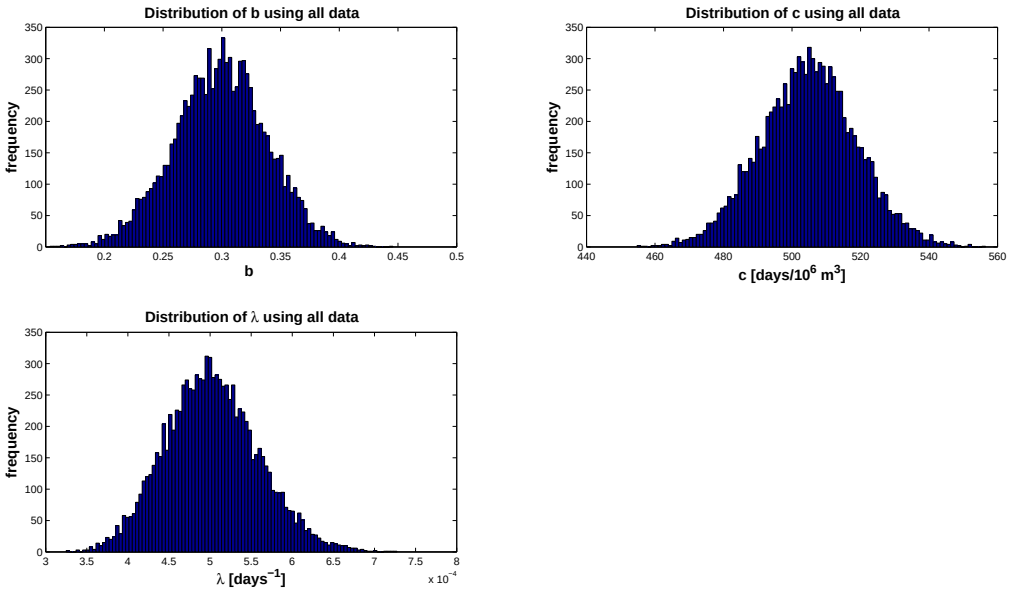

Figure 2.11: *Posterior distributions for BH_ TPMII parameters obtained using all data in the catalog: top left panel refers to b, top right to c and bottom left to λ.*

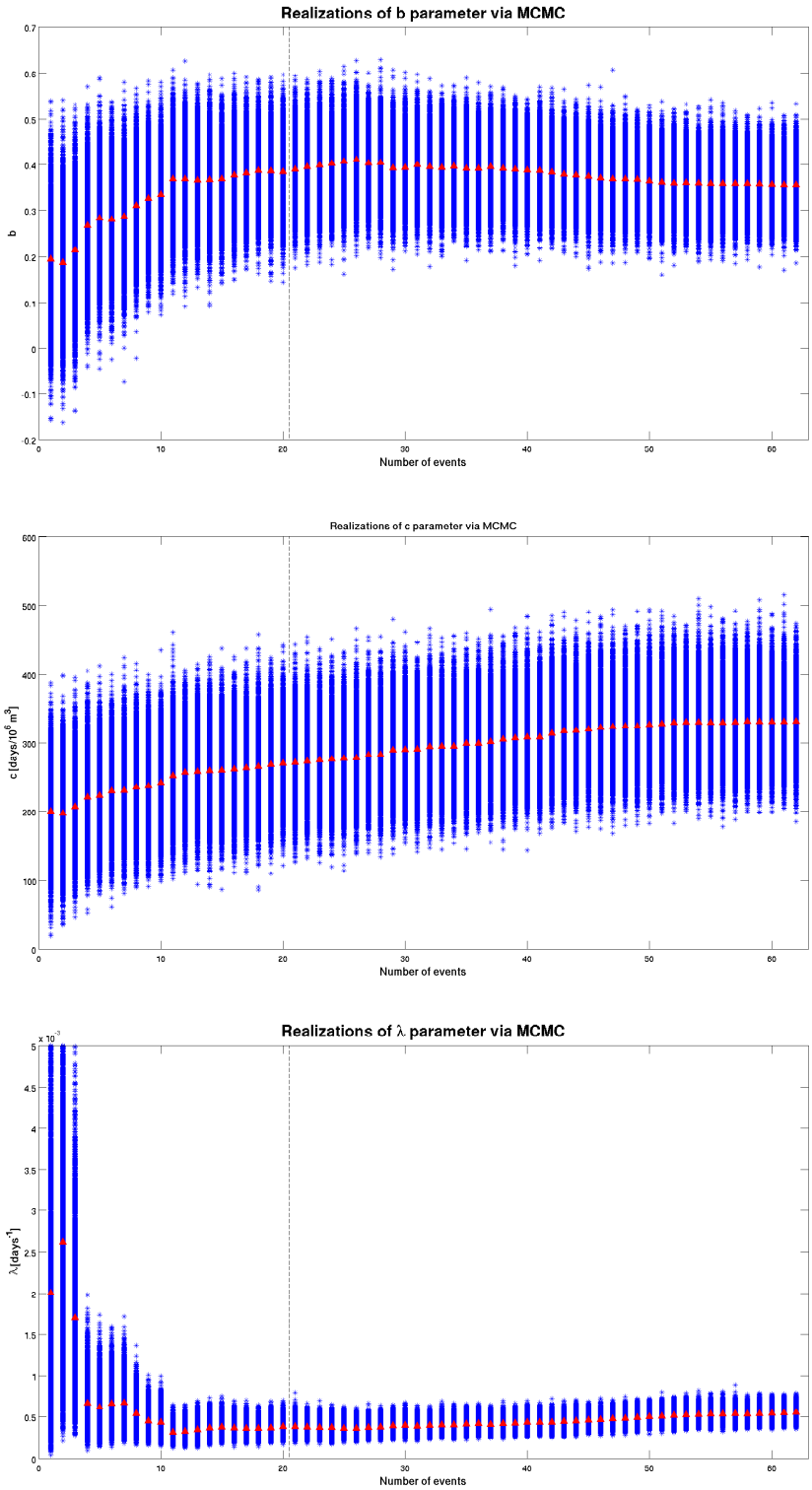

Figure 2.12: *Posterior distributions of: b parameter in top panel, c parameter in middle panel and λ in the bottom panel, all calculated using the sequential procedure discussed in the text. Black dashed line represents the learning phase. Red triangles are the mean*

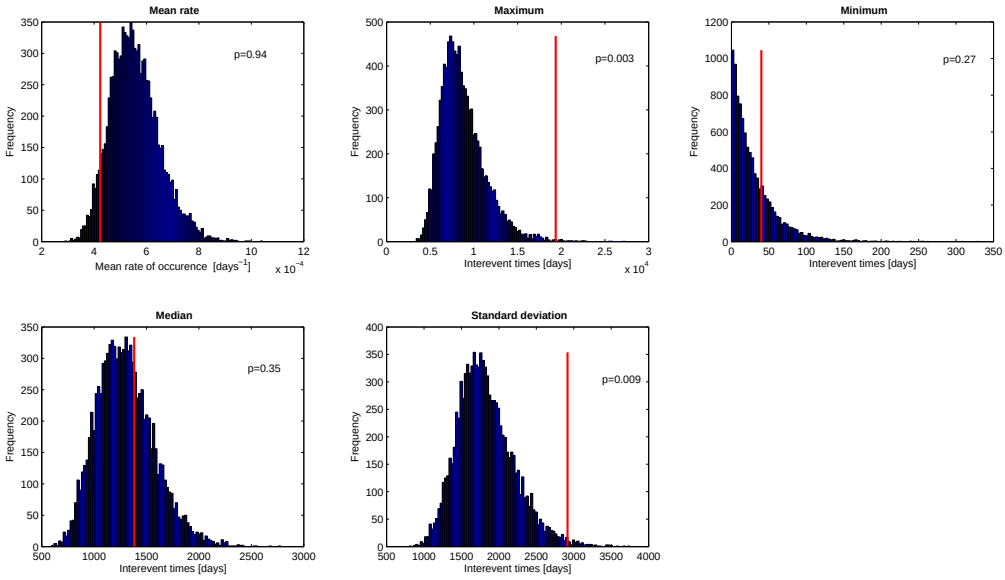

Figure 2.13: *Distributions of synthetic interevent times (blue bars) compared with observed values (red line) using descriptive statistic. This goodness-of-fit test (for more detail see the text) shows that BH_ TPMII predicts synthetic interevent times in good agreement with the observed data, except for the maximum and standard deviation where the observed quantities are reproduced in the tail behavior.*

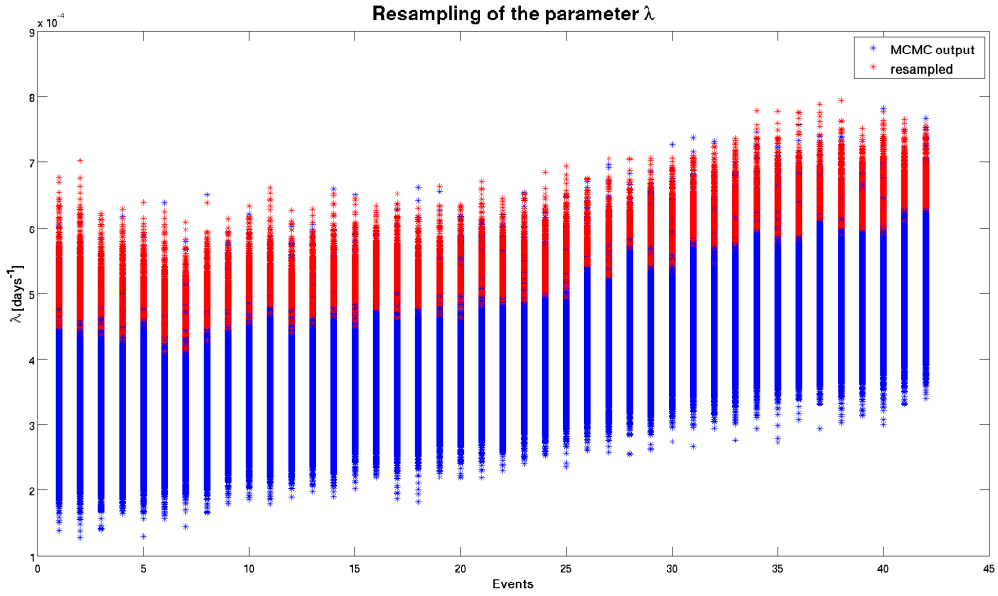

Figure 2.14: *Results for the SIR procedure applied to posterior distribution of λ's. In this plot we indicate with blue stars the posterior MCMC-realizations for λ^j while red stars refer to the resampled ones with SIR algorithm. Using the SIR procedure, described in Appendix A, we update each posterior distribution of λ with the information given by the observed volume under the sequential procedure discussed in the text. The SIR procedure is applied on λ's obtained after the learning phase as required in the sequential approach used (i.e. events from 20 to 62 in Table 1.1).*

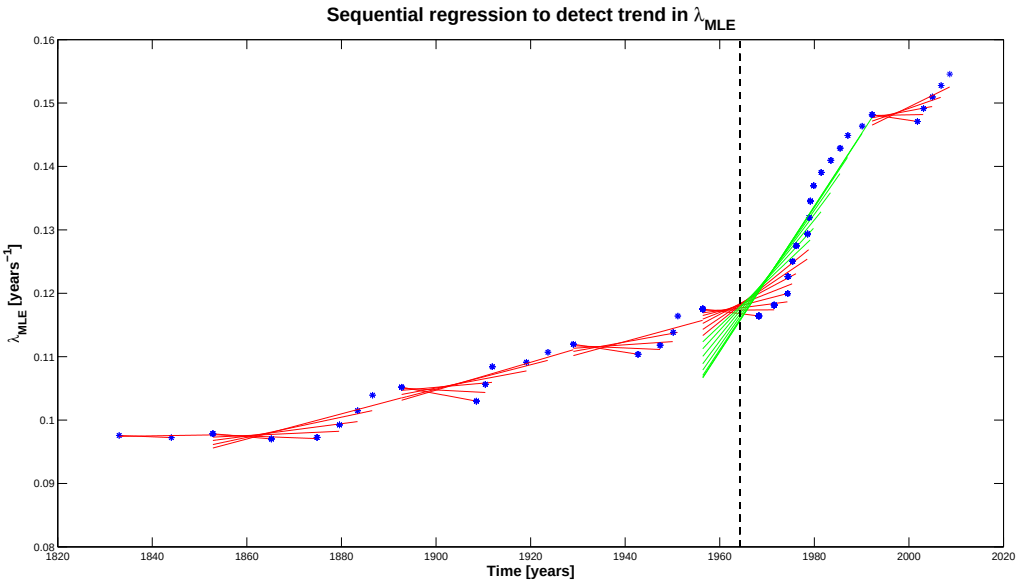

Figure 2.15: *Plot to detect the trend of intensity of a homogeneous Poisson process under the sequential procedure. Blue stars are the intensity λ_{MLE} calculated sequentially via MLE adding one data at a time plotted versus the time of each event. The λ_{MLE}'s are calculated after the learning phase. To figure out whether or not the intensity is increasing with time, we estimate its trend with linear regression, please refer to the text for more details. Red lines represent non significant regressions (at 1% level), green lines represents significant regressions. The black dashed line is the change point found by Smethurst et al 2009. Estimating sequentially the trend, one is able to detect the increasing trend only four events after the change point found by Smethurst et al., 2009, say, only after the 1975 AD eruption.*

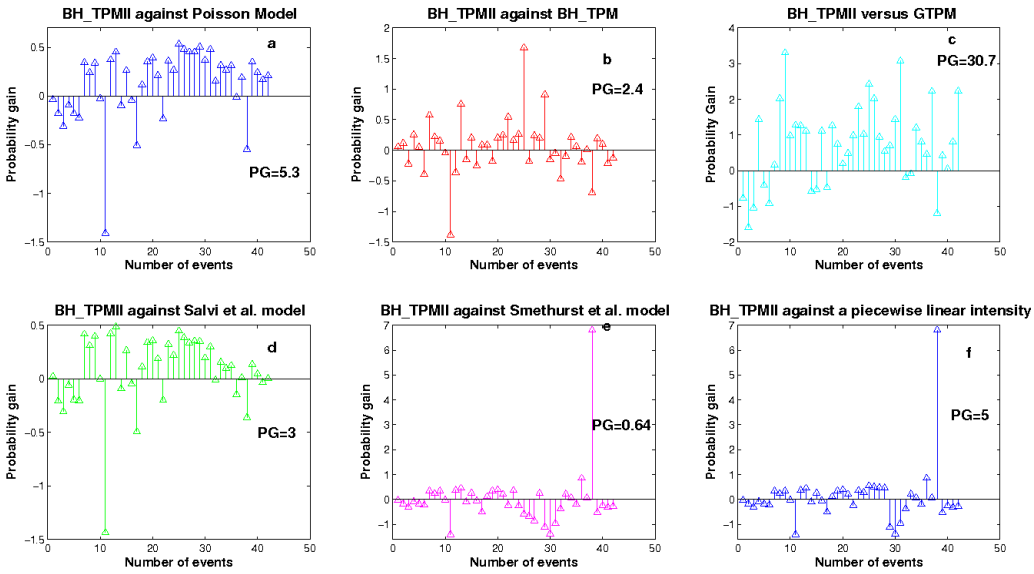

Figure 2.16: *"Punctual probability gain" of the BH_ TPMII for each event after the learning phase against: in panel* ***a*** *Poisson Model (Klein, 1982), in panel* ***b*** *BH_ TPM (Passarelli et al, 2010), in panel* ***c*** *GTPM (Sandri et al, 2005), in panel* ***d*** *Salvi et al, 2006 model, in panel* ***e*** *Smethurst et al, 2009 model and in panel* ***f*** *modified piecewise linear model of Smethurst et al, 2009 under the sequential procedure (please see the text for more details). Values greater than zero indicate when BH_ TPM model performs better forecast than the reference models. The inset in each panel is the total Probability gain, i.e. the sum of the punctual probability gains.*

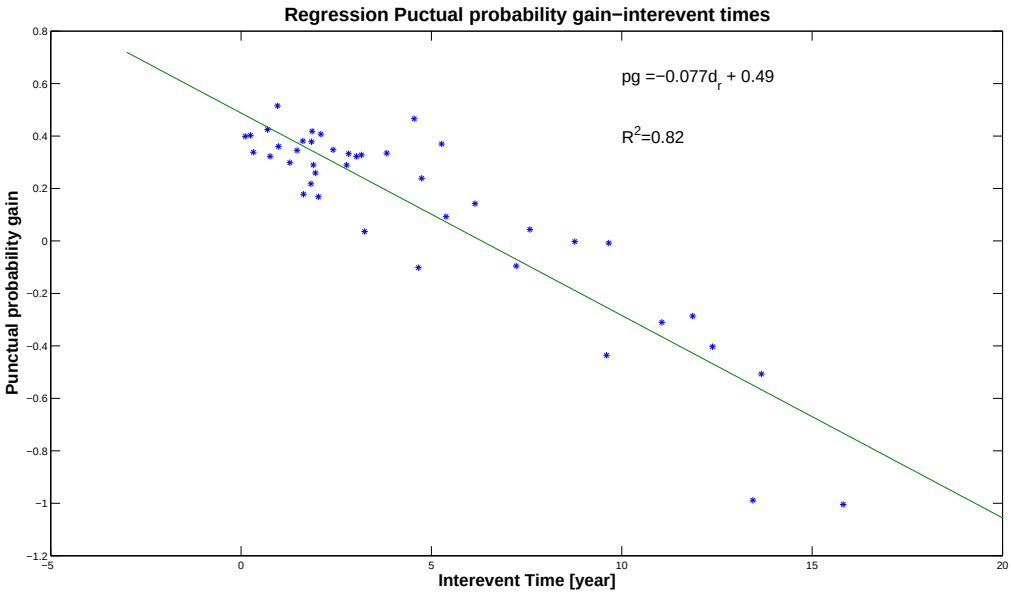

Figure 2.17: *Regression analysis for BH_ TPMII "punctual probability gain" against Poisson Model versus observed interevent times. The significant inverse linear relationship, whose best fit regression coefficients and R^2 are given, indicates a systematic negative probability gain for long interevent times. As discussed in the text, this means an additional complexity for long interevent times compared to the time predictable eruptive behavior. This causes a worse ability of our model, compared to Poisson model, to forecast long interevent times.*

Chapter 3

The Correlation Between Run-Up and Repose Times of Volcanic Eruptions

Abstract

Volcanoes usually show signs of unrest before an eruption. The intensity of these signals during the pre-eruptive phase varies greatly. Establishing physical controls on the duration of precursory activity, i.e. run-up time, could improve understanding of the dynamics of magma ascent from a shallow magma reservoir to the surface. Another observable indicative of eruption dynamics is the interevent repose time, i.e., the time between magmatic eruptions. The repose time could be associated with the mechanism that recharges the magmatic system. Both of these dynamic quantities are strongly dependent on magma composition and hence magma viscosity. In this work we investigate the inter-relationship between run-up time, repose time and viscosity by collecting together a database of 54 eruptions from 26 different volcanoes around the world. Run-up time and repose are strongly correlated with 60% of the variance in the data well-explained by a linear correlation with repose time equal to approximately 10^4 times the run-up time. The probability of the data being uncorrelated is $<0.1\%$. The data ranges from basaltic to dacitic systems, so we can investigate the gross influence of viscosity by using the silica content as a proxy. High silica, and thus by inference high viscosity, systems have longer repose times and run-up times. The run-up time observations are consistent with model where timescales are controlled by flow processes such as diking. The observed repose times are consistent with recharge rates inferred in other studies and thus appears to be reflecting the dynamics of deep crustal magma flow. The observed interrelationships provide

a new tool for constraining physical and probabilistic models for volcanic hazard mitigation.

3.1 Introduction

Volcanic eruptions commonly have geophysically observable precursors. Before an eruption, seismicity, ground deformation and gas emission may increase. The intensity of those precursory phenomena varies substantially in size and temporal duration for different volcanoes, yet most eruptions have at least some sign of the impending eruption.

The precursors are thought to be related to magma ascent beneath the volcanic edifice. For instance, at a variety of volcanoes the seismicity and ground deformation are associated with magmatic pressure, fluids exsolving from the magma chamber, and heat perturbing the stress distributions and pore fluids in surrounding host rocks (Lipman & Mullineaux, 1981; Tokarev, 1985; Yokoyama, 1988; Yokoyama *et al*, 1992; Cornelius & Voight, 1994; Druitt & Kokelaar, 2002; Newhall & Punongbayan, 1996; Aki & Ferrazzini, 2000; Yokoyama & Seino, 2000; Kilburn 2003; Cervelli *et al*, 2006; De La Cruz-Reyna *et al*, 2008). Therefore, the time of precursory activity, or run-up time, should reflect the physical properties of the magma. Most notably, viscosity should have a major effect of the dynamics of diking and thus the run-up time of activity (Rubin, 1995). However, discerning such a relationship on a single volcano is relatively difficult, in large part because of the lack of detailed constraints on the viscosity and state of the magma at depth.

Since the details of the magma viscosity are subject to large uncertainties, we need to use a large dataset which encompasses extreme variations. For that reason we focus on well-documented eruptions around the world during the last 70 years using all material available for pre-eruptive and eruptive period. Therefore, if we compare eruptions from a large variety of volcanoes with different silica-content, we can assemble a data set where viscosity of the magma varies by 7 orders of magnitude and thus becomes the most dominant parameter in the system.

In addition, magma viscosity may play a role in controlling another observable of the system: inter-event repose time. The time between eruptions is controlled by the recharge of the magma chamber and the accumulation of pressure. Both of these processes are also sensitive to magma viscosity and thus might be expected to vary from volcano to volcano. Again, a study at a single edifice would be difficult, but capitalizing on the large viscosity

variations from edifice to edifice might be instructive.

In this paper we investigate the interrelationships among run-up time, recurrence interval and viscosity by using 54 eruptions. Repose time, run-up times and silica content of each event are listed in Table 3.1. First, we take some time to carefully define and discuss the operational definitions of repose time and run-up time. Next we observe a strong correlation between recurrence time and repose time along with a dependency on petrology. We will then translate the petrologic constraints into viscosity using a rough proxy model based on silica content. Finally we interpret our results as manifestations of the control of viscosity via diking on the precursory process and magma recharge rate on the inter-eruptive processes.

3.2 Definitions

We define the time associated with a precursory phase before a magmatic eruption as the run-up time. The run-up time t_{run-up} is the time elapsed from the onset of observed magmatic unrest to the onset of a magmatic eruption. The run-up time defined in this way should be related to the time taken by the magma to move from a magma chamber to the surface. Although this definition of run-up seems a very straightforward one, it leads us to deal with very complicated questions: 1) How do you define a starting point for a magmatic eruption? 2) How do you define the starting point of magmatic unrest?

To answer question (1), we define the start of an eruption as when juvenile magma material is detected at the surface. Despite this simple definition, sometimes this information is not easily available for explosive eruptions because phreatic and phreato-magmatic activity can obscure when juvenile material is first ejected. We tackle this problem using information available in literature about petrography and petrology of the eruptive products. In Table 3.1 there are also indicates references for the magmatic composition and petrography of each eruption.

For most eruptions the onset time is well known with an error of at least 1 day, but for some historical eruptions it is impossible to know when juvenile material is ejected first. For eruptions without a clear onset in the literature we use the start date given by Smithsonian Institution-Global Volcanism Program datasets. In cases both day and month of an event are unknown we use 01 January as the onset date together with the given year. The relative error introduced by this approximation is always $<1\%$ and thus we can neglect it for all cases.

When only year and month are specified we use the 15th day of the month as a onset date.

Answering question (2) is a difficult matter. The defined starting point for volcanic unrest depends on the ability to detect precursory volcanic signals above variable background levels, and it is unavoidably related to a particular type of volcano. Signs of pre-eruptive unrest vary and eruptions in this study include both examples of elevated seismicity and increased ground deformation (See below). In addition the data for precursory activity usually are not easily available, are often strongly heterogeneous and in some cases are only qualitative (see Newhall & Dzurisin, 1988, Simkin & Siebert, 1994, Benoit & McNutt, 1996). This makes it very difficult to set a comprehensive scheme for defining the onset date of magmatic unrest and the relative run-up time for volcanic eruptions.

Our strategy in dealing with this complicated problem has arisen from reading the scientific work and reports about eruptions around the world. Given the great variability among eruptions and scarcity of detailed pre-eruptive data available for direct interpretation, we have deferred to the authors of each study and used the local definition of run-up time for this work. This strategy is inherently dangerous both because it does not use a quantitative or precise definition of background and because it uses a posteriori interpretation given by authors about volcanic signs. For instance, it does not account for the highly variable ability to detect precursory activity depending on the frequency of visual observation and the proximity to geophysical monitoring instrumentation. However, it is the only easily accessible method since there is no worldwide volcanic geophysical database available.

In many studies made after an eruption, authors describe the characteristics and duration of precursory activity well. For example in Aki & Ferrazzini (2000, Table 3), the authors give clear information about the precursory activity for eruptions from 1985 to 1996 at Piton de la Fournaise, a well-monitored volcano. This single dataset allows comparison of multiple eruptions in a consistent way. Another very helpful work about Popocatepetl Volcano 1994 eruption and its very long precursory activity is made by De la Cruz-Reyna *et al* (2008). In this case, the documentation is sufficient to make reasonable statements about the precursory activity for even a single event. Similar quantitative studies we found elsewhere in the literature identify the starting point for a magmatic unrest. The precise sources of documentation for each eruption in this study are listed in Table 3.1.

In most of these studies the time for the precursory activity is indicated by precursory

seismicity (see for example Tokarev, (1985); Yokoyama, (1988); Yokoyama *et al*, (1992); Gil Cruz & Chouet, (1997); Yokoyama & Seino, (2000); Soosalu *et al*, (2005) Table 1); a few cases have ground deformation and seismicity (for example Lockwood *et al*, (1987)) and one case has only ground deformation (Cervelli *et al*, 2006). To double check the information taken from the literature, we used the monthly and weekly report of Global Volcanism Program (www.volcano.si.edu) as a source of information. For example in the case of the 1999 eruption of Tungurahua Volcano there is no literature regarding the precursory activity, so we integrate the information from monthly report BGVN 24:11 from Global Volcanism Program web sites (http://www.volcano.si.edu). For such events where we found some discrepancy between seismicity and deformation as precursory signals, we always refer to the seismicity for the run-up time value. When only the month of precursory activity is known, we conventionally use the 15th day of the month as a starting date.

We also collected data on the relative repose time or interevent time t_{repose} defined as the time elapsed between two subsequent eruptions. As stated before, we consider the onset of an eruption as the time when first juvenile material is present in volcanic ejecta. We use the onset time rather than duration to define the time between eruptions (Klein, 1982, Mulargia, 1985, De la Cruz-Reyna, 1991, Burt *et al*, 1994, Bebbington & Lai 1996, Sandri *et al*, 2005, Marzocchi & Zaccarelli, 2006). The cited literature was supplemented by the Global Volcanism Program records to determine the eruptive history (See Table 3.1 for detailed onset times).

Finally we collected information for magma composition and silica content. However not all eruptions considered have direct petrologic data. In cases where we do not know the exact magma composition for a particular eruption, we use the magma composition information from the most recent eruption of that volcano. When more than one magma composition is given for a particular eruption we use the mean. Finally, we reserve a special mention for the 18 Piton de la Fournaise events. Direct compositional information from Villeneuve *et al* (2008) was available only for 1983, 1986 and 1998 eruptive event. Hence for all events between 1985 and 1998 we use the 1986 silica content which appears reasonable as Peltier *et al* (2009) suggest that there is no strong variations in the magma composition in the last 30 years (See Table 3.2).

For each eruption included in this analysis we report the volcano name, silica content, run-up time, repose or interevent time, volume erupted (tephra and lava) and reference list in

Table 3.1.

3.3 Observations

The data we have collected are shown in Figure 3.1. The log-log plot shows the repose and run-up times together with their magma composition. Petrological types are categorized by silica content using the standard classification of Le Bas *et al* (1986).

At first glance it is easy to see that both run-up and repose times vary over about six order of magnitude. For basaltic volcanoes repose times are of the order of months to a few years and run-up times are of the order of minutes to a few days. For high silica volcanoes repose times are of the order of several years up to several centuries and run-up time of the order of days to several months. The ratio between the run-up and repose times is always less than 1% except for 8 events which are less than 10%. Run-up time is always much shorter than repose time, so the first phenomenological evidence here is that the pre-eruptive activity is a small fraction of the time between two eruptions, which is consistent with our operational definitions.

The main physical insight from this plot is that repose times and run-up times are positively correlated. This is corroborated by the simple linear fit of the logarithmic data (Figure 3.1). The high value of R^2=0.60 in log-log space means 60% of the data are explained by the linear regression model. The value of R^2 allows us to reject the hypothesis of uncorrelated values (i.e. slope equal to zero) with an error of <0.001 (i.e. P-value of the hypotheses testing), according to an F-test (Draper & Smith, 1998). The P-value is the risk associated with rejecting the hypothesis, so in this case the probability that we have inappropriately rejected the uncorrelated hypothesis is less than 0.1%. The observed ratio of the repose times and run-up time in Figure 1 ranges between 10 and 10^5.

However, a regression is not sufficient to fully prove the significance of the correlation for these data. In regression analysis the data are assumed to have constant variance. In this case we can not say easily that run-up times have constant variance, because we can not know their exact errors. The error associated with run-up times is strongly dependent on the resolution with which one volcano is monitored and varies over time. Therefore, the goodness of fit test could be biased by the assumption of constant variance. So to corroborate our analysis, we perform a bootstrap regression analysis with 1000 data permutations and without any

assumption on the data. The bootstrap mean for the slope is 1.1 ± 0.1 and for intercept is -3.5 ± 0.3 where the error bars are 1 standard deviation. These values are again resolvably positive and we conclude that the positive correlation is robust.

Another observation in Figure 3.1 is that the magma composition seems to be correlated with run-up and repose times. Because the SiO_2 for Piton de la Fournaise eruptions has the same value for several eruptions, a different test of correlation is necessary than before. The repeated values will bias a regression and therefore we directly compute the correlation coefficient ρ from the raw data rather than embarking on a fit and interpreting R^2. The distinction is that R^2 tests the correlation between the prediction of a linear fit and the observed data, while ρ is simply a measure of the correlation between the variables, i.e., the covariance divided by the standard deviation of each individually (Draper & Smith, 1998). We found ρ=0.35 (P-value =0.01, null hypotheses is correlation coefficient equal to zero) for repose times and silica content and ρ=0.31 (P-value=0.02 null hypotheses is correlation coefficient equal to zero) for run-up times and silica content. The significantly greater than zero correlation value implies a relationship between the parameters, although it is not as strong as the relationship between repose and run-up times. The observation indicates that using the silica content as a fundamental parameter in describing the pre-eruption dynamics may be productive. But it is also a warning that other physical parameters like the crystal content in magma, magma temperature, tectonic and local stress distribution must be taken into account to fully model the pre-eruptive dynamics.

3.3.1 Unusual Individual Eruptions

Much of the scatter in Figure 3.1 is likely due to the great variability of individual eruptive circumstances. It is helpful to outline the limits of the proposed relationships by reviewing some of the peculiarities of the individual data points that lead to significant departures from the trend.

Shishaldin Volcano 1999 eruption shows a very long pre-eruption activity compared with other basaltic volcano with a run-up time that is 1/4 the repose time. This unusual ratio goes with an unusual sequence that includes a hiatus in the middle of the precursory activity. The precursory activity we consider here starts in late June 1998 with a series of small low-frequency earthquakes that continued until the end of October 1998. After October, the volcano became

quiet until the new increase in the precursory activity in early February, possibly indicating a new or renewed intrusion (Nye *et al*, 2002; Moran *et al*, 2002). Measuring the precursory interval from February results in a ratio of 1/40, which is still different from the mean, but less extraordinary. In Figure 3.1 and subsequent interpretations, we maintain consistency with the operational definition of Section 3.2 by choosing June 15, 1998 as the onset time, although it is possible that a shorter one would have been more appropriate physically.

Less easy to explain are Hekla and Okmok eruptions. These voluminous basaltic andesite eruptions have repose times consistent with their moderate silicate composition, but run-up times more typical of low silica systems, i.e., shorter than expected. The anomalously short warning was anecdotally noted for both systems as a cause for consternation to local observatories (Soosalu *et al*, 2005; Prejean *et al*, 2008). We speculate that in these systems, late stage evolution may have dropped the viscosity resulting in relatively fast magma migration to the surface.

3.4 Interpretation in terms of viscosity

To interpret the observations, we first need to translate the data into a likely physical control like viscosity. In order to do this, we will use the most important control on gross viscosity, silica content, as a means to delineate the variations between eruptive systems. Once this translation is complete, we will then model the run-up time in terms of viscous processes. The test of the model will be whether or not it predicts the observed ratio of run-up to viscosity for a reasonable set of model parameters. For repose time, we will not embark on a full-scale model but will rather connect the data to previous observations and models of inter-eruptive intervals.

3.4.1 Viscosity based on Silica content

Starting from the petrologic information available, we calculate the viscosity of magma for 17 events in catalog using the Conflow software package (Mastin & Ghiorso, 2000). Then we find a best-fit relationship between the viscosity and the relative silica content assuming that the log-viscosity varies linearly with silica content. Finally, we use this fit to infer the viscosity for all data in Table 3.1 from the silica content. Details about eruptions, magma

compositions and temperatures setting for Conflow are in Table 3.2. For all eruptions we choose to use a melt composition with 0 wt % of water owing to the lack of information about the magma melt water content. This dry viscosity may be an overestimate by as much as an order of magnitude. Since we are focusing on the gross variations of viscosity associated with silica content, this assumption will need to suffice. In the process of inferring viscosity, we are neglecting several other significant controls such as crystallinity and vesicularity. The justification for relying solely of silica content as a proxy is that silica content is the most reliably measurable parameter for the dataset and thus allows us to generate a reasonably uniform approximation. Furthermore, since eruptive temperature and silica content co-vary, regressing with respect to silica content captures the first-order viscosity signal robustly. The results for the linear best fit are in Figure 3.2. Again, we perform the F-test on the slope of the regression under the null hypotheses that the slope is equal to zero, and we reject with P-value$<$0.01. As stated before, we use the regression line to estimate the viscosity for all 54 events in the catalog from their SiO_2 content. This result is similar to Hulme (1976). The resultant viscosity for all events varies over 7 orders of magnitude from 10^1 to 10^8 Pa-s (Table 3.2). The calculated viscosity can now be used to study the compatibility of a simple physical model and the data. Performing the translation between silica content and inferred viscosity leads to Figure 3.3. Here the trends of increasing run-up and repose time with increasing silica content become clearly tied to increasing viscosity. The run-up time in seconds is on the order of 10^{-4} to 10^3 times the viscosity in Pa-s (or time in days is 10^{-9} to 10^{-2} times viscosity). The repose time in seconds is 10^1 to 10^5 times the viscosity in Pa-s (or time in days is 10^{-4} to 10 times the viscosity). We do not further quantify the correlation between repose time and run-up time with respect to viscosity simply because we will obtain the same result discussed for the correlation with silica content. Therefore, we will proceed to investigate physical models for the control of viscosity on both times.

3.4.2 Model for Run-up Times

We defined run-up time as a proxy for the time necessary for magma to travel from the magma chamber to the surface. We now model this process as a dike intrusion event. We will predict dike propagation time (and hence run-up time) as a function of viscosity by considering the movement of a pressure-driven, magma-filled crack. The observed run-up time to viscosity

ratio $\alpha = t_{run-up}/\eta$ is between 10^{-4} Pa^{-1} and 10^{3} Pa^{-1}, with mean value approximately equal to 10 Pa^{-1} . The mean value a is calculated as the mean ratio of the run-up time and the viscosity in logarithmic space. We use here the arithmetic mean of logarithm of run-up's and viscosities because these quantities vary over seven order of magnitude. The test of the model will be whether or not we can successfully predict this mean value for realistic parameters. The dike will be modeled as a 2-D planar pressure-driven crack with elliptical shape and minor axis w much smaller than the major axis and height L, propagating in an elastic medium subjected to a regional stress (Rubin, 1995). By analyzing the Poiseuille flow for a viscous fluid in a elliptical crack where the perturbation to the host rock stresses and the displacement due to the dike opening depend only upon the difference between internal magma pressure and the ambient compressive stress, Rubin (1995) calculates the velocity of the dike (Rubin, 1995). The order of magnitude dike propagation velocity under a linear pressure gradient p_0/L, assuming a laminar flow in the height direction, is given by:

$$u = \frac{1}{3}(\frac{p_0^3}{M^2})L \tag{3.1}$$

where η is the viscosity, p_0 is the magma pressure at the dike entrance, M is the elastic stiffness, L is the dike height and $w = (p_0^3/M^2)L$ is the half dike thickness (see Rubin, 1995).

The time necessary for ascent from the magma chamber to the surface is the propagation time of a dike with height L equal to the depth of magma chamber below the surface (Figure 3.4). Therefore,

$$t_{run-up} = \frac{L}{u} \tag{3.2}$$

Combining equation (3.1) and (3.2) we can evaluate the run-up time in terms of the viscosity

$$\alpha = \frac{t_{run-up}}{\eta} = \frac{3M^2}{p_o^3} \sim 10Pa^{-1} \tag{3.3}$$

when the pressure is $p_0 = 6$ MPa and the elastic stiffness is $M = 3 \times 10^{10}$Pa. For these reasonable parameters, the result is identical to the mean value of the observations. At this point the run-up times seem to be compatible with the dynamics of magma ascent, even though we are using a very simple model.

3.4.3 Model for Repose Times

Between eruptions, the magma chamber is recharged by a series of intrusions from depth. The speed of each individual intrusion is again related to viscosity through some combination of diking, diapirism and porous media flow (Annen *et al* 2006; Karlstorm *et al*, 2009). In all of these processes, recharge rate is inversely proportional to viscosity, therefore the higher silica systems are expected to take longer to fill a magma chamber and accumulate sufficient overpressure for an eruption. Studies of the duration of magma transfer in the crust based on uranium-series disequilibria show that magma differentiation time (i.e. cooling and crystal-liquid separation) is a function of silica content with high silica magma having greater intervals storage in crustal magma reservoir than low silica magma (Reid, 2003). Storage time from crystal ages for basaltic system are generally longer or equal to repose times; for higher silica systems the storage times are comparable or slightly shorter than repose times (White *et al*, 2006). A complete model of magma chamber recharge processes is beyond the scope of this paper. One simple conceptualization of magma reservoir is a storage system to which mass enters with a particular rate Q_i and is extracted at particular rate Q_e. In such cases when input and output are equal, i.e. $Q_i = Q_e$, it may attain quasi-steady-state condition and the magma residence time could be defined as VxQ_e^{-1} (Reid, 2003). Only fewer than 30% or likely the 10% of the sub-aerial volcanoes approximate these conditions (Pyle, 1992). For other volcanoes eruption is not the only output of magma reservoir: there is also sub-surface magma solidification as plutonism. In these non-steady-state cases, $Qi \leq Qe$ and the relationship between residence times and volumes is only approximate (Reid, 2003).

Here, we simply show that the observed repose time trend is consistent with recharge rates inferred by other means and thus appears to be reflecting the dynamics of deep crustal magma flow. We can make this connection by converting the repose time information into volcanic eruption extrusion rates, which is a quantity previously studied. The repose time is related to the extrusion rate Q_e by

$$Q_e = V/t_{repose} \tag{3.4}$$

where V is the volume of an individual eruption. From the information in Table 3.1, the average Q_e for the basaltic volcanoes is $(3.8 \pm 0.1) \times 10^{-2} Km^3/yr$, for basaltic andesites is $(3.7 \pm 0.9) \times 10^{-2} Km^3/yr$ for andesites is $(7.6 \pm 2.0) \times 10^{-3} Km^3/yr$ and dacites is $(5.1 \pm 1.0) \times 10^{-3} Km^3/yr$. Errors for extrusion rate are calculated using the error propagation formula

assuming a relative error for repose times and volumes equal to 1% and 25% respectively.

White *et al* (2006) inferred values for the output rate for a wide class of volcanism worldwide grouping volcanoes in only three class: basaltics, andesites and rhyolites. For those class of volcanoes they calculate average extrusion rates equal to $(2.6 \pm 1.0) \times 10^{-2} km^3/yr$, $(2.3 \pm 0.8) \times 10^{-3} km^3/yr$ and $(4.0 \pm 1.4) \times 10^{-3} km^3/yr$, respectively. The average output rates here calculated are compatible within the error bars those presented by White *et al* (2006) except for the the output rate of andesite volcanoes (Figure 3.5). The mean values are somewhat higher in this study. The discrepancy may in part be due to a difference in dataset definitions. White *et al* (2006) defined "repose time" as the duration between characteristic sized eruptions while here we study the interval between eruptions of any size and define Q_e based on the volume erupted after the repose interval. Despite the difference in absolute values, Figure 3.5 in both datasets shows a decreasing trend with silica content. This trend is compatible with the fact that high silica systems show longer repose times compared with basaltic ones. As a first order approximation, it should be seen as the role played by the viscosity in the magma reservoir recharging process (Reid, 2003). Finally this simple comparison highlights how the low silica systems take shorter time to refill the magma reservoir than high silica system, assuming the output rate as a rough measure of the magma recharge rate. For low silicic volcanoes with relatively low viscosity the recharge rate is higher; high silica systems show very low recharge rate compatible with their higher viscosity.

3.5 Conclusions and Implications for Eruption Forecasts

In this work we show the interrelationship between repose time, run-up time and viscosity. The data presented suggest a strong positive correlation between repose time and run-up time for all classes of magma composition volcanoes. In addition, both times seem to correlate with silica content and, therefore with gross variations in magma viscosity. Using extremely simplified models of magma ascent immediately before an eruption, we successfully match the observed dependencies of the run-up time times on viscosity. Propagation of a single, pressure-balanced dike from the chamber is consistent with the run-up time data. Using the relationships between run-up and repose time observed here provides a way to design a prediction window appropriate to a particular magmatic system. For instance, if unrest begins on a low silica system with short quiescent period, one should expect an eruption to occur

within hours to days, if it is going to happen. On the other hand, for a high silica system that has experienced a very long quiescent time, an alert period should remain open for a much longer period of time from days to years.

Bibliography

[1] Aki, K. & Ferrazini, V., 2000. Seismic monitoring and modeling of an active volcano for prediction, *J Geophys Res*, 105 B7, 16,617– 16,640.

[2] Annen, C., J.D. Blundy & R.S.J. Sparks. 2006. The genesis of intermediate and silicic magmas in deep crustal hot zones, *J of Petrology* 47(3), 505–539.

[3] Bebbington M.S. & Lai, C.D., 1996. Statistical analysis of New Zealand volcanic occurrence data, *J Volcanol Geotherm Res*, 74, 101–110.

[4] Benoit, J., R. & McNutt, S.R., 1996. Global volcanic earthquake swarm database 1979-1989. USGS Open-File Report 1996, 69, US Department of the Interior, Washington DC.

[5] Burt, M.L., Wadge, G. & Scott, W.A., 1994. Simple stochastic modeling of eruption history of basaltic volcano: Nyamuragira, Zaire, *Bull Volcanol* 56, 87–97.

[6] Cervelli, P. F., Fournier,T., Freymueller,J. & Power,J.A. 2006. Ground deformation associated with the precursory unrest and early phases of the January 2006 eruption of Augustine Volcano, Alaska, *Geophys Res Lett*, 33, L18304, doi:10.1029/2006GL027219.

[7] Cornelius, R.R. & Voight, B., 1994. Seismological aspects of the 1989-1990 eruption at Redoubt Volcano, Alaska: the Materials Failure Forecast Method (FFM) with RSAM and SSAM seismic data, *J Volcanol Geotherm Res*, 62, 469–498.

[8] De La Cruz-Reyna, S., 1991. Poisson-distributed patterns of explosive eruptive activity, *Bull Volcanol*, 54, 57–67.

[9] De la Cruz-Reyna, S., Yokoyama, I., Martinez-Bringas, A. & Ramos, E., 2008, Precursory seismicity of the 1994 eruption of Popocatepetl Volcano, central Mexico, *Bull Volcanol* 70, 753–767.

[10] Draper, N.R. & H. Smith, 1998, Applied Regression Analysis, 3rd Ed., Wiley.

[11] Druitt T.H. & Kokellar B.P., 2002. The eruption of Soufriere Hills volcano, Montserrat, from 1995 to 1999, Geol. Soc. London. Mem.

[12] Gil Cruz, F. & Chouet, B., 1997. Long-period events, the most characteristic seismicity accompanying the emplacement and extrusion of a lava dome in Galeras Volcano, Colombia, in 1991, *J Volcanol Geotherm Res*, 77, 121–158.

[13] Hulme, G., 1976. The determination of the Rheological proprierties and effusion rate of an Olympus Mons lava, *Icarus*, 27, 207–213.

[14] Karlstrom, L., Dufek.,J. & Manga, M., 2009. Magma chamber stability in arc and continental crust, *J Volcanol Geotherm Res*, doi:10.1016/j.jvolgeores.2009.10.003.

[15] Klein, F.W., 1982. Patterns of historical eruptions at Hawaiian Volcanoes, *J Volcanol Geotherm Res*, 12, 1–35.

[16] Kilburn C.R.J., 2003. Multiscale fracturing as a key to forecasting volcanic eruptions, *J Volcanol Geotherm Res* 125, 271–289. Le Bas, M.J., Le Maitre, R.W., Streckeisen, A. & Zanettin, B., 1986. A chemical classification of volcanic rocks based on the total alkali-silica diagram, *J of Petrol*, 27, 3, 745–750.

[17] Lipman, P.W. & Mullineaux, D.R., 1981. The 1980 eruptions of Mount St. Helens, Washington, U.S. Geological Survey Professional Paper 1250.

[18] Lockwood, J.P., Dvorak, J.J., English, T.T., Koyanagi, R.Y., Okamura, A.T., Summers, M.L. & Tanigawa, W.R., 1987. Mauna Loa 1974-1984: a decade of intrusive and extrusive activity, In: *Volcanism in Hawai'i*, U.S. Geological Survey Professional Paper 1350, 537–570, eds Decker, R.W, Wright, T.L. & Stauffer, P.H.. .

[19] Marzocchi, W. & Zaccarelli, 2006. A quantitative model for the time size distribution of eruptions, *J Geophys Res*, 111, B04204, doi:10.1029/2005JB003709.

[20] Mastin, L.G. & M. S. Ghiorso, M. S., 2000. A Numerical Program for Steady-State Flow of Magma-Gas Mixtures Through Vertical Eruptive Conduits, USGS Open-File Report 00-209.

[21] Moran, S.C., Stihler, S.D. & Power, J.A., 2002. A tectonic earthquake sequence preceding the April-May 1999 eruption of Shishaldin Volcano, Alaska, *Bull Volcanol*, 64, 520–524.

[22] Mulargia , F., Tinti, S. & Boschi, E., 1985. A statistical analysis of flank eruptions on Etna Volcano, *J Geophys Res*, 23, 263–272.

[23] Newhall, C., G., & Dzurisin D., 1988. Historical unrest at large calderas of the world, USGS Bull 1855:1108.

[24] Newhall, C., G. & Punongbayan R S, 1996. Fire and Mud: Eruptions and Lahars of Mount Pinatubo, Philippines. Quezon City, Philippines: Philippine Inst. Volc. Seism., and Seattle: Univ Wash Press.

[25] Nye, C.J., Keith, T.E.C., Eichelberger, J.C., Miller, T.P., McNutt, S.R., Moran, S.C., Scheneider, D.J., Dehn, J. & Schaefer, J.R., 2002. The 1999 eruption of Shishaldin Volcano, Alaska: monitoring a distant eruption, *Bull Volcanol*, 64, 507–519.

[26] Peltier,A., Bachelery,P. & Staudacher,T., 2009. Magma transport and storage at Piton de la Fournaise (La Reunion) between 1972 and 2007: a review of geophysical and geochemical data, *J Volcanol Geotherm Res* 184, 93–108.

[27] Prejean,S., Power,J. & Brodsky,E.E., 2008. Eruption Forecasting: Success and Surprise at Kasatochi and Okmok Volcanoes, *Eos Trans.AGU*, 89(53), Fall Meet. Suppl., Abstract A51J-01.

[28] Pyle, D.M., 1992. The volume and residence time of magma beneath active volcanoes determined by decay-series disequilibria methods, *Earth Planet Sci Lett*, 112, 61 – 73

[29] Reid , M.R., 2003. Timescales of magma transfer and storage in the crust, in *Treatise on Geochemistry*, 167–193, Elsevier, New York.

[30] Rubin, A., M., Propagation of magma-filled cracks, 1995, *Annu Rev Earth Planet Sci*, 23, 287-336.

[31] Sandri, L., Marzocchi, W. & Gasperini, P., 2005. Some insights on the occurrence of recent volcanic eruptions of Mount Etna volcano (Sicily, Italy), *Geophys J Int*, 163, 1203–1218.

[32] Simkin, T. & Siebert, L., 1994. Volcanoes of the world, 2nd edn., Geoscience Press, Tucson, Arizona, 1–349.

[33] Soosalu, H., Einarsson,P. & Þorbjarnardottir, B.S., 2005. Seismic activity related to the 2000 eruption of the Hekla volcano, Iceland, Bull. Volcanol. 68, 21–36.

[34] Tokarev, P.I., 1985. The prediction of large explosions of andesitic volcanoes, *J of Geodynamics* 3, 219–244.

[35] Villeneuve, N., Neuville, D.R., Boivin, P., Bachelery,P. & Richet,P., 2008. Magma crystallization and viscosity: A study of molten basalts from the Piton de la Fournaise volcano (La Reunion island), *Chemical Geology*, 256, 242–251.

[36] White, S. C., Crisp, J.A. & Spera, F.J., 2006. Long-term volumetric eruption rates and magma budgets, *Geochem Geophys Geosyst*, 7, Q03010, doi:10.1029/2005GC001002.

[37] Yokoyama, I., 1988. Seismic energy release from volcanoes, *Bull Volcanol* 50, 1–13.

[38] Yokoyama, I., De la Cruz-Reyna, S. & Espindola, J.M., 1992. Energy partition in the 1982 eruption of E1 Chichon volcano, Chiapas, Mexico, J. Volcanol. Geotherm. Res. 51, 1–21.

[39] Yokoyama, I. & Seino, M., 2000. Geophysical comparison of the three eruptions in the the 20th century of Usu Volcano, Japan, *Earth Plan Space* 52, 73–89.

	Volcano	**Magma** SiO_2 wt%	**Run-up** yyyy-mm-dd HHMMSS	**Repose time** yyyy-mm-dd HHMMSS	**Volume** $[10^6 m^3]$
1	AUGUSTINE (AU) 2006	Andesite 60.00[1]%	2005-11-17 00:00:00 1986-03-27 00:00:00	2006-01-11 00:00:00 2006-01-11 00:00:00	
2	BEZYMIANNY (Bz) 1956	andesite/dacite 59.90%	1955-09-29 00:00:00 1956-03-30 00:00:00	950-01-15 00:00:00* 1956-03-30 00:00:00	t:2800
3	EL CHICHON (EC) 1982	Andesite 55.88%	1981-01-15 00:00:00[2],** 1982-03-28 00:00:00	1432-01-01 00:00:00 1982-03-28 00:00:00 (∼550 years)	t:2300
4	GALERAS (Ga) 1992	andesite/dacite 59.40%	1988-06-15 00:00:00** 1991-10-09 00:00:00	1936-08-27 00:00:00 1991-10-09 00:00:00	
5	GRIMSVOTN (Gr) 2004	basaltic/andesite 50.00[3]%	2004-10-31 21:00:00 2004-11-01 00:00:00 (3 hour) [4]	1998-12-18 00:00:00 2004-11-01 00:00:00	
6	GUAGUA PICHINCHA 1999 (GP)	dacite 64.50%	1998-09-15 00:00:00 [5] 1999-09-26 00:00:00	1660-11-27 00:00:00 1999-09-26 00:00:00	l:> 6
7	HEKLA (Hk1) 1980	basaltic andesite 54.90%	1980-08-16 23:35:00 1980-08-17 00:00:00 (25 min)	1970-05-05 00:00:00 1980-08-17 00:00:00	l: 200 t: 70
8	HEKLA (Hk2) 1981	basaltic andesite 55.40%	1981-04-16 23:37:00 1981-04-17 00:00:00 (23 min)	1980-08-17 00:00:00 1981-04-09 00:00:00	l:120 t: 60
9	HEKLA (Hk3) 1991	basaltic andesite 54.70%	1991-01-16 23:30:00 1991-01-17 00:00:00 (30 min)	1981-04-09 00:00:00 1991-01-17 00:00:00	l: 150 t: 20
10	HEKLA (Hk4) 2000	basaltic andesite 55.00%	2000-02-25 22:41:00 2000-02-26 00:00:00 (79 min)	1991-01-17 00:00:00 2000-02-26 00:00:00	l:286 t: 10
11	MAUNA LOA (ML1) 1975	basalt 52.04%	1974-08-15 00:00:00** 1975-07-06 00:00:00	1950-06-01 00:00:00 1975-07-06 00:00:00	l:3
12	MAUNA LOA (ML2) 1985	Basalt 51.37%	1984-03-24 21:30:00 1984-03-25 00:00:00 (∼2 h 30m)	1975-07-06 00:00:00 1984-03-25 00:00:00	l: 220
13	MIYAKEJIMA (My) 2000	basaltic andesite 54.00%	2000-06-26 00:00:00 2000-06-27 00:00:00	1983-10-03 00:00:00 2000-06-27 00:00:00	t:9.3

[1]Based on 1986 eruption where range of SiO2 is 56-64%wt

[2]From Yokoyama [1988]

[3]From BGVN and Sigmarsson et al 2000 for previous eruption in 1998.

[4]Swarm 3 hours before eruption, probably increasing seismicity from 5-7 am Nov 1(from BGVN 29:10)

[5]From Garcia *et al* (2007), onset is mid-September

	Volcano	Magma SiO_2 wt%	Run-up yyyy-mm-dd HHMMSS	Repose time yyyy-mm-dd HHMMSS	Volume $[10^6 m^3]$
14	Mt. S. HELENS (MSH1)1980	Dacite 62.00%	1980-03-20 00:00:00 1980-05-18 00:00:00	1850-03-15 00:00:00 [6] 1980-05-18 00:00:00	l: 74 t:1200
15	Mt. S.HELENS (MSH2) 2004	Dacite 64.85%	2004-09-23 00:00:00 2004-10-01 00:00:00	1980-05-18 00:00:00 2004-10-01 00:00:00	l:93
16	Mt. SPURR (MSp) 1992	Andesite 56.00%	1991-08-15 00:00:00** 1992-06-27 00:00:00	1953-07-09 00:00:00 1992-06-27 00:00:00	t: 150
17	OKMOK (Ok) 2008	Basaltic andesite[7] 56.00%	2008-07-12 19:00:00 2008-07-12 19:43:00[8] (43 minutes)	1997-02-11 00:00:00 2008-07-12 19:43:00	
18	PAVLOF (Pv1) 1996	basaltic andesite 53.00[9]%	1996-09-13 00:00:00 1996-09-16 00:00:00	1986-04-16 00:00:00 1996-09-16 00:00:00	
19	PAVLOF (Pv1) 2007	basaltic andesite 53.00%	2007-08-14 00:00:00 2007-08-15 00:00:00	1996-09-16 00:00:00 2007-08-15 00:00:00	
20	PINATUBO (Pi) 1991	Dacite 64.00%	1991-03-15 00:00:00** 1991-06-07 00:00:00 (500years)	1491-01-01 00:00:00 1991-06-07 00:00:00	t:(1.1±0.5) x10^4 l: 4
21	PITON de la FOURNAISE (PF1)	Basalt 48.74%	1983-12-03 21:40:00 1983-12-04 00:00:00 (∼ 3 hr)	1981-02-03 00:00:00 1983-12-04 00:00:00	l:8
22	PITON de la FOURNAISE (PF2)	Basalt 47.78%	1983-12-03 23:00:00 1983-12-03 00:00:00 (∼ 1 hrs)	1983-12-04 00:00:00 1985-06-14 00:00:00	l: 1
23	PITON de la FOURNAISE (PF3)	basalt 47.78%	1985-08-13 21:23:00 1985-06-14 00:00:00 (2 h 37 min)	1985-06-14 00:00:00 1985-08-05 00:00:00	l:7
24	PITON de la FOURNAISE (PF4)	Basalt 47.78%	1985-09-05 22:48:00 1985-09-05 00:00:00 (1h 12 min)	1985-08-05 00:00:00 1985-09-06 00:00:00	l:14
25	PITON de la FOURNAISE (PF5)	basalt 47.78%	1985-11-30 23:43:00 1985-12-01 00:00:00 (17 min)	1985-09-06 00:00:00 1985-12-01 00:00:00	l: 0.7
26	PITON de la FOURNAISE (PF6)	Basalt 47.78%	1985-12-27 23:46:00 1985-12-28 00:00:00 (14 min)	1985-12-01 00:00:00 1985-12-28 00:00:00	l: 7

[6] Data taken from www.volcano.si.edu

[7] Personal communication Jessica Larsen (2009), Geophysical Institute, Fairbanks, AK

[8] Real onset time for run-up is known (see caption)

[9] Magma composition not available for 1996 eruption, so used the 2007 magma composition

	Volcano	**Magma** SiO_2 wt%	**Run-up** yyyy-mm-dd HHMMSS	**Repose time** yyyy-mm-dd HHMMSS	**Volume** $[10^6 m^3]$
27	PITON de la FOURNAISE (PF7)	Basalt 47.78%	17-03-1986 14:36:00 1986-03-18 00:00:00 (9h 24 min)	1985-12-28 00:00:00 1986-03-18 00:00:00	l: 14
28	PITON de la FOURNAISE (PF8)	basalt 47.78%	1987-07-18 21:47:00 1987-07-19 00:00:00 (2 h 13 min)	1987-06-10 00:00:00 1987-07-19 00:00:00	l: 0.8
29	PITON de la FOURNAISE (PF9)	Basalt 47.78%	1987-11-29 22:30:00 1987-11-30 00:00:00 (1h30)	1987-11-06 00:00:00 1987-11-30 00:00:00	l: 10
30	PITON de la FOURNAISE (PF10)	basalt 47.78%	1988-02-06 21:55:00 1988-02-07 00:00:00 (2 h 05 min)	1987-11-30 00:00:00 1988-02-07 00:00:00	l:8
31	PITON de la FOURNAISE (PF11)	basalt 47.78%	1988-05-17 23:29:00 1988-05-18 00:00:00 (31 min)	1988-02-07 00:00:00 1988-05-18 00:00:00	l: 15
32	PITON de la FOURNAISE (PF12)	basalt 47.78%	1988-08-30 21:35:00 1988-08-31 00:00:00 (2 h 25 min)	1988-05-18 00:00:00 1988-08-31 00:00:00	l: 7
33	PITON de la FOURNAISE (PF13)	basalt 47.78%	1988-12-13 19:29:00 1988-12-14 00:00:00 (4h 31 min)	1988-08-31 00:00:00 1988-12-14 00:00:00	l: 8
34	PITON de la FOURNAISE (PF14)	basalt 47.78%	1990-01-17 23:13:00 1990-01-18 00:00:00 (47 min)	1988-12-14 00:00:00 1990-01-18 00:00:00	l: 0.5
35	PITON de la FOURNAISE (PF15)	basalt 47.78%	1990-04-17 17:15:00 1990-04-18 00:00:00 6h 45 min	1990-01-18 00:00:00 1990-04-18 00:00:00	l: 8
36	PITON de la FOURNAISE (PF16)	basalt 47.78%	1991-07-17 23:08:00 1991-07-18 00:00:00 (52 min)	1990-04-18 00:00:00 1991-07-18 00:00:00	l: 2.8
37	PITON de la FOURNAISE (PF17)	basalt 47.78%	1992-08-26 23:03:00 1992-08-27 00:00:00 57 min	1991-06-18 00:00:00 1992-08-27 00:00:00	l: 5.5
38	PITON de la FOURNAISE (PF18)	basalt 48.74%	1998-03-07 12:00:00 1998-03-09 00:00:00 (36 h)	1992-08-27 00:00:00 1998-03-09 00:00:00	l:60
39	POPOCATEPETL (Pp) 1996	andesite/dacite 62.41%	1990-06-03 00:00:00 1996-03-01 00:00:00	1919-02-19 00:00:00 1996-03-01 00:00:00[10]	l: > 28

[10] Onset of dome extrusion, no information on previous juvenile material

	Volcano	**Magma** SiO_2 wt%	**Run-up** yyyy-mm-dd HHMMSS	**Repose time** yyyy-mm-dd HHMMSS	**Volume** $[10^6 m^3]$
40	RABAUL (Rb1) 1994	andesite/dacite 61.66%	1994-09-17 21:00:00 1994-09-19 00:00:00 (27hours)	1943-12-23 00:00:00 1994-09-19 00:00:00	l: 0.4
41	RABAUL (Rb2) 1995	andesite/dacite 61.40%	1995-11-27 00:00:00 1995-11-28 00:00:00 (24 hours)	1994-09-19 00:00:00 1995-11-28 00:00:00	l: 4.5±0.5
42	REDOUBT (Rd) 1989	Andesite 61.00[11] %	1989-12-13 01:00:00 1989-12-14 00:00:00 (∼ 23h)	1967-12-06 00:00:00 1989-12-14 00:00:00	l: 88 t: 210
43	RUAPEHU (Rh1) 1995	Andesite 58.50%	1995-04-15 00:00:00[12] 1995-09-17 00:00:00	1977-07-16 00:00:00 1995-09-17 00:00:00	t: 30±20
44	RUAPEHU (Rh2) 1996	Andesite 57.47 %	1996-06-14 08:00:00 1996-06-16 00:00:00 (40 hours)	1995-09-17 00:00:00 1996-06-16 00:00:00	t:4
45	SHISHALDIN (Shis) 1999	Basalt 51.94%	1998-06-15 00:00:00** 1999-04-17 00:00:00	1995-12-23 00:00:00 1999-04-17 00:00:00	l: 14
46	SHIVELUCH (Shiv) 1964	andesite/dacite 60.00%	1964-02-24 00:00:00 1964-11-11 00:00:00	1944-11-05 00:00:00 1964-11-11 00:00:00	t:750±50
47	SOUFRIERE HILLS 1995 (SHV)	Andesite 60.02%	1994-06-15 00:00:00 [13] 1995-09-25 00:00:00	1650-01-15 00:00:00* 1995-09-25 00:00:00	l:1.2 x 10^2
48	TOKACHI (Tk2) 1962	andesite 52.78%	1962-05-01 00:00:00[14] 1962-06-30 00:00:00	1924-05-24 00:00:00 1962-06-30 00:00:00	t: 72
49	TOKACHI (Tk1) 1988	Andesite 53.15%	1988-09-15 00:00:00[15] 1988-12-19 00:00:00	1962-06-30 00:00:00 1988-12-19 01:00:00	t: 0.75
50	TUNGURAHUA (Tg) 1999	andesite 58.58%	1999-05-15 00:00:00 1999-10-15 00:00:00 [16]	1916-03-03 00:00:00 1999-10-15 00:00:00	
51	UNZEN (Uz) 1990	dacite 65.31%	1989-11-15** 00:00:00 1991-02-12 00:00:00	1792-02-10 00:00:00 1991-02-12 00:00:00	l:150 t:>4.7
52	USU 1943 (Us1)	dacite/rhyolite 70.24%	1943-12-28 00:00:00 1944-08-15 00:00:00	1853-03-06 00:00:00 1944-08-15 00:00:00 [17]	l: 70? t:4

[11] Range of SiO2 content is 58.5-64%wt

[12] In Christenson [2000] the onset is not clear, but from www.volcano.si.edu BGVN(20:05) onset mid April

[13] from Kokelaar 2002, mid June, 1995-07-18 beginning of phreatic activity, poor information from seismicity before.

[14] from Yokoyama, 1964

[15] problematic onset run up time, choose mid September, but increase seismicity started in july 88 from Okada et al.,1990

[16] onset of both run up and repose time are from www.volcano.si.edu

[17] from Showa-Shinzan diary Aug, 17, 1944 with some ambiguity, so chose 08/15

	Volcano	**Magma** SiO_2 wt%	**Run-up** yyyy-mm-dd HHMMSS	**Repose time** yyyy-mm-dd HHMMSS	**Volume** $[10^6 m^3]$
53	USU 1977 (Us2)	dacite 69.65%	1977-08-05 16:00:00 1977-08-07 00:00:00 (32 hrs)	1944-08-15 00:00:00 1977-08-07 00:00:00	t:100
54	USU 2000 (Us3)	dacite 68.89%	2000-03-27 08:00:00 [18] 2000-03-31 13:10:00	1977-08-07 00:00:00 2000-03-31 00:00:00	

Table 3.1: Data set of run-up times, repose times, silica content and volume erupted. For some eruptions the run-up time duration is also bracketed together with the onset date. In those cases we only found the specification of the duration of the precursory activity and not the precise start time. The start date for those eruptions is a convention that allows us to use a homogeneous notation for all event and easily convert into Julian days. In nearly all cases the eruption start point is assumed to be at 00:00:00. The exceptions are Usu 2000 eruption and Okmok 2008 eruption where the real onset time for both precursory activity and eruption start are known. When eruptions are marked with * this means that month and day of onset are set as 01-15 by convention in absence of other information, while those marked with **, day of onset is set as 15th day of month by convention in absence of other information. In volume column l means lava and t tephra. The references list is given below with the same alphabetical order as in this table.

[18] real onset times

Volcano	**SiO_2 wt %**	**T [^{0}C]**	**Crystal** volume % of melt	**Main crystal phase**	**Viscosity [Pa s]** (melt + crystal)
Tokachi 1962	52.78	1000	48	Plagioclase	7.784×10^5
Tokachi 1988	53.15	1000	42	Plagioclase	2.981×10^5
Piton de la Fournaise 1983	48.74	1200	22	Olivine	6.707×10^1
Piton de la Fournaise 1986	47.78	1200	12	Olivine	2.100×10^1
Piton de la Fournaise 1998	48.74	1200	20	Olivine	6.795×10^1
El Chichon	55.88	850	53	Plagioclase	5.366×10^7
Galeras	59.90	900	50	Plagioclase	2.718×10^7
Mauna Loa 1975	52.04	1200	20	Olivine	1.321×10^2
Mauna Loa 1984	51.37	1200	20	Olivine	1.008×10^2
Popocatepetl	62.41	900	39	Plagioclase	3.650×10^6
Usu 1943	70.24	900	13	Plagioclase	4.914×10^7
Usu 1977	69.65	900	4	Plagioclase	2.074×10^7
Usu 2000	68.89	900	4	Plagioclase	1.769×10^7
Hekla 1970	54.90	1100	10	Plagioclase	2.111×10^2
Hekla 2000	55.00	1100	10	Plagioclase	4.475×10^3
Guagua Pichincha	65.79	900	10	Plagioclase	4.204×10^6
Soufriere Hills	60.02	900	40	Plagioclase	4.042×10^6

Table 3.2: Data used to calculate the viscosity, last column on the right using the software program Conflow (Mastin and Ghiorso, 2000). For the melt composition used as input, please refers to reference list of Table 1. Pressure is always chosen equal to 26 MPa and the melt water content is always zero. The value of viscosity refers to melt + crystal.

Reference list for Table 3.1

Augustine 2006

BGVN, Bulletin Global Volcanism Network monthly report 30:12 and 31:01 http://www.volcano.si.edu/.

Cervelli, P.F., Fournier,T., Freymueller,J. & Power,J.A., 2006. Ground deformation associated with the precursory unrest and early phases of the January 2006 eruption of Augustine Volcano, Alaska, *Geophys Res Lett*, 33, L18304, doi:10.1029/2006GL027219.

Roman,D.C., Cashman,K.V., Gardner,C.A., Wallace,C.A. & Donovan,C.A., 2006. Storage and interaction of compositionally heterogeneous magmas from the 1986 eruption of Augustine Volcano, Alaska, *Bull Volcanol*, 68, 240–254.

Bezymianny

Bogoyavlenskaya, G. E., Braitseva, O.A., Melekestsev, I.V., Kiriyanov, V.YU. & Miller, D.C., 1985. Catastrophic eruptions of the directed-blast type at Mount Saint Helens, Bezymianny and Shiveluch volcanoes, *J of Geodynamics*, 3, 189–218.

Tokarev, P.I. , 1985. The prediction of large explosions of andesitic volcanoes, *J of Geodynamics*, 3, 219–244.

El Chichon

De la Cruz-Reyna, S. & and Martin Del Pozzo, A.L. , 2009. The 1982 eruption of El Chichon volcano, Mexico: eyewitness of the disaster, *Geofisica Internacional* 48, 1, 21–31.

Havskov, J., De la Cruz-Reyna, S., Singh, S.K., Medina, F. & Gutierrez, C., 1983. Seismic activity related to the March-April, 1982 eruptions of El Chichon volcano, Chiapas, Mexico. *Geophys Res Lett*, 10, 4 293-296.

Jimenez, Z., Espindola, V. H. & Espindola, J.M. , 1999. Evolution of the seismic activity from the 1982 eruption of El Chichon Volcano, Chiapas, Mexico, *Bull Volcanol*, 61, 411–422, 1999.

Luhr, J., Carmichael, I.S.E. & Varekamp, J. C., 1984. The 1982 eruptions of El Chichon volcano, Chiapas, Mexico: mineralogy and petrology of the anhydrite-bearing pumices, *J Volcanol Geotherm Res*, 23, 69–108.

Macias, J. L. , Arce, J. L., Mora, J. C., Espindola, J. M., Saucedo,R. & Manetti, P. , 2003. A 550-year-old Plinian eruption at El Chichon Volcano, Chiapas, Mexico: Explosive volcanism linked to reheating of the magma reservoir, *J Geophys Res*, 108, B122569, doi:10.1029/2003JB002551.

Tilling, R. I., 2009. El Chichon "surprise" eruption 1982: lessons for reducing volcano risk, *Geofisica Internacional*, 48, 1, 3–19.

Yokoyama, I., 1988. Seismic energy release from volcanoes, *Bull Volcanol* 50,1–13.

Yokoyama, I., De la Cruz-Reyna, S. & Espindola, J.M., 1992. Energy partition in the 1982 eruption of E1 Chichon volcano, Chiapas, Mexico, *J Volcanol Geotherm Res*, 51, 1–21.

Galeras

Calvache, M.L. & Williams, S.N., 1997. Emplacement and petrological evolution of the andesitic dome of Galeras Volcano, 1990-1992, *J Volcanol Geotherm Res*, 77, 57–69.

Calvache, M.L., Cortes, G.P. & Williams, S.N., 1997. Stratigraphy and chronology of the Galeras volcanic complex, Colombia, *J Volcanol Geotherm Res*, 77, 5–19.

Cortes, G.P. & Raigosa J.A., 1997. A synthesis of the recent activity of Galeras volcano, Colombia: Seven years of continuous surveillance, 1989-1995, *J Volcanol Geotherm Res*, 77, 101–114.

Gil Cruz, F. & Chouet, B., 1997. Long-period events, the most characteristic seismicity accompanying the emplacement and extrusion of a lava dome in Galeras Volcano, Colombia, in 1991, *J Volcanol Geotherm Res*, 77, 121–158.

Grimsvotn 2004

BGVN, Bulletin Global Volcanism Network monthly report 29:10 http://www.volcano.si.edu/.

Hjaltadottir,S., Geirsson,H. & Skaftadottir,Þ., 2005. Seismic activity in Iceland during 2004, Jökull, 55,107-119 http://en.vedur.is/earthquakes-and-volcanism/reports-and-publications/.

Sigmarsson,O., Karlsson, H. R. & Larsen, G. 2000. The 1996 and 1998 subglacial eruptions beneath the Vatnajökull ice sheet in Iceland: contrasting geochemical and geophysical inferences on magma migration, *Bull Volcanol* , 61, 468–476.

Sturkell,E , Einarsson P, Sigmundsson,F., Geirsson, H., Olafsson,H., , Pedersen, R., de Zeeuw-van Dalfsen,E, Linde, A.T., Sacks, S.I. & Stefansson R, 2006. Volcano geodesy and magma dynamics in Iceland, *J Volcanol Geotherm Res* 150, 14 – 34

Guagua Pichincha

BGVN, Bulletin Global Volcanism Network monthly report from 23:08 to 24:10 http://www.volcano.si.edu/ .

Garcia-Aristizabal,A., Kumagai, H. , Samaniego,P. , Mothes,P., Yepes, H. & Monzier, M., 2007. Seismic, petrologic, and geodetic analyses of the 1999 dome-forming eruption of Guagua Pichincha volcano, Ecuador, *J Volcanol Geothem Res*, 161, 333–351.

Wright, H. M. N., Cashman,K.V., Rosi, M. & Cioni, R., 2007. Breadcrust bombs as indicators of Vulcanian eruption dynamics at Guagua Pichincha volcano, Ecuador, *Bull Volcanol* 69, 281–300.

Hekla

Moune, S., Gauthier, P.J., Gislason, S.R. & Sigmarsson, O., 2006. Trace element degassing and enrichment in the eruptive plume of the 2000 eruption of Hekla volcano, Iceland, *Geochim Cosmochim Acta* 70, 461–479.

Sverrisdottir,G., 2007. Hybrid magma generation preceding Plinian silicic eruptions at Hekla, Iceland: evidence from mineralogy and chemistry of two zoned deposits, *Geol Mag* 144, 4 ,643–659.

Soosalu, H., Einarsson,P., Þorbjarnardottir,B.S., 2005. Seismic activity related to the 2000 eruption of the Hekla volcano, Iceland, *Bull Volcanol*, 68, 21–36.

Mauna Loa

Lockwood, J.P., Dvorak, J.J., English, T.T., Koyanagi, R.Y., Okamura, A.T., Summers, M.L. & Tanigawa, W.R., 1987. Mauna Loa 1974-1984: a decade of intrusive and extrusive activity, In: in Decker, R.W, Wright, T.L., and Stauffer, P.H., (eds.), *Volcanism in Hawai'i*, U.S. Geological Survey Professional Paper 1350, 537–570.

Miyakejima

Nakada, S., Nagai, M., Kaneko, T., Nozawa, A. & Suzuki-Kamata, K., 2005. Chronology and products of the 2000 eruption of Miyakejima Volcano, Japan, *Bull Volcanol*, 67, 219–230.

Saito, G., Uto, K., Kazahaya, K., Satoh, H., Kawanabe, Y. & Shinohara, H., 2005. Petrological characteristics and volatile content of magma from the 2000 eruption of Miyakejima Volcano, *Bull Volcanol* 67, 268–280.

Uhira, K., Baba, T., Mori, H., Katayama, H. & Hamada, N., 2005. Earthquake swarms preceding the 2000 eruption of Miyakejima volcano, Japan, *Bull Volcanol*, 67, 219-230.

Mount Saint Helens

Christiansen, R.L. & Peterson, D.W., 1981. Chronology of the 1980 eruptive activity, In: *The 1980 eruptions of Mount St. Helens, Washington*, Lipman, P.W., Mullineaux, D.R., U.S. Geological Survey Professional Paper 1250, 3–17.

Endo, T.E., Malone, S.D., Noson, L. L. & Weaver, C.S., 1981. Locations, magnitude, and statistics of the March 20 - May 18 earthquake sequence, In: *The 1980 eruptions of Mount St. Helens, Washington*, Lipman, P.W., Mullineaux, D.R., U.S. Geological Survey Professional Paper 1250, 93–108.

Lipman, P.W., Norton, D.R., Taggart, Jr, J.E., Brandt, E. L. & Engleman, E. E., 1981. Compositional variations in 1980 magmatic deposits, In: *The 1980 eruptions of Mount St. Helens, Washington*, Lipman, P.W., Mullineaux, D.R., U.S. Geological Survey Professional Paper 1250, 631-649.

Moran, S.C., Malone, S.D., Qamar, A.I., Thelen, W.A., Wright, A.K. & Caplan-Auerbach, J., 2008. Seismicity associated with renewed dome building at Mount St.Helens, 2004-2005, In: *A volcano rekindled; the renewed eruption of Mount St. Helens, 2004-2006*,

Sherrod, D.R., Scott, W.E., and Stauffer, P.H., U.S. Geological Survey Professional Paper 1750, 2, 27–54.

Pallister, J.S., Thornber, C.R., Cashman, K.V., Clynne, M.A., Lowers, H.A., Mandeville, C.W., Brownfield, I.K. & Meeker, G.P., 2008. Petrology of the 2004-2006 Mount St. Helens lava dome-implications for magmatic plumbing and eruption triggering, In: *A volcano rekindled; the renewed eruption of Mount St. Helens, 2004-2006*, Sherrod, D.R., Scott, W.E., and Stauffer, P.H., U.S. Geological Survey Professional Paper 1750, 30, 647-702.

Mount Spurr

Gardner, C.A., Cashman, K.V. & Neal, C.A., 1998. Tephra-fall deposits from the 1992 eruption of Crater Peak, Alaska: implications of clast textures for eruptive processes, *Bull Volcanol* 59, 537–555.

Power, J.A., Jolly, A.D., Nye, C.J. & Harbin, M.L., 2002. A conceptual model of the Mount Spurr magmatic system from seismic and geochemical observations of the 1992 Crater Peak eruption sequence, *Bull Volcanol* 64, 206–218.

Okmok

BGVN, Bulletin Global Volcanism Network monthly report 33:06
http://www.volcano.si.edu/ .

Silica content Jessica Larsen personal communication.

Pavlof

Alaskan Volcanoes Observatory, Reported activity about Pavlof volcano 2007 eruption http://www.avo.alaska.edu/volcanoes/volcact.php?volcname=Pavlof.

BGVN, Bulletin Global Volcanism Network monthly report from 32:08
http://www.volcano.si.edu/ .

Roach, A.L., Benoit, J.P., Dean, K.G. & McNutt, S.R., 2001. The combined use of satellite and seismic monitoring during the 1996 eruption of Pavlof volcano, Alaska, *Bull Volcanol* 62, 385–399.

Waythomas, C.F., Prejean, S.G. & McNutt, S.R., 2008 Alaska's Pavlof Volcano ends 11-year repose, *Eos*, 89, 23, 209–211.

Pinatubo

Wolfe,E.W. & Hoblitt, R.P., 1996 Overview of the eruption, In: *Fire and Mud: Eruptions and Lahars of Mount Pinatubo, Philippines*, Newhall C. G., Punongbayan R. S., Quezon City, Philippines: Philippine Inst. Volc. Seis.m, and Seattle: Univ Wash Press, 3–20.

Newhall, C.G., Daag, A.S., Delfin, F.G.J., Hoblitt, R.P., McGeehin, J., Pallister, J.S., Regalado, Ma.T.M., Rubin, M., Tubianosa, B.S., Tamayo, R.A.J. & Umbal, J.V., 1996. Eruptive history of Mount Pinatubo In: *Fire and Mud: Eruptions and Lahars of Mount Pinatubo, Philippines,* Newhall C. G., Punongbayan R. S., Quezon City, Philippines: Philippine Inst. Volc. Seism., and Seattle: Univ Wash Press, 165–196.

Hoblitt, R.P., Wolfe,E.W., Scott, W.E., Couchman, M.R., Pallister, J. & Javier, D., 1996. The preclimatic eruptions of Mount Pinatubo, June 1991, In: *Fire and Mud: Eruptions and Lahars of Mount Pinatubo, Philippines,* Newhall C. G., Punongbayan R. S., Quezon City, Philippines: Philippine Inst. Volc. Seism. and Seattle: Univ Wash Press, 457–512

Pallister, J.S., Hoblitt, R.P., Meeker, G.P., Knight, R.J. & Siems, D.F., 1996. Magma mixing at Mount Pinatubo: Petrographic and chemical evidence from the 1991 deposits, In: *Fire and Mud: Eruptions and Lahars of Mount Pinatubo, Philippines,* Newhall C. G., Punongbayan R. S., Quezon City, Philippines: Philippine Inst. Volc. Seism. and Seattle: Univ Wash Press, 165–196.

Luhr, J.F. & Melson, W.G., 1996. Mineral and glass compositions in June 15, 1991 pumices: Evidence for dynamics disequilibrium in the dacite of Mount Pinatubo, In: *Fire and Mud: Eruptions and Lahars of Mount Pinatubo, Philippines,* Newhall C. G., Punongbayan R. S., Quezon City, Philippines: Philippine Inst. Volc. Seism. and Seattle: Univ Wash Press, 165–196.

Piton de la Fournaise

Aki,K. & Ferrazzini,V., 2000. Seismic monitoring of an active volcano for prediction, *J Geophys Res*, 105 no B7 16617–16640.

BGVN, Bulletin Global Volcanism Network monthly report from 8:11 to 23:03 http://www.volcano.si.edu/ .

Peltier,A., Bachelery,P. & Staudacher,T., 2009. Magma transport and storage at Piton de la Fournaise (La Reunion) between 1972 and 2007: a review of geophysical and geochemical data, *J Volcanol Geotherm Res* 184, 93–108.

Villeneuve, N., Neuville, D.R., Boivin, P., Bachelery,P. & Richet,P., 2008. Magma crystallization and viscosity: A study of molten basalts from the Piton de la Fournaise volcano (La Reunion island), *Chemical Geology*, 256, 242–251.

Popocatepetl

De la Cruz-Reyna, S., Yokoyama, I., Martinez-Bringas, A. & Ramos, E., 2008. Precursory seismicity of the 1994 eruption of Popocatepetl Volcano, central Mexico, *Bull Volcanol*, 70, 753-767.

De la Cruz-Reyna, S. & Siebe, C., 1997. The giant Popocatepetl stirs, *Nature* 388, 17 July 1997.

Witter, J. B., Kress, V.C. & Newhall, C.G.,1997. Volcan Popocatepetl, Mexico. Petrology, magma mixing, and immediate sources of volatiles for the 1994 - present eruption, (2005) *J of Petrol*, 46, 11, 2337–2366.

Rabaul

BGVN, Bulletin Global Volcanism Network monthly report 19:09 and 20:11/12 http://www.volcano.si.edu/.

Cunningham, H. , Turner,s. P., Dosseto, A., Patia, H., Eggins,S. M. & Arculus, R. J., 2009, Temporal Variations in U-series Disequilibria in an Active Caldera, Rabaul, Papua New Guinea, *J of Petrol*, 50, 3, 507-529.

Williams, S. N. , 1995, Erupting Neighbors - At Last, *Science* 267, 340-341.

Roggensack,K., Williams, S. N., Schaefer, S.J. & Parnell, R.A.J., 1996. Volatiles from 1994 Eruptions of Rabaul : Understanding large caldera system, *Science* 273,490–493.

Redoubt

Chouet, B.A., Page,R.A., Stephens,C.D., Lahr, J.C. & Power,J.A., 1994. Precursory swarms of long-period events at Redoubt Volcano (1989-1990), Alaska: Their origin and use as a forecasting tool, *J Volcanol Geotherm* Res. 62, 95–135.

Wolf, K.J. & Eichelberger, J.C., 1997. Syneruptive mixing, degassing, and crystallization at Redoubt Volcano, eruption of December, 1989 to May 1990., *J Volcanol Geotherm Res* 75, 19–37.

Ruapehu

BGVN, Bulletin Global Volcanism Network monthly report 20:05
http://www.volcano.si.edu/ .

Bryan, C.J. & Sherburn, S., 1999. Seismicity associated with the 1995-1996 eruptions of Ruapehu volcano, New Zealand: narrative and insights into physical processes, *J Volcanol Geotherm Res*, 90,1–18.

Christenson, B.W., 2000. Geochemistry of fluids associated with the 1995-1996 eruption of Mt. Ruapehu, New Zealand: signatures and processes in the magmatic-hydrothermal system, *J Volcanol Geotherm Res*, 97,1–30.

Nakagawa,M., Wada, K. & Wood, C.P., 2003. Mixed Magmas, Mush Chambers and Eruption Triggers: Evidence from Zoned Clinopyroxene Phenocrysts in Andesitic Scoria from the 1995 Eruptions of Ruapehu Volcano, New Zealand, *J of Petrol* 43, 12, 2279–2303.

Sherburn, S., Bryan, C.J., Hurst, A.W., Latter, J.H. & Scott, B.J., 1999. Seismicity of Ruapehu volcano, New Zealand, 1971-1996: a review, *J Volcanol Geotherm Res*, 88, 255–278.

Shishaldin

Moran, S.C., Stihler, S.D. & Power, J.A., 2002. A tectonic earthquake sequence preceding the April-May 1999 eruption of Shishaldin Volcano, Alaska, *Bull Volcanol*, 64, 520–524.

Nye, C.J., Keith, T.E.C., Eichelberger, J.C., Miller, T.P., McNutt, S.R., Moran, S.C., Scheneider, D.J., Dehn, J. & Schaefer, J.R., 2002. The 1999 eruption of Shishaldin

Volcano, Alaska: monitoring a distant eruption, *Bull Volcanol*, 64, 507–519.

Stelling, P., Beget, J., Nye, C., Gardner, J., Devine, J. D. & George, R. M. M., 2002. Geology and petrology of ejecta from the 1999 eruption of Shishaldin Volcano, Alaska, *Bull Volcanol*, 64, 548–561.

Shiveluch

Bogoyavlenskaya, G. E., Braitseva, O.A., Melekestsev, I.V., Kiriyanov, V.YU. & Miller, D.C., 1985. Catastrophic eruptions of the directed-blast type at Mount Saint Helens, Bezymianny and Shiveluch volcanoes, *J of Geodynamics*, 3, 189–218.

Tokarev, P.I., 1985. The prediction of large explosions of andesitic volcanoes, *J of Geodynamics*, 3, 219–244.

Soufriere Hills

Devine, J.D., Murphy, M.D., Rutherford, M.J., Barclay, J., Sparks, R.S.J., Carroll,M.R., Young, S.R. & Gardner, J.E., 1998. Petrologic evidence for pre-eruptive pressure-temperature conditions, and recent reheating, of andesitic magma erupting at the Soufriere Hills Volcano, Montserrat, W.I., *Geophys Res Lett*, 25, 19, 3669–3672.

Gardner, C.A. & White, R.A., 2002. Seismicity, gas emission and deformation from 18 July to 25 September during the initial phreatic phase of the eruption of Soufriere Hills Volcano, Montserrat In: *The eruption of Soufriere Hills volcano, Montserrat, from 1995 to 1999*, Druitt, T.H., Kokelaar, B.P., Geol. Soc. London. Mem., 21, 567–582.

Kokelaar, B.P., 2002. Setting, chronology and consequences of the eruption of Soufriere Hills Volcano, Monserrat (1995-1999), In: *The eruption of Soufriere Hills volcano, Montserrat, from 1995 to 1999*, Druitt, T.H., Kokelaar, B.P., Geol. Soc. London. Mem., 21, 1–44.

Watts, R.B., Herd, R.A., Sparks, R.S.J. & Young, S.R., 2002. Growth pattern and emplacement of the andesitic lava dome at Soufriere Hills volcano, In: *The eruption of Soufriere Hills volcano, Montserrat, from 1995 to 1999,* Druitt, T.H., Kokelaar, B.P., Geol Soc London Mem, 21, 115-152.

Tokachi

BGVN, Bulletin Global Volcanism Network monthly report from 13:11 to 14:06 http://www.volcano.si.edu/.

Goto,A., Oshima, H. & Nishida, Y., 1997. Empirical method of calculating the viscosity of peraluminous silicate melts at high temperatures. *J Volcanol Geotherm Res*, 76,319–327.

Ikeda,Y., Katsui,Y., Nakagawa, M., Kawachi, S., Watanabe, T., Fujibaiashi, N., Shibata, T. & Kagami, H., 1990. Petrology of the 1988-89 essential ejecta and associated glassy rocks of Tokachi-dake volcano in central Hokkaido, *Japan Bull Volcanol Soc Jpn* 35, 2, 147–162.

Katsui, Y., Kawachi, S., Kondo, Y., Ikeda, Y., Nakagawa, M., Gotoh, Y.,Yamagishi, H., Yamazaki, T. & Sumita, M., 1990. The 1988-1989 explosive eruption of Tokachi-dake, central Hokkaido, its sequence and mode, *Bull Volc Soc Jpn*, 35, 2, 557–583.

Murai, I., 1963. A brief note on the eruption of the Tokachi-dake Volcano of June 29 and 30, 1962, *Bull Earthquakes Res Institute*, 41, 185–208.

Nishimura, Y., Miyamachi, H., Ueki, S., Nishimura, T., Shimizu,H., Ohmi, S. & Okada, H.,1990. Joint seismometrical observations by the National University team during the 1988-1989 eruptive activity of Mt. Tokachi, Hokkaido, *Bull Volc Soc Jpn*, 35, 2, 163-173.

Okada, H., Nishimura, Y., Miyamachi, H., Mori, H. & Ishihara, K., 1990. Geophysical significance of the 1988-1989 explosive eruptions of Mt. Tokachi, Hokkaido, Japan, *Bull Volcanol Soc Jpn*, 35, 2, 175–203.

Yokoyama, I., 1964. Seismometrical Observation of the 1962 Eruption of Volcano Tokati, Hokkaido, Japan, *Bull Volcanol* 27, 217–223.

Yokoyama, I., 1988. Seismic energy release from volcanoes, *Bull Volcanol* 50, 1–13.

Tungurahua

Arellano, S.R., Hall,M., Samaniego, P., Le Pennec, J.-L., Ruiz,A., Molina, I. & Yepes, H., 2008. Degassing pattern of Tungurahua volcano (Ecuador) during the 1999-2006

eruptive period, inferred from remote spectroscopic measurements of SO2 emissions, *J Volcanol Geotherm Res* 176, 151–162.

BGVN, Bulletin Global Volcanism Network monthly report from 24:09 to 24:11 http://www.volcano.si.edu/ .

Hall, M.L., Robin, C., Beate, B., Mothes, P. & Monzier, M., 1999. Tungurahua Volcano, Ecuador: structure, eruptive history and hazards, *J Volcanol Geotherm Res*, 91,1–21.

Unzen

BGVN, Bulletin Global Volcanism Network monthly report from 15:07 to 16:05 http://www.volcano.si.edu/.

Nakada, S., Shimizu, H. & Ohta K., 1999. Overview of the 1990-1995 eruption at Unzen Volcano, *J Volcanol Geotherm Res*, 89, 1–22.

Nakada, S. & Motomura ,Y., 1999. Petrology of the 1990-1995 eruption at Unzen: effusion pulsation and groudmass cristallization *J Volcanol Geotherm Res*, 89, 173–196.

Watanabe, K., Danhara,T., Watanabe, K., Terai,K. & Yamashita, T., 1999. Juvenile volcanic glass erupted before the appearance of 1991 lava dome, Unzen Volcano, Kyushu, Japan *J Volcanol Geotherm Res*, 89, 113–121.

Usu

Mimatsu M, 1995. Showa-Shinzan Diary: Expanded Reprint. Sobetsu, Hokkaido: Sobetsu Town Office.

Matsubara,W., Yomogida,K., Koyama,J., Kasahara,M., Ichiyanagi,M., Kawakatsu,H. & Yamamoto,M., 2004. Distribution and characteristic in waveform and spectrum of seismic events associated with the 2000 eruption of Mt. Usu, *J Volcanol Getherm Res* 136, 141–158.

Tomiya, A., & Takahashi, E., 1995. Reconstruction of an evolving magma chamber beneath Usu Volcano since the 1663 eruption, *J of Petrology*, 36, 3, 617–636.

Tomiya, A., & Takahashi, E., 2005. Evolution of magma chamber beneath Usu Volcano since 1663: a natural laboratory for observing changing phenocryst composition and textures, *J of Petrology*, 36, 3, 617–636.

Yoshida, M. & Nishimura,Y., 2004, Temporal variation of erupting rate during the 1978 activity of Usu Volcano, northern Japan, revealed by the eruptive deposits and volcanic tremor, *J Volcanol Geotherm Res*, 135, 285–298.

Yokoyama, I. & Seino, M., 2000. Geophysical comparison of the three eruptions in the the 20th century of Usu Volcano, Japan, *Earth Plan Space* 52, 73-89.

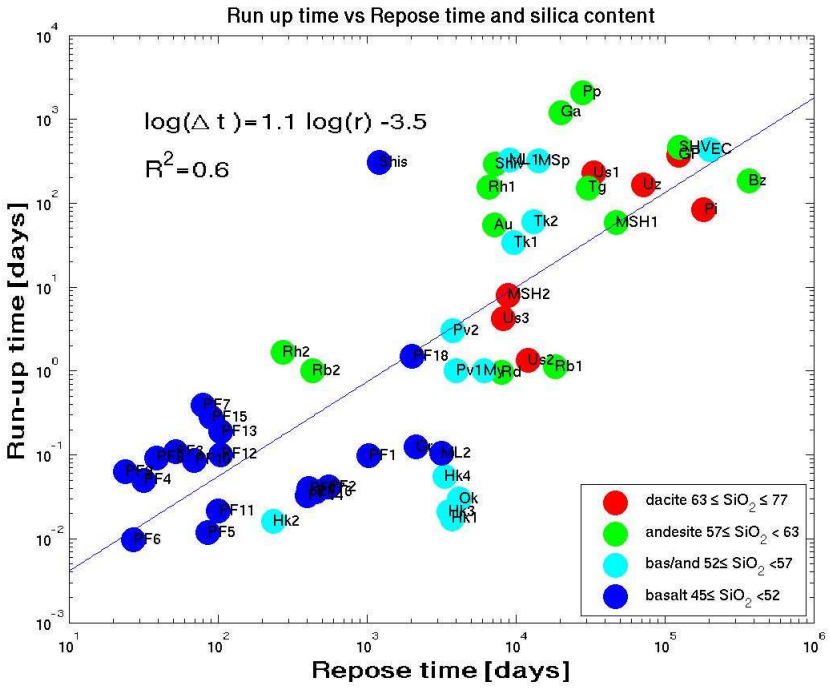

Figure 3.1: *Repose time versus run-up time data. The error associate with the slope of the regression is equal to 0.3 and with the intercept is 0.1. Labels of individual points correspond to each eruption documented in Table 1. Magma composition is based on the Le Bas et al (1986) classification.*

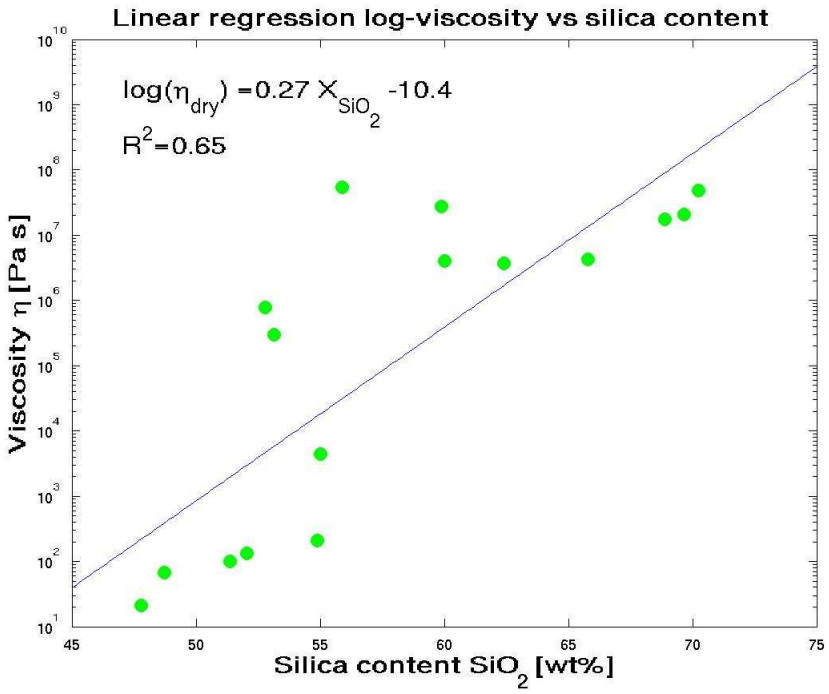

Figure 3.2: *Regression analysis to infer an empirical relationship between silica content and viscosity. Viscosity is calculated using Conflow with reported compositional information (Mastin & Ghiorso, 2000). Please refer to Table 2 for more details.*

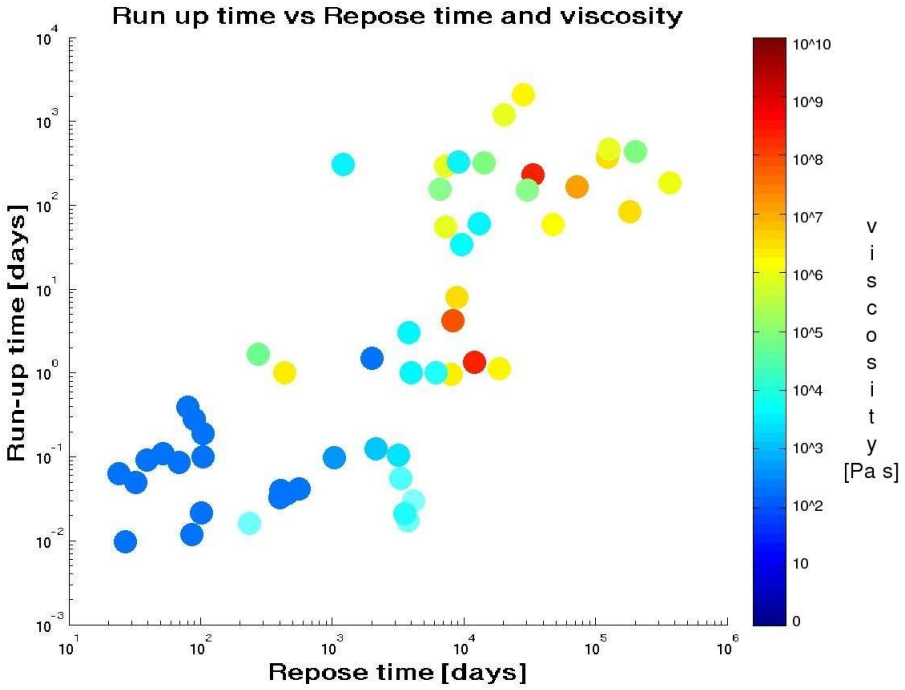

Figure 3.3: *Repose time versus run-up time with viscosity calculated using the regression line in Figure 2 for each eruption.*

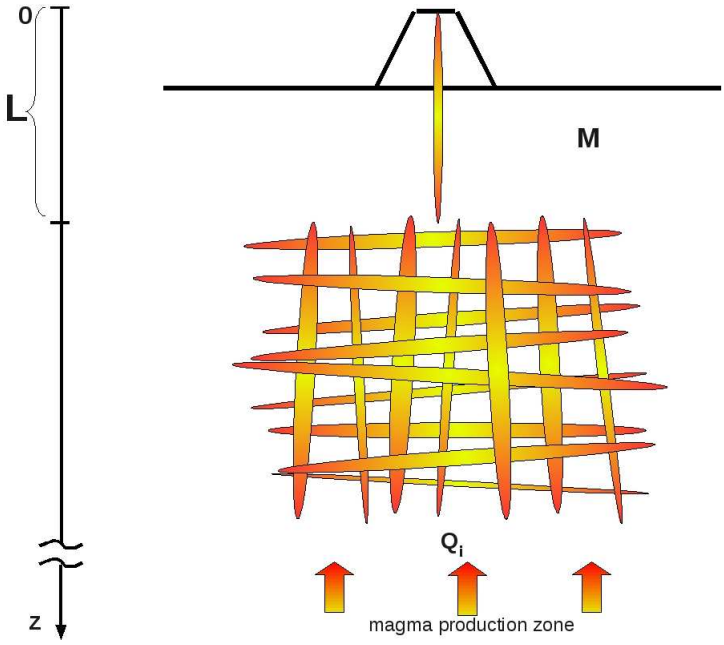

Figure 3.4: *Schematic illustration of the physical model used in the text. Q_i is the magma supply rate. For more details, please refer to the text.*

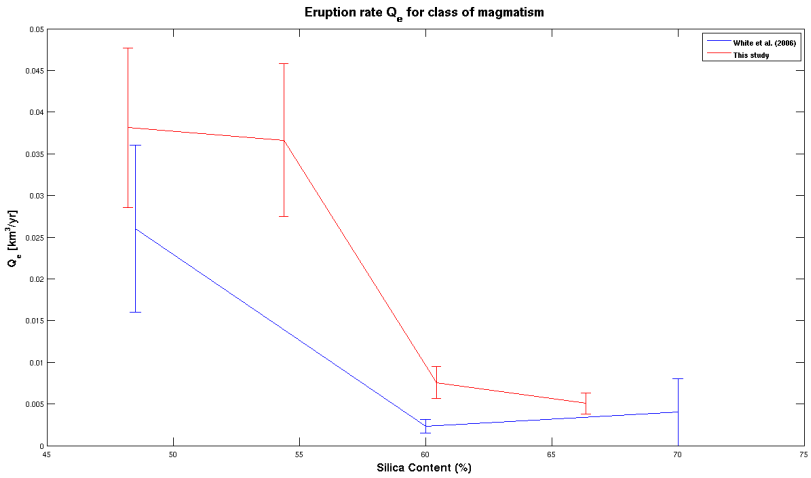

Figure 3.5: *Average extrusion rate Q_e, red ones, are calculated using repose times and volumes in Table 1 and compared with those from White et al (2006), blue ones. The Q_e's are calculate for different class of magma composition. For more detail please refer to the text.*

Conclusions

In this dissertation we presented the three project developed during my PhD studies. We have carried out two time predictable models embedded in a hierarchical Bayesian structure (BH_TPM and BH_TPMII), to describe the behavior of eruptive catalog of open conduit volcanoes. The use of a Bayesian structure allows to explicitly and formally include in the analysis any kind of uncertainty (relative to data, models, and parameters). While in the last chapter we have presented the inter-relationship between repose time, run-up time and viscosity.

We have applied the BH_TPM to Kilauea eruptive catalog from 1923 to 1983 AD. The results have shown that interevent times depend on the previous erupted volume, as in a Generalized Time Predictable Model (Sandri *et al.* 2005; Marzocchi & Zaccarelli 2006). The model has shown a reasonable fit with the data observed at Kilauea volcano, although it was not able to capture all the features and variability of the real catalog. We have found also that the Kilauea volcano has a weak time predictable eruptive behavior. However, these discrepancies do not seem to affect the forecasting capability of BH_TPM, that remains superior to the forecasting capability of a stationary Poisson model, a Log-Normal model and Generalized Time Predicable Model.

In the second chapter we have carry out, as improvement of the BH_TPM, a new Bayesian Hierarchical model to test time predictability, the BH_TPMII. We have applied the model to Kilauea eruptive catalog from 1923 to 1983 AD and to Mount Etna flank eruptions from 1607 to 2008 AD. The results have shown both volcanoes having time predictable eruptive behavior. The model have shown a good fit with the observed data for both volcanoes and is also able to capture extreme values as a tail behavior of the distributions. In addition, the BH_TPMII have improved the data fitting compared with those of BH_TPM. The forecasts obtained by BH_TPM II are superior to those provided by other statistical models for both

volcanoes. In particular we have improved the forecast performance compared with those of BH_TPM which corroborate the hypotheses of building up the present model.

The numerical values of the time predictable model parameters, inferred in both models, suggest the amount of the erupted volume could change the dynamics of the magma chamber refilling process during the repose period. This is an important feature that should be taken into account in modeling the magma chamber recharging process for both Kilauea and Mt Etna volcanoes.

Both BH_TPM and BH_TPMII have shown some limits in forecasting eruptions after long quiescence periods compared with a Poisson process. This feature could be interpreted an additional complexity for long interevent times compared to the time predictable eruptive behavior. A possible explanation may be addressed in the transition between open conduit regime and closed conduit regime where the time predictable assumption may fails (Marzocchi & Zaccarelli, 2006).

Finally, in the last chapter looking at the inter-relationship between repose time, run-up time and viscosity, data have shown a strong positive correlation between repose time and run-up time for all classes of magma composition volcanoes. In addition, both times reasonably correlated with silica content and, therefore with gross variations in magma viscosity. Using extremely simplified models of magma ascent immediately before an eruption, we have successfully matched the observed dependencies of the run-up time times on viscosity. This preliminary results for the relationships between run-up and repose time observed here provides a way to design a prediction window appropriate to a particular magmatic system. For instance, if unrest begins on a low silica system with short quiescent period, one should expect an eruption to occur within hours to days, if it is going to happen. On the other hand, for a high silica system that has experienced a very long quiescent time, an alert period should remain open for a much longer period of time from days to years.

Acknowledgements

I am very grateful with Dr Laura Sandri for guiding and supporting during my PhD studies. I would like also to thanks Prof. Bruno Sanó to give me the possibility of working with him at UCSC being patient with my weird slow time-schedule. I am indebted with Prof. Emily Brodsky, she gave me the possibility to discover new aspects of the geophysical science.

Bibliography

[1] Bebbington M.S. & Lai C. D. 1996a. Statistical analysis of New Zealand volcanic occurrence data, *J. Volcanol. Geotherm. Res.*, 74, 101–110.

[2] Bebbington M.S. & Lai C. D. 1996b. On nonhomogeneous models for volcanic eruptions, *Math. Geology*, 28,5, 585–600.

[3] Burt M.L., Wadge G. & Scott W.A., 1994. Simple stochastic modelling of eruption history of basaltic volcano: Nyamuragira, Zaire, *Bull. Volcanol.*, 56, 87–97.

[4] De la Cruz-Reyna S., 1991. Poisson-distributed patterns of explosive eruptive activity, *Bull. Volcanol.*, 54, 57–67

[5] Gelman A., Carlin J.B., Stern H.S. & Rubin D.B.,2000. *Bayesian Data Analysis*, reprinted edn, Chapman & Hall/CRC,Boca Raton-Florida.

[6] Marzocchi W.,1996. Chaos and stocasticity in volcanic eruptions the case of Mount Etna and Vesuvius, *J. Volcanol. Geotherm. Res.*,70, 205-212.

[7] Marzocchi W., Sandri L. & Selva J.,2008. BET_EF: a probabilistic tool for long- and short-term eruption forecasting, *Bull. Volcanol.*, 70, 623–632

[8] Marzocchi W. & Zaccarelli L.,2006. A quantitative model for the time size distribution of eruptions, *J Geophys Res*, 111, doi:10.1029/2005JB003709.

[9] Mulargia F.,Tinti S. & Boschi E.,1985. A statistical analysis of flank eruptions on Etna Volcano, *J Volcanol Geotherm Res* , 23, 263–272.

[10] Salvi, F., Scandone, R. & Palma, C., 2006. Statistical analysis of the historical activity of Mount Etna, aimed at the evaluation of volcanic hazard, *J Volcanol Geotherm Res*, 154, 159–168, doi:10.1016/j.jvolgeores.2006.01.002.

[11] Sandri L., Marzocchi W. & Gasperini P., 2005. Some inside on the occurrence of recent volcanic eruptions of Mount Etna volcano (Sicily,Italy), *J. Geophys. Res.*, 163, 1203–1218.

[12] Sparks, R.S.J., 2003. Forecasting volcanic eruptions,*Earth Planet. Sci. Lett.*, 210, 1–15.

[13] Newhall C.G. & Hoblitt,R.P., 2002. Constructing event trees for volcanic crises, *Bull. Volcanol.*, 64, 3–20.